USE OF THE BOUNDARY ELEMENT METHOD FOR

ANALYSIS OF GALVANIC CORROSION IN

NONHOMOGENEOUS ELECTROLYTES

By

JUAN CARLOS ORTIZ

Bachelor of Science in Civil Engineering
Louisiana State University
Baton Rouge, Louisiana
1984

Master of Science in Civil Engineering
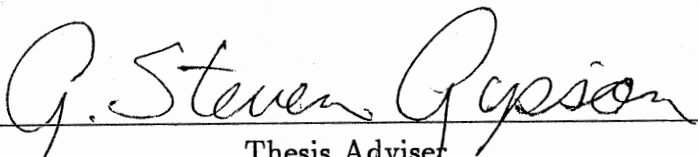Louisiana State University
Baton Rouge, Louisiana
1986

Submitted to the Faculty of the Graduate College
of the Oklahoma State University
in partial fulfillment of the requirements
for the Degree of
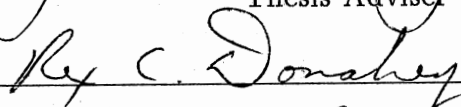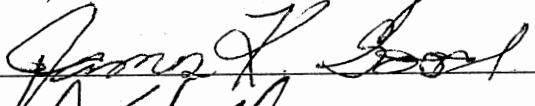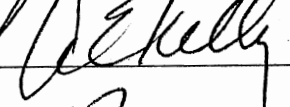DOCTOR OF PHILOSOPHY
December 1989

Thesis
1989D
O77u
cop.2

USE OF THE BOUNDARY ELEMENT METHOD FOR

ANALYSIS OF GALVANIC CORROSION IN

NONHOMOGENEOUS ELECTROLYTES

Thesis Approved:

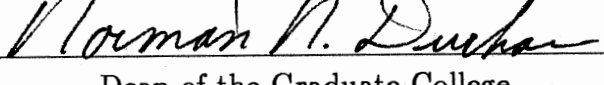_G. Steven Gipson_

Thesis Adviser

Ry C. Donahey

James K. Good

D. E. Kelly

Norman N. Durham

Dean of the Graduate College

ii

1360185

ACKNOWLEDGMENTS

TABLE OF CONTENTS

LIST OF TABLES

LIST OF FIGURES

CHAPTER I

INTRODUCTION

The economical impact of galvanic corrosion dictates that large amounts of capital and engineering time be invested in the design and construction of protection systems. Rational and accurate application of these systems can result in significant savings for industry. Certainly, misdesign of protection systems may result in accelerated damage. It is important, therefore, that accurate methods for prediction of corrosion activity and for design of protection systems be developed. The boundary element method (BEM) has been used successfully in the design and analysis of cathodic protection systems [1].

The boundary element method is a numerical procedure for the solution of partial differential equations (PDEs), where only the boundary of the analysis region is modeled. BEM may be used to predict the electropotential distribution across an electrolyte in a galvanic cell, which is governed by Laplace's PDE. The electropotential values on the electrolyte surfaces are an essential element in the design of cathodic protection systems. Ease in the development of models, speed in the analysis, and accuracy of the results are all important considerations which make BEM a preferred alternative to other numerical procedures for the solution of PDEs, such as finite

element (FEM), and finite difference (FDM) methods.

The major shortcoming common to all current BEM applications is their limitation to applications in which the electrolyte is homogeneous with constant resistivity. In fact, electrochemical resistivity is not constant in most real world problems. Examples of structures existing in nonhomogeneous electrolytes include underground storage tanks, offshore oil rigs, and reinforcing steel in chloride contaminated concrete. The resistivity of the soil in which storage tanks are embedded may vary with each soil layer and even within each layer. The resistivity of the seawater in which offshore oil structures exist may vary significantly with depth, and the difference in the electropotentials obtained from analyses performed with and without accounting for material nonhomogeneity is significant [2]. The resistivity of chlorine contaminated concrete varies with depth, since it is dependent on the chloride concentration and moisture [3].

The need for a BEM system which accounts for nonhomogeneous electrolytes is apparent. Such a system would take advantage of the superiority of BEM over FEM and FDM while enhancing its current capabilities. It is this kind of system that is developed in this work.

CHAPTER II

LITERATURE REVIEW

General Aspects of Corrosion and Cathodic Protection

In this section, a general overview of galvanic corrosion with emphasis on cathodic protection is presented, based on the books by Morgan, and Fontana and Greene [4,5].

Electrochemical corrosion of a metal, such as iron, is the result of an chemical reaction occurring with a non-metal such as oxygen. For example, the chemical reaction which occurs when iron is immersed in water can be expressed as:

$$Fe + 2H_2O + O_2 \rightarrow 2Fe^{+2} + 4OH^- \rightarrow 2Fe(OH)_2 \downarrow \qquad (1)$$
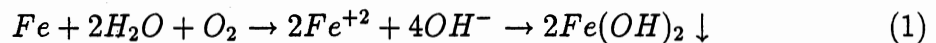
The resulting ferrous salt, $2Fe(OH)_2$, oxidizes into the ferric salt $2Fe(OH)_3$, which is the familiar rust. This reaction may be thought of a combination of two separate reactions, occurring simultaneously and at the same rate on the metal surface:

Oxidation (anodic reaction) $Fe \rightarrow Fe^{+2} + 2e$

Reduction (cathodic reaction) $O_2 + 2H_2O + 4e \rightarrow 4OH^- \qquad (2)$
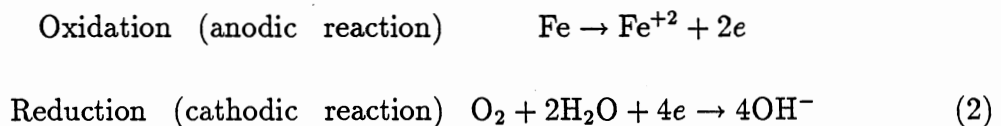
Two dissimilar metals, if electrically connected and immersed in an electrolyte, will produce an electron flow and the ensuing corrosion reactions. On the surface of the more resistant metal, the cathodic reaction will take place, and the metal surface will experience deposition. On the surface of the less resistant metal the anodic reaction will take place causing the metal to corrode. Accordingly, the resistant metal is called the cathode and the active metal is called the anode. The resulting system is called a galvanic cell.

The electropotential difference existing between two different locations within an electrolyte is the driving force behind the galvanic corrosion reaction. This potential difference may exist either at a macroscopic level or at a microscopic (molecular and crystal) level. Macroscopic galvanic cells are generally created in the presence of two dissimilar metals submerged in an electrolyte. Microscopic galvanic cells generally exist at small imperfections within a single metal submerged in an electrolyte.

Selection of the proper material for a particular corrosive environment, alteration of the environment to make it less corrosive, and coating materials used to isolate the affected material from the hostile medium are all effective methods which may be used to prevent corrosion. In many cases, economic and/or physical constraints prevent the use of any protective measures and the engineer may prefer to design the structure with allowances for corrosion. An alternative to these methods is cathodic protection, briefly described below.

A metal which would normally experience uniform corrosion by the formation

of microscopic galvanic cells on its surface can be forced to become a cathode in a macroscopic galvanic cell. This can be accomplished by introducing a sacrificial piece of material which is anodic with respect to the material to be protected, thus assuring that the protected metal acts as a cathode throughout its surface and eliminating the microscopic cells. A suitably defined electropotential distribution determines which segments of a structure act cathodically and which segments act anodically. Thus, the surface of a particular metal is said to be "cathodically protected" if the potential is raised to a level greater than any potential difference that can possibly exist on the metal surface.

Since the cathodic reaction is achieved by supplying electrons to the cathode, as seen in Equation 2, cathodic protection may also be achieved by creating a current with an external power supply instead of galvanic coupling. Therefore, two methods of cathodic protection may be used to force the protected material to become a cathode in a macroscopic galvanic cell: imposed current methods and sacrificial anode methods. The type of cathodic protection used is determined by each particular situation.

While cathodic protection may not be the only method to prevent corrosion, for many cases it is the most effective. Mudd [6] quotes the Federal Highway Administration as concluding that the only technique capable of completely stopping the corrosion of the reinforcing steel in concrete is cathodic protection, either alone or in combination with other corrosion preventing techniques. Offshore structures are

routinely protected from corrosion using cathodic protection; the weight and cost of coatings prevent their use, and the alteration of the seawater environment is impossible.

Mathematical Modeling

From the previous discussion on the general aspects of corrosion, we can conclude that the rate of corrosion of a particular anode depends on its electrochemical properties, its electrochemical potential, and the electrochemical properties of the electrolyte in which it is immersed. For most cases encountered in engineering practice, the properties of the anode and the electrolyte can be determined experimentally. The electrochemical potential (Φ) over the electrolyte in a galvanic system is governed by the familiar Laplace equation:

$$\frac{\partial^2 \Phi}{\partial x^2} + \frac{\partial^2 \Phi}{\partial y^2} + \frac{\partial^2 \Phi}{\partial z^2} = \nabla^2 \Phi = 0 \tag{3}$$

Several researchers have been able to verify measured potential distributions utilizing analytical procedures. Successful applications have, however, been limited to simple cases where the boundary conditions and geometries allow a closed-form solution to Laplace's equation [7–17]. In general, real structures or components have complex boundary conditions and geometries. Therefore, numerical approximations, such as FEM and FDM, are required. FEM and FDM have both been used to calculate

potential distributions in galvanic cells [18–22], for the design of cathodic protection systems of offshore platforms [23–26], and for the analysis of cathodic protection systems for reinforced concrete structures [27].

In the analysis of cathodic protection systems, the primary objective is to evaluate the electropotentials at the cathodes and the anodes, i.e. the metal surfaces within the electrolyte. Electropotential distribution throughout the electrolyte is unimportant. Unfortunately, both FEM and FDM require that the electrolyte body be modeled. A large amount of computation time is therefore used to calculate nonessential information: the potentials throughout the electrolyte body. An alternative — in which computation time and, more importantly, modeling time are used to calculate only the essential information (the electropotentials at the anode and cathode) — is BEM.

The boundary element method, based on Green's third formula to transform the volume derivative in Laplace's equation into a surface integral over the boundary of the domain, has been shown to be the superior analysis technique for the corrosion problem [1,28]. The boundary element method requires only that the boundaries of the domain be modeled and that only the potentials on the boundary surfaces are initially calculated. This is an important advantage, since both modeling and computation times are reduced considerably. BEM has proven to be very effective for predicting the electropotential in galvanic cells [21,29,30]. Several researchers have also used the method very effectively for the design and analysis of cathodic protection systems for offshore platforms [1,31–33].

Nonhomogeneous Electrolytes

The successful application of BEM is directly dependent on the availability of a Green's function associated with the equation governing the physical problem [34]. The potential distribution of a galvanic corrosion process within a homogeneous electrolyte is governed by Laplace's equation subject to nonlinear boundary conditions [31]. The Green's function associated with Laplace's equation is well known. Green's functions for equations governing galvanic corrosion systems with nonhomogeneous properties, however, are not readily available.

Darcy's equation, the governing equation for the flow of groundwater through non-homogeneous soils, may also be applied to galvanic corrosion problems with varying resistivity. This equation may be written as

$$\vec{\nabla} \cdot (k\vec{\nabla}\Phi) = 0 \tag{4}$$

where k is the spatially varying conductivity (inverse of the resistivity) of the electrolyte, and Φ is the electropotential. If k is constant throughout the electrolyte, Equation 4 reduces to Laplace's equation. Cheng [35] has demonstrated that a Green's function may be obtained for Equation 4 for the case where $\sqrt{k}$ satisfies Laplace's equation:

$$\nabla^2(\sqrt{k}) = 0 \tag{5}$$

There are numerous functions satisfying this contraint on k which may be easily used to model measured resistivity data.

CHAPTER III

BEM SYSTEM DEVELOPMENT

Boundary Element Methods for the Solution
of Laplace's Equation

Laplace's equation, without reference to electropotential theory and without reference to any particular coordinate system, is expressed as:

$$\nabla^2(\Phi) = 0 \tag{6}$$

where Φ is the potential distribution over the region Ω, shown in Figure 1 reproduced from Gipson [36]. The region Ω is bounded by a surface Γ on which two types of boundary conditions exist. The entire surface Γ will be composed of the cartesian sum of two surface types, Γ_1 and Γ_2, on which the different boundary conditions are specified. The related boundary conditions are:

$$\Phi = \bar{\Phi} \text{ on } \Gamma_1 \text{ and } \frac{\partial \Phi}{\partial n} = q = \bar{q} \text{ on } \Gamma_2 \tag{7}$$
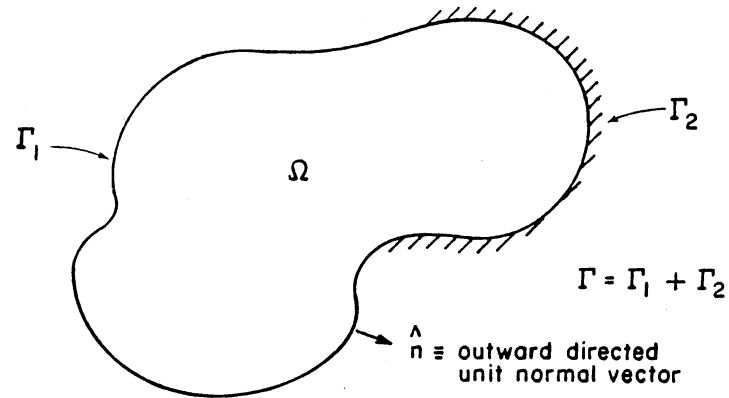
Figure 1. Nomenclature For General Laplace's Equation
Problem

where $\frac{\partial}{\partial n}$ is the derivative in a direction normal to the surface Γ, defined as:

$$\frac{\partial}{\partial n} = \hat{n} \cdot \vec{\nabla} \tag{8}$$

and $\hat{n}$ is a unit vector pointing in the outward direction normal to the surface Γ. q is then defined as the flux in the outward normal direction. $\bar{\Phi}$ and $\bar{q}$ are specified boundary conditions. It is important to understand that, in a well-posed problem, the entire boundary surface is either of the Γ_1 or of the Γ_2 type.

Using a weighted residual method, Laplace's equation is converted into surface integral form. The weighted residual statement may be written as:

$$\int_\Omega \nabla^2 \hat{\Phi}\, W\, d\Omega + \int_{\Gamma_1} (\hat{\Phi} - \bar{\Phi})\, \bar{W}\, d\Gamma + \int_{\Gamma_2} (\hat{q} - \bar{q})\, \bar{\bar{W}}\, d\Gamma = 0 \qquad (9)$$

where $\hat{\Phi}$ and $\hat{q}$ are the approximations to Φ and q, respectively. W, $\bar{W}$, and $\bar{\bar{W}}$ are the weighting functions. Integrating by parts twice, and, without loss of generality, making the following restrictions on the weighting functions:

$$\bar{W} = \frac{\partial W}{\partial n} \quad \text{on } \Gamma_1 \quad \text{and} \quad \bar{\bar{W}} = -W \quad \text{on } \Gamma_2 \qquad (10)$$

we obtain what is called the inverse statement:

$$\int_\Omega \nabla^2 W\, \Phi\, d\Omega + \int_{\Gamma_1} \left(\hat{q} W - \bar{\Phi}\frac{\partial W}{\partial n} \right) d\Gamma + \int_{\Gamma_2} \left(\bar{q} W - \hat{\Phi}\frac{\partial W}{\partial n} \right) d\Gamma = 0 \qquad (11)$$

where the Laplacian operator (∇^2) is now acting on the weighting function W. Since no restrictions have been placed on the weighting function, we can now choose W such that:

$$\nabla^2 W = \delta(\vec{r} - \vec{r}_\ell) \qquad (12)$$

where δ is the Dirac Delta function, and $\vec{r}$ and $\vec{r_\ell}$ are position vectors. This restriction on W produces the basic equation used for boundary element analysis:

$$C\hat{\Phi}(\vec{r_\ell}) = \int_\Gamma (\Phi\,\frac{\partial W}{\partial n} - W\,\frac{\partial \Phi}{\partial n})\,d\Gamma \tag{13}$$

which is strictly in terms of surface integrals. The function satisfying Equation 12 is the fundamental solution for the Laplacian operator, also referred to as the Green's function for Laplace's equation in unbounded space. Equation 13 holds for any particular point $\vec{r_\ell}$ whether or not it is on the boundary. The constant C is 1.0 for points inside the boundary, zero for points outside the boundary, and some fraction of unity for points on the boundary [34].

The idea now is to discretize the boundary into a system of elements, each of which have a defined behavior of Φ and q. In order to achieve this, a set of shape functions is defined. The shape function set consists of one normalized function per node, and is used to approximate Φ and q in the following manner:

$$\Phi = <\Phi^n>\{N\} \quad \text{and} \quad q = <q^n>\{N\} \tag{14}$$

where $<\Phi^n>$ and $<q^n>$ are row vectors containing the values of Φ and q at the nodes of the element, and $\{N\}$ denotes a column vector containing the shape functions corresponding to each node. The notation used here to differentiate between row ($<>$) and column ($\{\ \}$) vectors will be used throughout the rest of this work.

Equation 13, after substituting the approximations to Φ and q, may be rewritten as:

$$C\hat{\Phi}(\vec{r}_\ell) = <\Phi^n> \int_\Gamma \frac{\partial W}{\partial n}\{N\}\,d\Gamma - <q^n> \int_\Gamma W\{N\}\,d\Gamma \tag{15}$$

where the vectors $<\Phi^n>$ and $<q^n>$ have been factored out of the integrals. By evaluating Equation 15 at every node, we obtain a set of simultaneous equations relating the unknown Φ's with the known q's and the unknown q's with the known Φ's. The equations thus obtained have the form:

$$[H]\{\Phi\} = [G]\{q\} \tag{16}$$

where the matrices $[H]$ and $[G]$ depend only on the boundary definitions and geometry, i.e., the integrals over the boundary.

As mentioned previously, in a well-posed boundary value problem, either Φ or q is known at a point on the boundary. With the boundary conditions defined, one can rearrange Equation 16 to obtain a system of simultaneous equations of the form:

$$[A]\{x\} = \{y\} \tag{17}$$

in which the $\{x\}$ vector contains all the unknown quantities and the $\{y\}$ vector contains all the known quantities. This system of fully-populated equations can be solved to obtain the unknown boundary values at the nodes. Once all the unknown boundary data are calculated, Equation 15 may be reused to calculate values for the

potential at any internal point. Also, by differentiating Equation 15, values of the components of the fluxes may be obtained at any internal points.

The success of the method depends on one being able to find a weighting function W which satisfies Equation 12. As mentioned previously, a function which satisfies this restriction on W, and allows the most latitude for program development, is the fundamental solution for Laplace's equation. The Green's function in unbounded two-dimensional space, or fundamental solution, for Laplace's equation is given by:

$$W = \frac{1}{2\pi} \ln |\vec{r} - \vec{r}_\ell| \tag{18}$$

In three-dimensional space, the Green's function for Laplace's equation is expressed as:

$$W = \frac{1}{4\pi} \frac{1}{|\vec{r} - \vec{r}_\ell|} \tag{19}$$

Using these two expressions, the solution to Laplace's equation is obtained after performing the integrals involved in Equation 15. For a complete discussion of this procedure see Gipson [36].

Galvanic Corrosion

The equation governing the electropotential distribution within the electrolyte in a galvanic corrosion process is derived from the steady state charge conservation

equation [20]

$$\vec{\nabla} \cdot i = 0 \tag{20}$$

where i is the current density per unit volume. By substituting Ohm's law

$$i = k\mathrm{E} \tag{21}$$

where E is the electric field intensity and k is the conductivity of the electrolyte, the steady state continuity equation becomes

$$\vec{\nabla} \cdot k\mathrm{E} = 0 \tag{22}$$

Including the relationship for electric field density

$$\mathrm{E} \equiv \vec{\nabla}\Phi \tag{23}$$

where Φ is the electropotential, the continuity equation becomes:

$$\vec{\nabla} \cdot k\vec{\nabla}\Phi = 0 \tag{24}$$

which is also known as Darcy's equation, the equation governing the flow of groundwater through nonhomogeneous soils. This equation reduces to the better known Laplace's equation for homogeneous electrolytes with constant conductivity k.

The reduction and oxidation reactions occurring at the electrodes determine the corrosion rates in a galvanic cell. The corrosion rate at an electrode is a function of its material composition, the current density and electropotential existing on its surface, and the electrolyte in which it is immersed. This relationship, also referred to as the polarization behavior of the chemical reaction occurring on the electrode, may be expressed as a mathematical function in the form of:

$$q_e = f_e(\Phi_e) \tag{25}$$

where q_e represents the current density at the electrode, Φ_e is the electropotential at the electrode, and f_e is a function of a variety of chemical factors depending on how the electrode behaves in the particular electrolyte in which it is immersed. Thus, the corrosion rates for a galvanic corrosion process may be predicted if the electropotential Φ is known on the affected area.

For most metals in commonly encountered electrolytes, the polarization behavior can usually be expressed as an approximation of Φ in terms of linear functions of the logarithm of q. Figure 2 shows a typical polarization function for reinforcing steel in chloride contaminated concrete, where Φ is with respect to a $Cu/CuSO_4$ (half cell) [27].

Equation 25 determines the boundary conditions at the electrodes used in the mathematical analysis. Using the BEM, as shown in the previous section, the solution to Darcy's equation is reduced to solving the set of equations in Equation 16, repeated
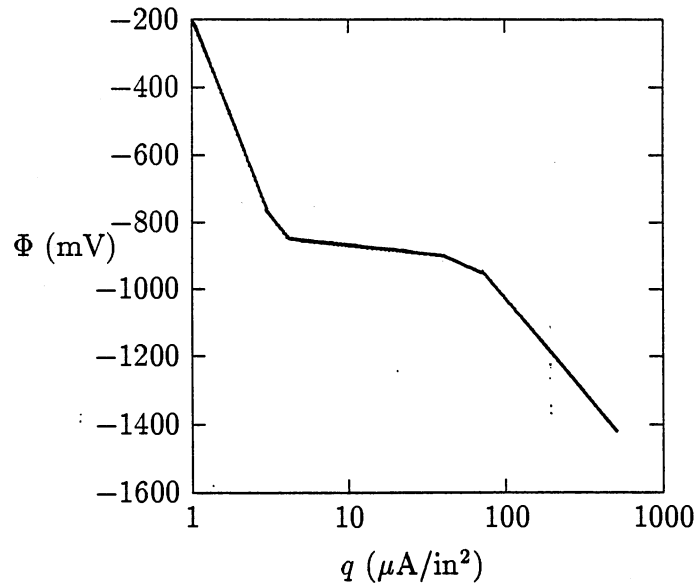
Figure 2. Typical Polarization Behavior of Steel in Concrete

here:

$$[H]\{\Phi\} = [G]\{q\} \tag{16}$$

where the matrices $[H]$ and $[G]$ depend only on the geometry of the electrolyte

boundary, and the column vectors $\{\Phi\}$ and $\{q\}$ represent the electropotential and the

current density, respectively, at the boundary nodes. With the boundary conditions

defined in Equation 25, Equation 16 may be rearranged into a standard system of

nonlinear equations of the form:

$$[A]\{x'\} = \{y'\} \tag{26}$$

in which the vectors $\{x'\}$ and $\{y'\}$ are related through the polarization curve in

Equation 25. This system of nonlinear equations may be solved by using the Newton-Raphson iteration technique briefly described below.

Using the same notation used in the work by Press, et al. [37], the solution to a set of N functions F_i, in the same number of variables x_i

$$F_i(x_1, x_2, \ldots, x_N) = 0 \quad i = 1, 2, \ldots, N \qquad (27)$$

to be zeroed, may be found by solving the system of equations

$$[\alpha]\{\delta x\} = \{\beta\} \qquad (28)$$

where

$$\alpha_{ij} \equiv \frac{\partial F_i}{\partial x_j} \quad \text{and} \quad \beta_i \equiv -F_i \qquad (29)$$

for the corrections δx_j. These corrections are then added to the solution vector $\{x\}$:

$$x_i{}^{new} = x_i{}^{old} + \delta x_i \quad i = 1, \ldots, N \qquad (30)$$

and the process is repeated until convergence is reached.

In applying the Newton-Raphson method, it should be noticed that not all of the equations in the system in Equation 26 contain nonlinear functions, since not all of the boundaries of the electrolyte will be electrodes. There may be some boundaries in the corrosion cell which have specified electropotential values (such as anodes

with impressed currents) and some boundaries with specified current density (such as insulated surfaces, which would have a zero flux boundary condition). To take advantage of this fact, the following scheme may be used to implement the Newton-Raphson iterative solution to the resulting system of nonlinear equations.

Using the known polarization behavior, the electropotential Φ may be expressed as a function g_e of the current density q:

$$\Phi_e = g_e(q_e) \tag{31}$$

We may rewrite Equation 16 as

$$[H']\{u\} = [G']\{v\} \tag{32}$$

where the $\{u\}$ vector contains the unknown q_e's at the electrode surfaces and the unknown data at the nonelectrode boundaries, the $\{v\}$ vector contains known quantities on the nonelectrode boundary and the values of $\Phi_e = g_e(q_e)$ at the electrodes, and the matrices $[H']$ and $[G']$ are the properly adjusted matrices $[H]$ and $[G]$ from Equation 16. The right hand side of Equation 32 may be rewritten as the sum of two matrix multiplications:

$$[G']\{v\} = [G']\{v'\} + [K]\{\Phi_e\} \tag{33}$$

The vector $\{v'\}$ contains the actual known quantities on the boundaries and zeros in place of the calculated values Φ_e. The matrix $[K]$ contains only those terms from

$[G']$ which would be multiplied by the values of Φ_e in vector $\{v\}$. The terms in $[K]$ are actually the negatives of the corresponding columns from the matrix $[H]$ in Equation 16, thus, $[K]$ is not a square matrix. The number of rows in $[H]$ is equal to the number of equations in the system, and the number of columns is equal to the number of electrolytes with specified polarization functions. The vector $\{\Phi_e\}$ contains only the values $\Phi_e = g_e(q_e)$, and its length is equal to the number of electrolytes with specified polarization functions.

If we multiply the matrix $[G']$ by the vector $\{v'\}$, we obtain the vector $\{y\}$ in Equation 17 from the previous section, where any value which corresponds to a node at an electrode has been zeroed. Notice that the matrix $[H']$ is equal to the matrix $[A]$, also from Equation 17. This is an important consideration, since the matrix $[A]$ and the vector $\{y\}$ in Equation 17 are used in the solution of Laplace's equation without nonlinear boundary conditions. Thus, the only new complexity that we have added to the normal solution of Laplace's equation is the formation of the $[K]$ matrix and the vector $\{\Phi_e\}$.

After the $[K]$ matrix is formed, the $[\alpha]$ matrix from Equation 28 is then obtained from

$$\alpha_{ij} = H'_{ij} - K_j \frac{\partial g_e}{\partial q_j} \tag{34}$$

since the polarization function g at a node is only a function of the value of q at that

node. The vector $\{\beta\}$ in Equation 28 is obtained from

$$\beta_i = -[H']\{u\} + \{y\} + [K]\{\Phi_e\} \tag{35}$$

Solving for $\{\delta x\}$ and using

$$\{u_{new}\} = \{u_{old}\} + \lambda\{\delta x\} \tag{36}$$

we can start an iteration process which is ended when the norms of the vectors $\{F\}$ and $\{\delta x\}$ are less than a tolerance given by the user. In this work, the norm $||v||$ of any vector $\{v\}$ is defined as the eucledian L_2 norm, given by

$$||v|| = \sqrt{\sum_{i=1}^{N} v_i^2} \tag{37}$$

where N is the size of the vector $\{v\}$. The initial value for $\{u_{old}\}$ is obtained by assuming a value of $q = 0$ in Equation 32 and solving for the vector $\{u\}$. The factor λ is used as a correction on the vector $\{\delta x\}$ to prevent the "step" size of the iteration process from becoming too large. λ is calculated by computing the norm $||F_{old}||$ of the vector $\{F\}$ (in Equation 27) using $\{u_{old}\}$ and halving the initial value of $\lambda = 1$ until the norm $||F_{new}||$, computed using $\{u_{new}\}$, is smaller than $||F_{old}||$.

This self-correcting Newton-Raphson technique prevents the solution from diverging when the computed $\{\delta x\}$ becomes too large, which occurs when the gradients in

the nonlinear system of equations are large. This is often the case when singularities are present in the problem to be solved.

Nonhomogeneous Electrolytes

As seen in the previous section, the fundamental solution for the particular differential equation to be solved is essential for the success of the boundary element method. Laplace's equation governs the electropotential distribution within a homogeneous electrolyte in a galvanic cell. The governing equation for distribution of the electropotential within a nonhomogeneous electrolyte is Darcy's equation:

$$\vec{\nabla} \cdot (k \vec{\nabla} \Phi) = 0 \tag{38}$$

where k is the conductivity of the electrolyte, which may or may not be constant throughout the region. Generally, the Green's function corresponding to Equation 38 does not exist if k is completely arbitrary. For some specific cases, however, where the behavior of the conductivity k is known, the governing Green's functions are obtainable.

For example, consider the case of an orthotropic two-dimensional domain, where the conductivity does not vary with position, but is different in each of the cartesian directions x and y. The governing equation, Darcy's equation with the specified

conductivity k, is given by:

$$\nabla_k{}^2 \Phi = \frac{\partial}{\partial x}(k_x \frac{\partial \Phi}{\partial x}) + \frac{\partial}{\partial y}(k_y \frac{\partial \Phi}{\partial y}) = 0 \tag{39}$$

where k_x and k_y are the constant conductivities in the x and y directions, respectively. The Green's function W governing this equation may be obtained, as seen previously, from the solution of

$$\nabla_k{}^2 W = \delta(\vec{r} - \vec{r}_\ell) \tag{40}$$

where $\vec{r}$ and $\vec{r}_\ell$ are position vectors in the x-y plane. By making a coordinate transformation of the form

$$X = \frac{x}{\sqrt{k_x}} \quad \text{and} \quad Y = \frac{y}{\sqrt{k_y}} \tag{41}$$

and substituting into Equation 40, we obtain the following equation:

$$\nabla^2 W = \frac{1}{\sqrt{k_x k_y}} \delta(\vec{R} - \vec{R}_\ell) \tag{42}$$

with

$$\vec{R} = \frac{x}{\sqrt{k_x}}\hat{\imath} + \frac{y}{\sqrt{k_y}}\hat{\jmath} \quad \text{and} \quad \vec{R}_\ell = \frac{x_\ell}{\sqrt{k_x}}\hat{\imath} + \frac{y_\ell}{\sqrt{k_y}}\hat{\jmath} \tag{43}$$

where $\hat{\imath}$ and $\hat{\jmath}$ are unit vectors in the x and y directions, respectively [36]. The only difference between Equation 42 and Equation 12 (from which we obtained the Green's function for Laplace's equation) is the multiplicative factor $\frac{1}{\sqrt{k_x k_y}}$. Therefore, the solution to Equation 42 is given by the Green's function for Laplace's equation

in two dimensions multiplied by $\frac{1}{\sqrt{k_x k_y}}$:

$$W = \frac{1}{2\pi\sqrt{k_x k_y}} \ln|\vec{R} - \vec{R}_\ell| \qquad (44)$$

Thus, the Green's function is obtained for the specific case where the constant conductivity k is different in each of the cartesian directions. Substituting this function for W into Equation 15, the solution to Darcy's equation in orthotropic media may be obtained by using the boundary element method.

Orthotropic electrolytes, governed by the particular case of Darcy's equation just discussed, are observed mostly in underground situations. Drilling wells, underground pipes, and underground tanks are all affected by corrosion. The ground, acting as the electrolyte in the corrosion process, behaves like an orthotropic material: the conductivity may be different in the horizontal and vertical directions. More importantly, the different layers within the soil may each have different properties. This leads to the consideration of corrosion processes occurring across different electrolytes.

If the corrosion process occurs across electrolytes with different properties, each electrolyte must be treated as a separate subregion, each having its own distinct boundary element mesh, as shown in Figure 3. At the interfaces of the different electrolytes, the subregions share nodes and elements where both the electropotential and the current flux values are unknown. The boundary element equations are assembled separately for each region in the same manner as that described previously. However, the resulting equations cannot be solved until the physical conditions of compatibility
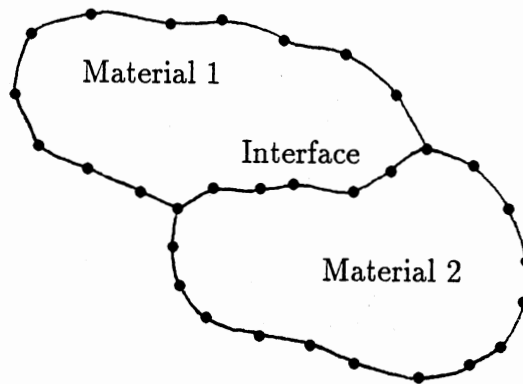
Figure 3. Nomenclature for BEM Problem Consisting of Two
Different Regions

and equilibrium are enforced at the interfaces. Mathematically, this involves invoking

the constraint across an interface I, connecting regions labeled 1 and 2, as follows:

$$\Phi_{I_1} = \Phi_{I_2} \quad \text{and} \quad q_{I_1} = q_{I_2} \tag{45}$$

where Φ_{I_i} and q_{I_i} represent the values of the electropotential Φ and the current flux

q at the interface I as computed from the ith electrolyte region. The resulting set

of equations may then be solved for the solutions at each boundary including the

interface. Again, for a more detailed explanation of the treatment of zoned media,

the reader is referred to Gipson [36].

What may be even more common with nonhomogeneous electrolytes are cases in

which the conductivity k actually varies with some known behavior throughout the

electrolyte. For instance, within reinforced concrete bridge decks, the conductivity will vary according to the saline concentration within the concrete matrix. Since the concrete deck is affected by deicing salts, the concentration of salt will be higher at the top of the deck, where infiltration starts, than it will be toward the bottom. This leads to a variation in the electrical conductivity along the vertical distance of the deck. Another example of an electrolyte with varying conductivity is seawater. The electrochemical conductivity of water changes with temperature; thus, in deep water situations, the conductivity at the bottom of the structure may be very different from the conductivity at the seawater surface level [2]. Such variations in conductivity cannot be handled as easily as the cases where the conductivity is constant throughout the electrolyte. However, as previously mentioned, it has been shown that for the special case where the square root of the conductivity satisfies Laplace's equation, a Green's function W_{sp} for the specialized Darcy's equation may be obtained [35].

This particular Green's function is obtained using the following identity:

$$\nabla^2(g^{\frac{1}{2}} f) = g^{-\frac{1}{2}}[\vec{\nabla} \cdot (g\vec{\nabla}f)] + f(\nabla^2 g^{\frac{1}{2}}) \tag{46}$$

where g and f are functions. Equation 38 (Darcy's equation), repeated here for convenience

$$\vec{\nabla} \cdot (k\vec{\nabla}\Phi) = 0 \tag{38}$$

may be rewritten, using the identity in Equation 46, as

$$\vec{\nabla} \cdot (k\vec{\nabla}\Phi) = k^{\frac{1}{2}}[\nabla^2(k^{\frac{1}{2}}\Phi) - \Phi(\nabla^2 k^{\frac{1}{2}})] = 0 \tag{47}$$

If the square root of the conductivity k satisfies Laplace's equation, in other words, if we place the restriction on the conductivity k

$$\nabla^2 k^{\frac{1}{2}} = 0 \tag{48}$$

then Equation 47 becomes

$$\vec{\nabla} \cdot (k\vec{\nabla}\Phi) = k^{\frac{1}{2}} \nabla^2(k^{\frac{1}{2}}\Phi) = 0 \tag{49}$$

Thus, Darcy's equation is reduced to

$$k^{\frac{1}{2}} \nabla^2(k^{\frac{1}{2}}\Phi) = 0 \tag{50}$$

which involves the Laplacian operator for which we have already defined a Green's function. By making the substitution

$$\Psi = k^{\frac{1}{2}}(\vec{r}) \, \Phi \tag{51}$$

we are left with simply finding a Green's function W' for the Laplacian equation

$$k^{\frac{1}{2}}(\vec{r})\ \nabla^2(\Psi) = 0 \tag{52}$$

which is done using the same technique used previously. We simply find a solution to the equation

$$\nabla^2(W') = k^{-\frac{1}{2}}(\vec{r}_\ell)\ \delta(\vec{r} - \vec{r}_\ell) \tag{53}$$

which differs from Equation 12 only by the multiplicative factor $k^{-\frac{1}{2}}(\vec{r}_\ell)$. Therefore, the solution to Equation 53 is given by the Green's function for Laplace's equation W multiplied by $k^{-\frac{1}{2}}(\vec{r}_\ell)$

$$W' = k^{-\frac{1}{2}}(\vec{r}_\ell)\ W \tag{54}$$

and since $\Phi = k^{-\frac{1}{2}}(\vec{r})\Psi$, we conclude that the Green's function W_{sp} for the specialized Darcy's equation with the restriction on k in Equation 48, is

$$W_{\mathrm{sp}} = k^{-\frac{1}{2}}(\vec{r})\ k^{-\frac{1}{2}}(\vec{r}_\ell)\ W \tag{55}$$

thus enabling one to use the boundary element method to approximate a solution to Darcy's equation for the special case where the conductivity k satisfies the restriction imposed by Equation 48.

As mentioned in the previous chapter, there exist simple functions satisfying the restriction placed on the conductivity by Equation 48 which may be used to model

field resistivity data. Among these is the square of the general trilinear polynomial:

$$(a + bx + cy + dz + exy + fxz + gyz + hxyz)^2 \tag{56}$$

where a through g are constants. The resulting polynomial may be easily used to model measured resistivity data. Figure 4 shows some examples of possible representations for k using this function. The conductivity k in Figure 4 varies only with the depth y, typical of underground, underwater, and concrete situations [2,3,38]. In Figure 4, k has been nondimensionalized with respect to a reference conductivity k_o, and the y depth has been nondimensionalized with respect to a reference depth d. The examples clearly illustrate that conductivity functions satisfying Equation 48 may be used to represent field data of more commonly known functions. Using the new Green's function W_{sp}, the boundary element method may therefore be efficiently applied to solve galvanic corrosion problems in which the electrolyte is not homogeneous.

Element Types

In BEM, the boundary is discretized into a series of distinct elements and a certain number of nodes associated with each element. We represent the elements using
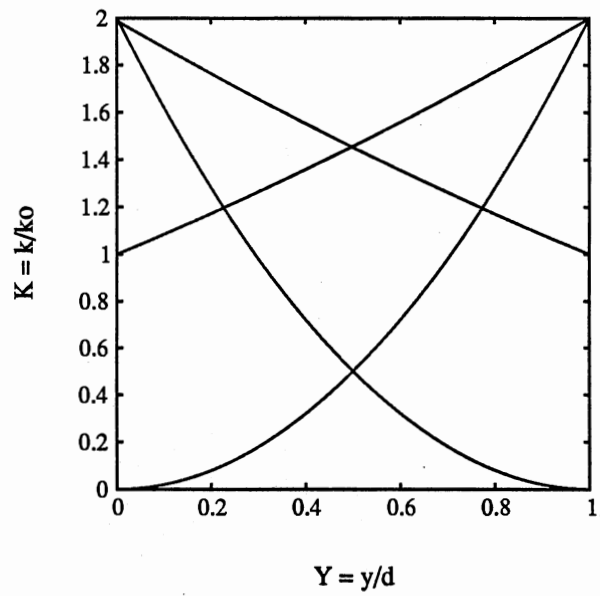
Figure 4. Several Examples of Nondimensionalized Conductivity K as a Function of the Nondimensionalized Depth Y

parametric curves or surfaces which are defined by the nodes on the element by:

$$\Phi = <\Phi^n> \{N\} \quad \text{and} \quad q = <q^n> \{N\} \tag{57}$$

where the shape function set $\{N\}$ is composed of parametric functions which vary along the element curve or surface according to their prescribed order. $<\Phi^n>$ and $<q^n>$ are vectors containing the values of Φ and q at the nodes of the element. The shape function set $\{N\}$ is also used to define the geometry of the element. The generalized coordinate x_i is represented by

$$x_i = <x_i{}^n> \{N\} \tag{58}$$

where $<x_i{}^n>$ is a vector containing the values of the coordinate x_i at each node of the element. The resulting parametric curves or surfaces are such that they give the nodal values of the variable under consideration when they are evaluated at the nodes, and vary between the nodes according to the order of the shape functions.

The parametric curves used to define the elements used in two-dimensional analysis are constructed by fitting a simple polynomial through the nodes associated with the element. The order of the polynomial used to define the element is determined by the number of nodes associated with the element [39] — it is equal to the number of nodes defining that element minus one.

The parametric surfaces used to define the elements used in three-dimensional

analysis are constructed by fitting a polynomial surface through the nodes associated with the element. The elements used in this work are defined by nodes which lie strictly on the edges of the element. In FEM analysis, this family of elements is referred to as the serendipity family [40]. The advantage of using this type of element lies in its lack of nodes internal to the element and not shared by any other element. Elements which contain nodes internal to an element lead to an undesirable increase in the total number of nodes used in a model, as compared to a similar model using the serendipity family of elements.

The following sections describe the different element types used in the BEM system developed for this work. The techniques for performing the integrations over the elements are also described.

Two-Dimensional Elements

In any BEM modeling, the selection of the element type affects modeling and computation time, as well as the accuracy of the analysis. In the current system, four elements have been implemented: linear, quadratic, standard cubic, and the Overhauser cubic element. It has been shown previously that while adequate results can be obtained using simple linear elements, the use of higher ordered elements leads to more accurate results [41,42]. The Overhauser elements [42,41] have the added advantage of maintaining C^1 continuity at the interelement connections, leading to a more accurate representation of curved boundaries than can be achieved with linear and standard higher order elements, and thus more accurate results.
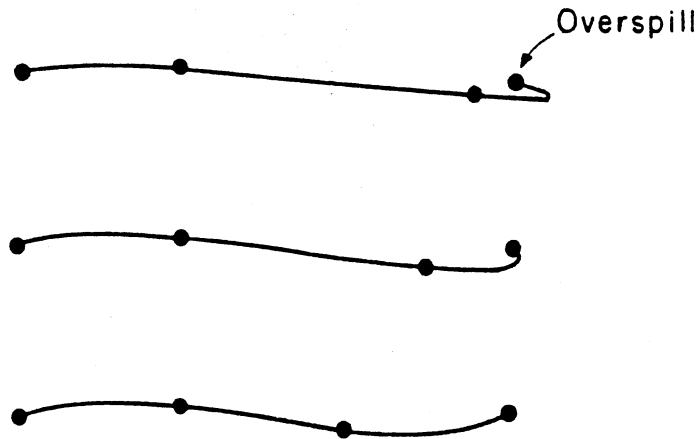
Figure 5. Nonunique Mapping of Geometry Due to Irregular
Spacing of Nodes Within Element: "Overspill"

A problem encountered with the higher ordered elements is a nonunique mapping

of the function under consideration, also called "overspill" [40]. As shown in Figure 5,

higher ordered curves may produce overspills when the geometry of the nodal spacing

of the nodes within an element is not regular. These distortions may also appear near

singularities and locations where high gradients in the field variable are present. Care

must be taken when using these elements so as to not cause unwanted distortions.

Nodes should be equally spaced within an element, and in some cases, it may be

preferable to use linear elements near singularities.

The simplest element is the standard linear element, defined by two nodes. The

two corresponding shape functions are

$$N_1 = 1 - t$$

$$N_2 = t \tag{59}$$

where t is the parameter defined in element coordinates, normalized to be zero at the first node of the element and 1 at the second node.

The next element, in order of complexity, is the standard quadratic element, defined by three nodes. Its three corresponding shape functions are

$$N_1 = 2t^2 - 3t + 1$$

$$N_2 = -4t^2 + 4t$$

$$N_3 = 2t^2 - t \tag{60}$$

where the first node of the element lies at $t = 0$, the second node lies at $t = \frac{1}{2}$ and the third at $t = 1$.

There exist two types of cubic elements, both defined by four nodes. One is a standard cubic element, with shape functions given as

$$N_1 = -\frac{9}{2}t^3 + 9t^2 - \frac{11}{2}t + 1$$

$$N_2 = \frac{27}{2}t^3 - \frac{45}{2}t^2 + 9t$$

$$N_3 = -\frac{27}{2}t^3 + 18t^2 - \frac{9}{2}t$$

$$N_4 = \frac{9}{2}t^3 - \frac{9}{2}t^2 + t \tag{61}$$

where the four nodes lie at $t = 0$, $t = \frac{1}{3}$, $t = \frac{2}{3}$, and $t = 1$, in order. The other cubic element is the Overhauser element, developed by Ortiz et al. in previously published work [41,42]. The corresponding shape functions for the Overhauser element are

$$
\begin{aligned}
N_1 &= -\frac{1}{2}t^3 + t^2 - \frac{1}{2}t \\
N_2 &= \frac{3}{2}t^3 - \frac{5}{2}t^2 + 1 \\
N_3 &= -\frac{3}{2}t^3 + 2t^2 - \frac{1}{2}t \\
N_4 &= \frac{1}{2}t^3 - \frac{1}{2}t^2
\end{aligned}
\tag{62}
$$

where the second node lies at $t = 0$, the third node lies at $t = 1$, and the first and fourth nodes lie outside of the element (Figure 6). The first and fourth node are used to define the parametric derivatives existing at the two end nodes (the second and third nodes). By overlapping the Overhauser elements, where the second, third and fourth nodes of one element are the first, second and third nodes of the next element, we insure that the parametric derivative is continuous at the nodes where the elements are joined together. For a more detailed explanation of the use of Overhauser elements in BEM analysis, see Ortiz et al. [41,42], and Walters et al. [43,44].

As may be seen from the previous sections, integrations are major tasks in boundary element analyses. Performing these integrations accurately and quickly is essential
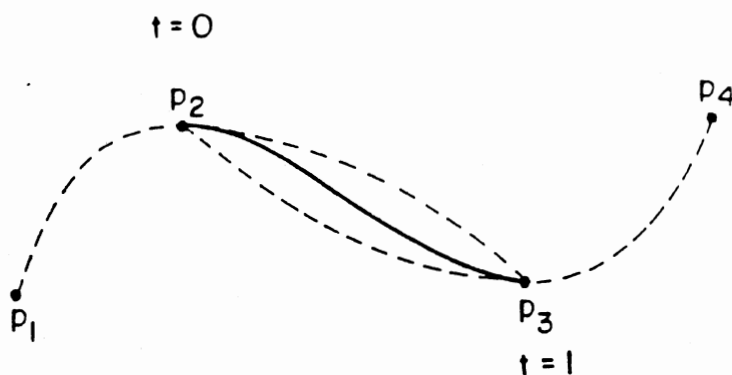
Figure 6. Definition of Overhauser Element in Parametric t
Space

to the success of any boundary element system. The numerical integrations in the
current BEM system are performed using Gaussian integration formulas developed
by Stroud and Secrest [45]. Gaussian integration is relatively fast and, for most of the
integrals occurring in BEM, is the only practical way of performing the integrations.

Planar Analysis. The solution of Laplace's equation will be used here to il-
lustrate the integration scheme used in the current BEM system. The solution to
Darcy's equation, whether it involves orthotropic regions, or regions with variable
conductivity, is approached in the same manner.

Substituting the fundamental solution of the two-dimensional Laplace's equation

$$W = \frac{1}{2\pi} \ln |\vec{r} - \vec{r}_\ell| \qquad (63)$$

and its normal derivative

$$\frac{\partial W}{\partial n} = -\frac{1}{2\pi}\frac{(\vec{r} - \vec{r}_\ell)\cdot\hat{n}}{|\vec{r} - \vec{r}_\ell|^2} \tag{64}$$

into Equation 15, repeated here for convenience

$$C\hat{\Phi}(\vec{r}_\ell) = <\Phi^{\mathrm{n}}> \int_\Gamma \frac{\partial W}{\partial n}\{N\}\,d\Gamma - <q^{\mathrm{n}}> \int_\Gamma W\{N\}\,d\Gamma \tag{15}$$

we obtain the following

$$C\hat{\Phi}(\vec{r}_\ell) = -<\Phi^{\mathrm{n}}> \frac{1}{2\pi}\int_\Gamma \frac{(\vec{r} - \vec{r}_\ell)\cdot\hat{n}}{|\vec{r} - \vec{r}_\ell|^2}\{N\}\,d\Gamma - <q^{\mathrm{n}}> \frac{1}{2\pi}\int_\Gamma \ln|\vec{r} - \vec{r}_\ell|\{N\}\,d\Gamma \tag{65}$$

Evaluations of the integrals are done in a localized coordinate system. Utilizing the Jacobian transformation

$$d\Gamma = |J(t)|\,dt = \sqrt{\left(\frac{dx}{dt}\right)^2 + \left(\frac{dy}{dt}\right)^2}\,dt \tag{66}$$

where x and y are defined by Equation 58, the integrals in Equation 65 become:

$$-\frac{1}{2\pi}\int_0^1 \frac{(\vec{r} - \vec{r}_\ell)\cdot\hat{n}}{|\vec{r} - \vec{r}_\ell|^2}\{N\}\,|J(t)|\,dt \tag{67}$$

and

$$\frac{1}{2\pi}\int_0^1 \ln|\vec{r} - \vec{r}_\ell|\{N\}\,|J(t)|\,dt. \tag{68}$$

All integrals are evaluated using standard Gaussian quadrature formulas [45] except for the case where the source node is actually on the element being integrated. If the source node is on the element being integrated, one must deal with a singularity in the Green's function, since $\vec{r} = \vec{r}_\ell$ at $t = 0$. The normal derivative of the Green's function is also singular in this case, but the singularity is canceled because the shape functions which do not correspond to the node in question are exactly zero at the point of singularity (at $t = 0$). The shape function corresponding to node 1 is exactly one at the point of singularity, thus not canceling it; but this integral does not need to be calculated — it is determined using physical considerations [36].

The singular integrals which need to be performed, those containing the Green's function, are evaluated using the formula developed for singular logarithmic integrals by Stroud and Secrest [45]

$$\int_0^1 g(x) \ln(x) \, dx \simeq \sum_{i=1}^n \omega_i g(x_i) \tag{69}$$

where $g(x)$ is a function of x, ω_i are the n Gaussian weights, and x_i are the corresponding Gaussian points. Simply using the Pythagorean theorem to find the magnitude of the vector inside the logarithm, the integral involving the Green's function in Equation 68 becomes

$$\frac{1}{4\pi} \int_0^1 \{N\} \, \ln[\,(x - x_\ell)^2 + (y - y_\ell)^2\,]\,|J(t)|\, dt \tag{70}$$

Expanding the terms inside the logarithm (which are defined by the shape functions) to a polynomial p, we obtain

$$\frac{1}{4\pi} \int_0^1 \{N\} \ln[\, p(t)\,]\, |J(t)|\, dt \tag{71}$$

where

$$p(t) = c_0 t^6 + c_1 t^5 + c_2 t^4 + c_3 t^3 + c_4 t^2 \tag{72}$$

and the constants c_0-c_4 are defined by the coordinates of the nodes on the element and the source node. By factoring a t^2 from the polynomial p inside the logarithm, the integral can now be written as two separate integrals:

$$\frac{1}{4\pi} \int_0^1 \{N\} \ln(\mathcal{I})\, |J(t)|\, dt + \frac{1}{2\pi} \int_0^1 \{N\} \ln(t)\, |J(t)|\, dt \tag{73}$$

where

$$\mathcal{I} = c_0 t^4 + c_1 t^3 + c_2 t^2 + c_3 t^1 + c_4 \tag{74}$$

The first of these integrals is evaluated using standard Gaussian integration, and the second is evaluated using the previously discussed formula developed for singular logarithmic integrals [45].

The integrations involving the Green's functions developed for Darcy's equation are treated similarly. The idea is to isolate the singularity involved with the logarithmic term and use the special Gaussian logarithmic quadrature, in combination with
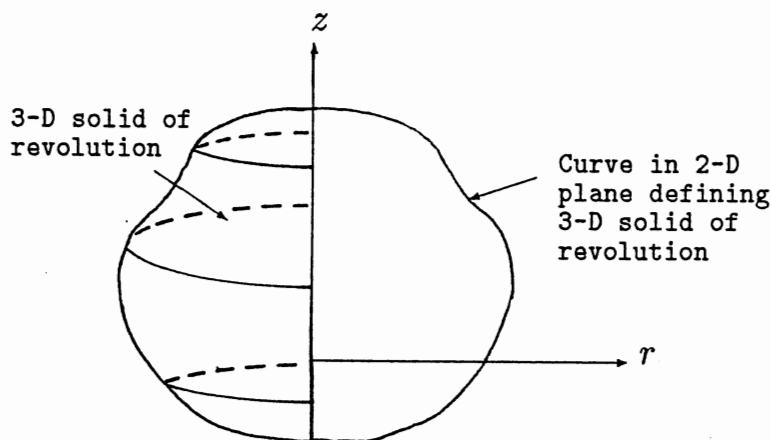
Figure 7. Axisymmetric Domain For Boundary Element Analysis in the r-z Coordinate System

standard Gaussian quadrature, to evaluate the resulting integrals.

Axisymmetric Analysis. Domains defined by solids of revolution and having a field variable (in our case, the electropotential Φ) which lacks angular dependency may be modeled as curves in the two-dimensional r-z plane (Figure 7). Thus, the same elements which are used for the two-dimensional planar analysis may be used for axisymmetric analysis.

The fundamental solution for Laplace's equation expressed in polar coordinates is not angularly independent. Therefore, in order to model axisymmetric domains using BEM, the Green's function for the general three-dimensional problem must be specialized to take advantage of the axial symmetry. The following description of how to obtain the Green's function for axisymmetric analysis of Darcy's equation, where the square root of the spatially varying conductivity k satisfies Laplace's equation, is based on Gipson's text [36], where a detailed explanation is provided.

The Green's function associated with Darcy's equation, as previously defined,

$$W = \frac{-1}{4\pi \sqrt{k(\vec{r})} \sqrt{k(\vec{r}_\ell)} |\vec{r} - \vec{r}_\ell|} \tag{75}$$

may be expressed in r, θ, z polar coordinates as

$$W = \frac{-1}{4\pi \sqrt{k(r,z)} \sqrt{k(r_\ell, z_\ell)} \sqrt{r^2 + r_\ell^2 - 2rr_\ell \cos(\theta - \theta_\ell) + (z - z_\ell)^2}} \tag{76}$$

Equation 15, once again repeated here for convenience,

$$C\hat{\Phi}(\vec{r}_\ell) = <\Phi^n> \int_\Gamma \frac{\partial W}{\partial n}\{N\}\, d\Gamma - <q^n> \int_\Gamma W\{N\}\, d\Gamma \tag{15}$$

may be expressed, for axisymmetric analysis, as

$$C\hat{\Phi}(r,z) = <\Phi^n> \int_{\Gamma'_e} \frac{\partial W}{\partial n}\{N\}\, r\, d\Gamma_e - <q^n> \int_{\Gamma'_e} W\{N\}\, r\, d\Gamma_e \tag{77}$$

where the boundary has been discretized into curved elements on the r-z plane, and the integrations around the surface will be performed across the elemental boundary $d\Gamma_e$ and around the circular-strip surface Γ'_e (Figure 8). The integrals which need to be evaluated are then

$$\int_{\Gamma'_e} \frac{\partial W}{\partial n}\{N\}\, r\, d\Gamma_e \quad \text{and} \quad \int_{\Gamma'_e} W\{N\}\, r\, d\Gamma_e \tag{78}$$
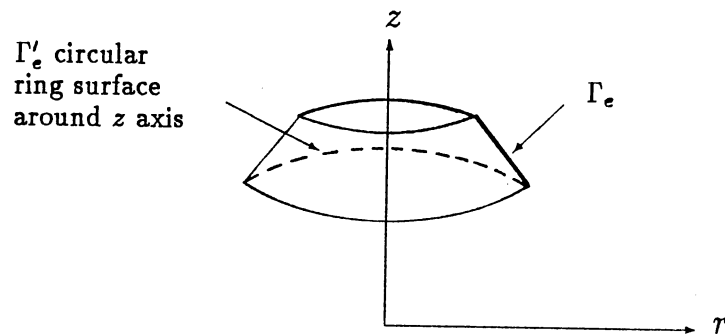
Figure 8. Definition of Axisymmetric "Ring" Boundary Element in the r-z Coordinate System

which, because both the shape functions and the outward pointing normal $\hat{n}$ are independent of the θ coordinate, may be rewritten as

$$\int_{\Gamma_e} \{N\} \frac{\partial}{\partial n} \left[\int_0^{2\pi} W \, d\theta \right] r \, d\Gamma_e \quad \text{and} \quad \int_{\Gamma_e} \{N\} \left[\int_0^{2\pi} W \, d\theta \right] r \, d\Gamma_e \tag{79}$$

The integral over θ

$$\int_0^{2\pi} W \, d\theta = \frac{-1}{4\pi \sqrt{k(r,z)} \sqrt{k(r_\ell, z_\ell)}} \int_0^{2\pi} \frac{1}{\sqrt{r^2 + r_\ell^2 - 2rr_\ell \cos\theta - \theta_\ell + (z - z_\ell)^2}} \, d\theta \tag{80}$$

may be written as

$$\int_0^{2\pi} W \, d\theta = \frac{-K(a)}{\pi \sqrt{k(r,z)} \sqrt{k(r_\ell, z_\ell)} \sqrt{(r + r_\ell)^2 + (z - z_\ell)^2}} \tag{81}$$

where $K(a)$ is an elliptic integral of the first kind, and its argument a is

$$a = \sqrt{\frac{4\,r\,r_\ell}{(r + r_\ell)^2 + (z - z_\ell)^2}} \tag{82}$$

Thus, the integrals which need to be evaluated

$$\int_{\Gamma_e'} W\{N\}\, r\, d\Gamma_e \quad \text{and} \quad \int_{\Gamma_e'} \frac{\partial W}{\partial n}\{N\}\, r\, d\Gamma_e \tag{83}$$

can be rewritten as

$$\int_{\Gamma_e'} \frac{-K(a)}{\pi \sqrt{k(r,z)}\sqrt{k(r_\ell,z_\ell)}\sqrt{(r + r_\ell)^2 + (z - z_\ell)^2}} \{N\}\, r\, d\Gamma_e \tag{84}$$

and

$$\int_{\Gamma_e'} \frac{\partial}{\partial n} \left[\frac{-K(a)}{\pi \sqrt{k(r,z)}\sqrt{k(r_\ell,z_\ell)}\sqrt{(r + r_\ell)^2 + (z - z_\ell)^2}} \right] \{N\}\, r\, d\Gamma_e \tag{85}$$

Therefore, we can take the Green's function for axisymmetric analysis to be

$$W_{\text{ax}} = \frac{-K(a)}{\pi \sqrt{k(r,z)}\sqrt{k(r_\ell,z_\ell)}\sqrt{(r + r_\ell)^2 + (z - z_\ell)^2}} \tag{86}$$

and its normal derivative

$$\frac{\partial W_{\text{ax}}}{\partial n} = \frac{\partial}{\partial n} \left[\frac{-K(a)}{\pi \sqrt{k(r,z)}\sqrt{k(r_\ell,z_\ell)}\sqrt{(r + r_\ell)^2 + (z - z_\ell)^2}} \right] \tag{87}$$

with $\frac{\partial}{\partial n}$ defined as $\hat{n} \cdot \vec{\nabla}_k$. It can be shown that the normal derivative of the specialized

Green's function for axisymmetric analysis is

$$
\begin{aligned}
\frac{\partial W_{\mathrm{ax}}}{\partial n} = & \frac{\sqrt{k(r,z)}}{\pi\sqrt{k(r_\ell,z_\ell)}\,R^3} \\
& \left\{ K(a) \left[\left(\frac{r_\ell^2 - r^2 + (z - z_\ell)^2}{2r} + (r + r_\ell) + \frac{R}{2k(r,z)}\frac{\partial k(r,z)}{\partial r} \right) n_r + \right. \right. \\
& \left. \left. \frac{R}{2k(r,z)}\frac{\partial k(r,z)}{\partial z}\, n_z \right] + \frac{E(a)}{(1 - a^2)} \left[(z - z_\ell)n_z - \frac{r_\ell^2 - r^2 + (z - z_\ell)^2}{2r} n_r \right] \right\}
\end{aligned}
\tag{88}
$$

where n_r and n_z are the components of the outward normal vector $\hat{n}$ in the r and z directions, respectively, $E(a)$ is the elliptic function of the second kind, and

$$
R = (r + r_\ell)^2 + (z - z_\ell)^2
\tag{89}
$$

With the Green's function and its derivative specialized for axisymmetric analysis, the solution to Equation 15 may be obtained by accurately performing the integrations involved. The specialized Green's function W_{ax} and its derivative are well behaved and can be efficiently integrated using standard Gaussian quadrature, except where $\vec{r}$ and $\vec{r}_\ell$ are at the same location.

The elliptic function of the first kind $(K(a))$ is singular when its argument a is equal to 1. The argument a to the elliptic functions is equal to 1 when $\vec{r} = \vec{r}_\ell$. Therefore, integrals involving the elliptic function of the first kind, may not be evaluated using standard Gaussian quadrature when $\vec{r}$ and $\vec{r}_\ell$ are at the same location. It can be shown that these are the only integrals which become singular in axisymmetric analysis.

To evaluate the integrals involving $K(a)$, we will use the following technique. $K(a)$ is expanded as [46]

$$K(a) = A + B \ln \frac{4}{a'} \tag{90}$$

where a' is equal to $\sqrt{1 - a^2}$, and the factors A and B are dependent on a' as follows:

$$A = \sum_{m=0}^{\infty} \begin{pmatrix} -\frac{1}{2} \\ m \end{pmatrix} (-b_m)(a')^{2m} \tag{91}$$

$$B = \sum_{m=0}^{\infty} \begin{pmatrix} -\frac{1}{2} \\ m \end{pmatrix} (a')^{2m} \tag{92}$$

and

$$\begin{pmatrix} x \\ m \end{pmatrix} = (-1)^m \frac{(-x)(-a-1)(-a-2)\ldots(-a-m+1)}{m!} \tag{93}$$

The factors A and B have been approximated by Abramowitz and Stegun [47] as

$$A = a_0 + a_1(1 - a^2) + \cdots + a_4(1 - a^2)^4 \tag{94}$$

$$B = b_0 + b_1(1 - a^2) + \cdots + b_4(1 - a^2)^4 \tag{95}$$

in which a_0-a_4 and b_0-b_4 are [47]:

$$
\begin{aligned}
a_0 &= 1.38629\ 436112 & b_0 &= 0.5 \\
a_1 &= 0.09666\ 344259 & b_1 &= 0.12498\ 593597 \\
a_2 &= 0.03590\ 092383 & b_1 &= 0.06880\ 248576 \\
a_3 &= 0.03742\ 563713 & b_1 &= 0.03328\ 355346 \\
a_4 &= 0.01451\ 196212 & b_1 &= 0.00441\ 787012
\end{aligned}
$$

The integral of any function F multiplied by $K(a)$ (where a is defined in Equation 82) over a the parameter t (along one of the previously defined elements) is given by

$$
\int_0^1 F\,K(a)\,dt = \int_0^1 F\left[A + B\ln\frac{R}{\mathcal{I}}\right] dt - \int_0^1 2FB\,\ln t\,dt \tag{96}
$$

where $\mathcal{I}$ is given by Equation 74 in the previous section, and R is given by Equation 89. Of these two integrals, only the second is singular, but it can be evaluated using the formula developed for singular logarithmic integrals by Stroud and Secrest [45], discussed in the previous section. The first integral may be evaluated using standard Gaussian quadrature — it is not singular.

Using this procedure, the singular integrals which arise in axisymmetric analysis may be effectively evaluated and the analysis of axisymmetric problems can be performed as easily as the planar analysis. As a matter of fact, all of the singular integrals in two-dimensional analysis can be evaluated using the same routines, since they are all very similar: one integral which is singular due to the logarithmic term

and one integral which is not singular. By taking advantage of this fact, only one efficient integration routine is needed for all element types and all two-dimensional Green's functions.

Three-Dimensional Elements

Four different types of surface elements for three-dimensional analyses were developed for the system. Again, the different element types are necessary to create a flexible and efficient BEM analysis system. Linear and quadratic serendipity-type elements of both triangular and rectangular shapes are used in the system developed in this work.

As mentioned in the previous sections, the elements consist of surface patches in space connected by nodes; the number of nodes determines the order of the parametric surface in ζ and η (Figure 9). The parameters ζ and η are normalized such that they both vary from 0 to 1 for rectangular elements. For triangular elements the parameter ζ is normalized to vary from 0 to 1, while η varies from 0 to $1 - \zeta$. Each shape function is associated with a node, such that the shape function value is equal to 1 at its corresponding node and zero at any other node.

The integrations of the fundamental solution and its derivative over the surface patches have been found to be very sensitive to element distortion [48]. Therefore, care must be taken to ensure that the elements do not deviate considerably from their original parametric shape. In other words, elements which are defined as rectangles
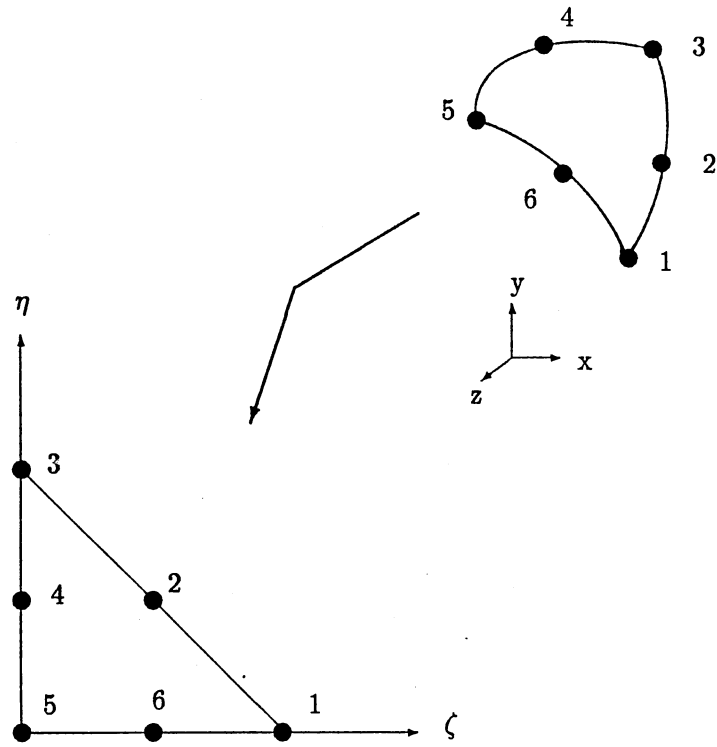
Figure 9. Mapping of Surface Elements From Three-Dimensional X-Y-Z Space to Localized Parametric ζ-η Space

in parameter space, should closely resemble rectangular surface patches in three-dimensional space, and elements which are defined as triangles in parameter space should also resemble triangles in three-dimensional space. Also, nodes located at corners of the element in parameter space should map into nodes at vertices of the element in three-dimensional space, and one can say the same about nodes which lie on the sides of the elements. Therefore, it is important to know the order in which the nodes are on the element in parameter space. The element definitions, including figures depicting the location of the nodes on the element in parameter space, are given in the following discussion.

The simplest element of the system consists of a triangular planar surface defined by three nodes. This element linearly interpolates the value of the unknown function between each node. As previously mentioned, the integrations over the element are performed in a localized coordinate system. Mapping of the element from three-dimensional space to the localized ζ-η system is achieved through the use of the parametric shape functions. These shape functions corresponding to the planar element are:

$$
\begin{aligned}
N_1 &= \zeta \\
N_2 &= \eta \\
N_3 &= 1 - \zeta - \eta
\end{aligned}
\tag{97}
$$

where the first node lies at $(\zeta = 1, \eta = 0)$, the second node at $(\zeta = 0, \eta = 1)$, and and the third node at $(\zeta = 0, \eta = 0)$, as shown in Figure 10.

The four-noded rectangular element, or bilinear element, interpolates the value of the unknown function with a bilinear surface between the nodes of the element. The mapping from three dimensional space to the localized coordinate system used to perform the integrations is achieved with the following parametric shape functions:

$$
\begin{aligned}
N_1 &= 1 - \zeta - \eta + \zeta\eta \\
N_2 &= \zeta - \zeta\eta \\
N_3 &= \zeta\eta \\
N_4 &= \eta - \zeta\eta
\end{aligned}
\tag{98}
$$

where the nodes are placed on the element in the order shown in Figure 11.

The six-noded triangular element interpolates the value of the unknown function and surface geometry with a quadratic surface connecting the nodes on the element. Mapping of the element from three dimensional space to the localized ζ-η coordinate system used for integration is done through the following parametric shape functions:

$$
\begin{aligned}
N_1 &= 2\zeta^2 - \zeta \\
N_2 &= 4\zeta\eta \\
N_3 &= 2\eta^2 - \eta
\end{aligned}
$$
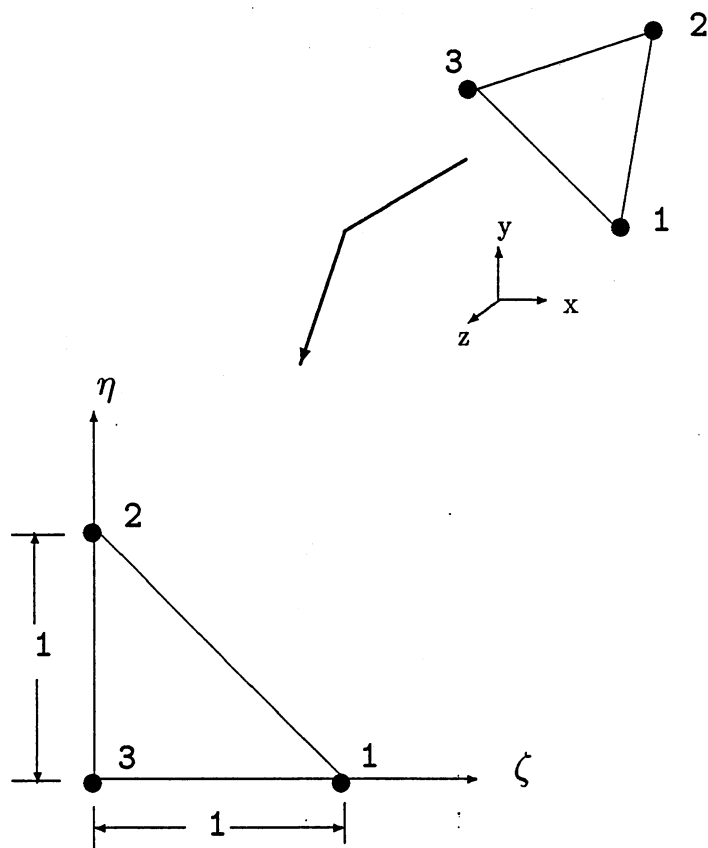
Figure 10. Mapping of Linear Element From Three Dimensional Space to Localized ζ-η Coordinate System
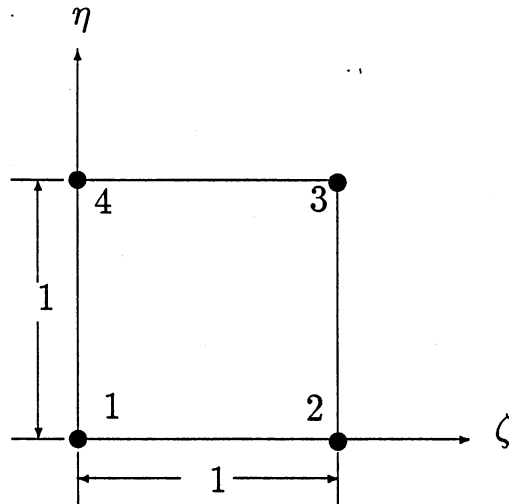
Figure 11. Bilinear Element in Localized ζ-η Coordinate System

$$N_4 = -4\eta^2 - 4\zeta\eta + 4\eta$$

$$N_5 = 1 - 3\zeta - 3\eta + 4\zeta\eta + 2\zeta^2 + 2\eta^2$$

$$N_6 = 4\zeta - 4\zeta\eta - 4\zeta^2 \tag{99}$$

where the order of the nodes on the element is shown in Figure 12. As Figure 12 indicates, the first, third, and fifth nodes of a triangular element must always be at the corners of the triangle; and the second, fourth, and sixth nodes should be at approximately the midpoint of the sides of the triangle.

The eight-noded rectangular element interpolates the value of the unknown function with a semi-cubic surface between each node on the element. Figure 13 shows

the order of the nodes for the eight-noded rectangular element. The shape functions for the eight-noded element are:

$$N_1 = -2\eta^2\zeta - 2\eta\zeta^2 + 2\eta^2 + 2\zeta^2 + 5\eta\zeta - 3\eta - 3\zeta + 1$$

$$N_2 = 4\eta^2 - 4\eta^2 - 4\eta\zeta + 4\eta$$

$$N_3 = -2\eta^2\zeta + 2\eta\zeta^2 + 2\eta^2 - \eta\zeta - \eta$$

$$N_4 = -4\eta\zeta^2 + 4\eta\zeta$$

$$N_5 = -2\eta^2\zeta + 2\eta\zeta^2 - 3\eta\zeta$$

$$N_6 = -4\eta^2\zeta + 4\eta\zeta$$

$$N_7 = 2\eta^2\zeta - 2\eta\zeta^2 + 2\zeta^2 - \eta\zeta - \zeta$$

$$N_8 = 4\eta\zeta^2 - 4\zeta^2 - 4\eta\zeta + 4\zeta \tag{100}$$

As with the two-dimensional analysis, performing the integrations over each element accurately and efficiently is imperative for the success of the BEM system. Gaussian quadrature is the most effective way to perform most of the integrations involved.

Equation 15 is repeated here for convenience:

$$C\hat{\Phi}(\vec{r}_\ell) = <\Phi^n> \int_\Gamma \frac{\partial W}{\partial n}\{N\}\, d\Gamma - <q^n> \int_\Gamma W\{N\}\, d\Gamma \tag{15}$$
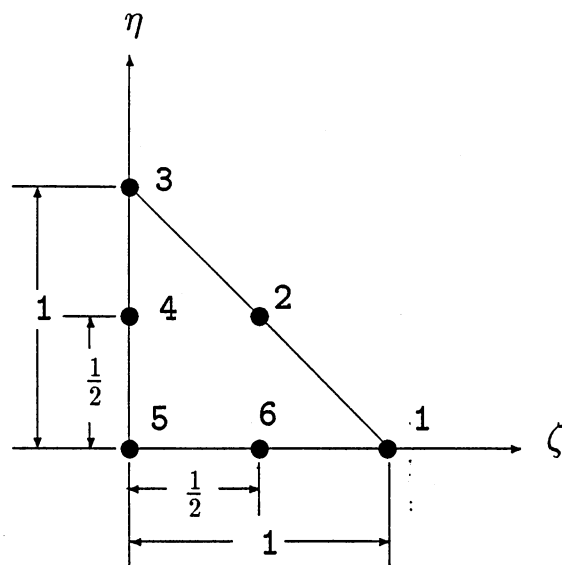
Figure 12. Six-Noded Triangular Element in Localized ζ-η Coordinate System
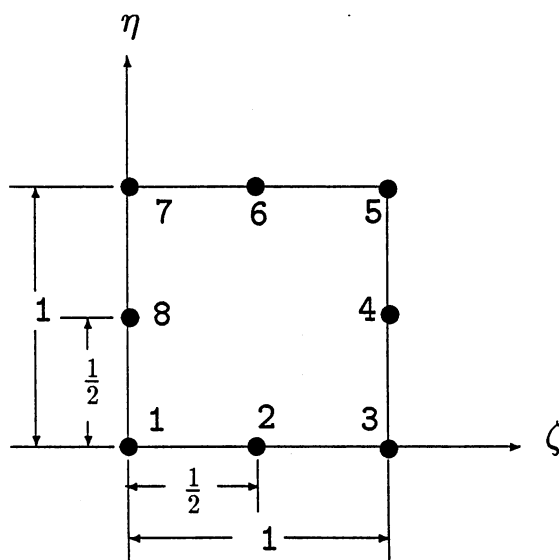
Figure 13. Eight-Noded Rectangular Element in Localized ζ-η Coordinate System

By substituting the fundamental solution of the three dimensional Laplace's equation

$$W = \frac{1}{4\pi} \frac{1}{|\vec{r} - \vec{r}_\ell|} \tag{101}$$

and its normal derivative

$$\frac{\partial W}{\partial n} = -\frac{1}{4\pi} \frac{(\vec{r} - \vec{r}_\ell) \cdot \hat{n}}{|\vec{r} - \vec{r}_\ell|^3} \tag{102}$$

into Equation 15, we obtain

$$C\hat{\Phi}(\vec{r}_\ell) = - < \Phi^n > \frac{1}{4\pi} \int_\Gamma \frac{(\vec{r} - \vec{r}_\ell) \cdot \hat{n}}{|\vec{r} - \vec{r}_\ell|^3} \{N\} \, d\Gamma - < q^n > \frac{1}{4\pi} \int_\Gamma \frac{1}{|\vec{r} - \vec{r}_\ell|} \{N\} \, d\Gamma \tag{103}$$

The integrations of Equation 103, which must be performed over the surface elements in space, are evaluated in the localized coordinate system, using the following Jacobian transformation:

$$d\Gamma = |J(\zeta, \eta)| \, d\zeta \, d\eta = \sqrt{g_1^2 + g_2^2 + g_3^2} \, d\zeta \, d\eta \tag{104}$$

where

$$
\begin{aligned}
g_1 &= \frac{\partial y}{\partial \zeta} \frac{\partial z}{\partial \eta} - \frac{\partial y}{\partial \eta} \frac{\partial z}{\partial \zeta} \\
g_2 &= \frac{\partial z}{\partial \zeta} \frac{\partial x}{\partial \eta} - \frac{\partial z}{\partial \eta} \frac{\partial x}{\partial \zeta} \\
g_3 &= \frac{\partial x}{\partial \zeta} \frac{\partial y}{\partial \eta} - \frac{\partial x}{\partial \eta} \frac{\partial y}{\partial \zeta}
\end{aligned}
\tag{105}
$$

For rectangular elements, the two integrals from Equation 103 that must be evaluated become

$$\frac{1}{4\pi} \int_0^1 \int_0^1 \frac{(\vec{r} - \vec{r}_\ell) \cdot \hat{n}}{|\vec{r} - \vec{r}_\ell|^3} \{N\} |J(\zeta, \eta)| \, d\eta \, d\zeta$$

$$\text{and} \tag{106}$$

$$\frac{1}{4\pi} \int_0^1 \int_0^1 \frac{1}{|\vec{r} - \vec{r}_\ell|} \{N\} |J(\zeta, \eta)| \, d\eta \, d\zeta$$

For triangular elements, the upper limits of the integral over the η-coordinate becomes $1 - \zeta$. Numerically, the integrations are evaluated using two one-dimensional Gaussian quadratures over the elemental surface. This integration technique provides accurate results as long as the integrals are not singular.

Singular integrals arise when integrating the Green's function over an element which contains the source node. These singular integrals cannot be evaluated accurately with standard Gaussian quadrature and care must be taken to obtain acceptable results.

Several different techniques have been developed to evaluate the singular integrals arising in boundary element analysis [48–54]. The most effective of these analytically cancel the singularity [49–51]; with this technique, errors as low as 0.0001% have been found for plane triangles and rectangles. This method is used in the current system.

For all four element types, only the case where the singularity is located at the first node need be considered. The nodes may be renumbered for each different case

in such a way that the source node always lies on node one. This is done internally by the current BEM system.

Consider the linear element with the vector $\vec{r}_\ell$ placed at the same location as node 1 of the element. In this case, the integrand of Equation 106 is singular at $(\zeta = 1, \eta = 0)$. The integrals to be evaluated are:

$$-\frac{1}{4\pi} \int_0^1 \int_0^{1-\zeta} \frac{(\vec{r} - \vec{r}_\ell) \cdot \hat{n}}{|\vec{r} - \vec{r}_\ell|^3} \{N\} |J(\zeta, \eta)| \, d\eta \, d\zeta \tag{107}$$

and

$$\frac{1}{4\pi} \int_0^1 \int_0^{1-\zeta} \frac{1}{|\vec{r} - \vec{r}_\ell|} \{N\} |J(\zeta, \eta)| \, d\eta \, d\zeta \tag{108}$$

The singularity may be removed analytically by mapping the triangular element into a square, as shown in Figure 14. As seen from Figure 14, node 1 of the element becomes a side of the square, in the new u-v coordinate system, the three sides of the triangle becoming the other three sides of the square. This mapping is achieved by the coordinate transformation

$$
\begin{aligned}
\zeta &= u & d\zeta &= du \\
\eta &= (1-u)v & d\eta &= (1-u)dv
\end{aligned}
\tag{109}
$$

The integrals to be evaluated now become:

$$\frac{1}{4\pi} \int_0^1 \int_0^1 \frac{(\vec{r} - \vec{r}_\ell) \cdot \hat{n}}{|\vec{r} - \vec{r}_\ell|^3} \{N\} |J(u, v)|(1-u)dv \, du$$

$$\text{and} \tag{110}$$

$$\frac{1}{4\pi} \int_0^1 \int_0^1 \frac{1}{|\vec{r} - \vec{r}_\ell|} \{N\} |J(u, v)|(1 - u) dv\, du$$

It is simple to show that the $|\vec{r} - \vec{r}_\ell|$ term appearing in both integrals can be written in the form:

$$|\vec{r} - \vec{r}_\ell| = (1 - u)\mathcal{F}(u, v, \vec{r}_1, \vec{r}_2, \vec{r}_3) \tag{111}$$

where the vectors $\vec{r}_1, \vec{r}_2, \vec{r}_3$ are simply the coordinates of the nodes of the elements. The function $\mathcal{F}$ is:

$$\mathcal{F} = \sqrt{(x_3 + vx_2 - vx_3 - x_1)^2 + (y_3 + vy_2 - vy_3 - y_1)^2 + (z_3 + vz_2 - vz_3 - z_1)^2}. \tag{112}$$

The offending term, $(1 - u)$, in the denominator may now be canceled with the $(1 - u)$ term in the numerator; thus, the integrals in Equation 110 may be written as:

$$-\frac{1}{4\pi} \int_0^1 \int_0^1 \frac{(\vec{r} - \vec{r}_\ell) \cdot \hat{n}}{(1 - u)^2 \mathcal{F}^3} \{N\} |J(u, v)| dv\, du \tag{113}$$

and

$$\frac{1}{4\pi} \int_0^1 \int_0^1 \frac{1}{\mathcal{F}} \{N\} |J(u, v)| dv\, du \tag{114}$$

These integrals may now be evaluated using standard Gaussian quadrature — neither one is singular since $\mathcal{F}$ is not zero at any point of the element. Even though the first integral still contains the $(1 - u)^2$ term in the denominator, it is not singular. A
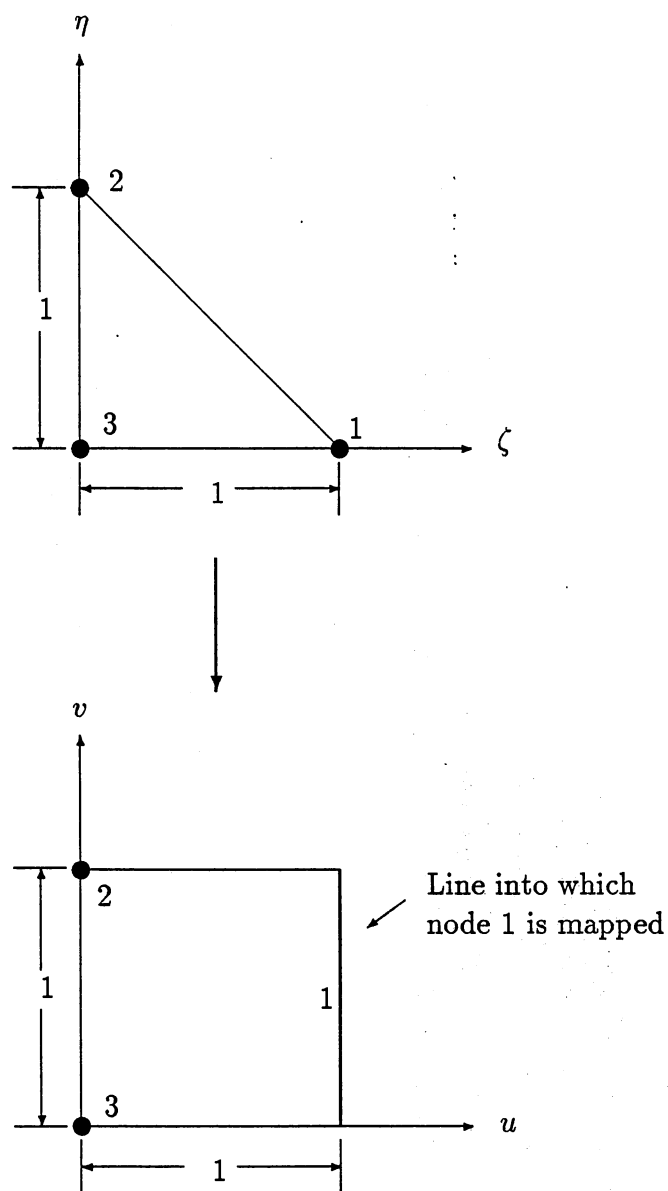
Figure 14. Mapping of Triangular Linear Element in ζ-η Coordinate System to Rectangle in u-v Coordinate System

$(1 - u)$ term may be factored out of the numerator, canceling one of the $(1 - u)$ terms in the denominator. The shape functions $\{N\}$ are exactly zero at the singular point (except the shape function corresponding to node one, but this integral may be calculated using physical considerations [36]), canceling the last of the $(1 - u)$ terms in the denominator.

The four-noded, six-noded, and eight-noded elements are treated in a similar fashion, except that one must deal with nodes which are not at corners of a triangle. For example, consider the four-noded element, with $\vec{r}_\ell$ located at node 1 of the element (see Figure 11 for location of the node). To deal with the singularity at this node, the element must be divided into two other triangular elements as shown in Figure 15. This mapping is achieved by using the following coordinate transformations:

$$\zeta = v_1$$

$$\eta = 1 - u_1 \tag{115}$$

and

$$\zeta = 1 - u_1$$

$$\eta = 1 - u_1 - v_1 \tag{116}$$

These two triangles, with the singularity at node 1 of each, are then mapped into squares as is done with the linear element.

The six-noded triangle is treated exactly the same as the linear element when the singularity exists at node 1 of the element. If the singularity exists at one of the mid-side nodes, the element must be split into two triangles as shown in Figure 16, where the singularity is at node 2. The mapping is achieved using the coordinate transformations:

$$\zeta = \frac{1}{2}u_1$$
$$\eta = \frac{1}{2}u_1 + v_1 \tag{117}$$

and

$$\zeta = 1 - \frac{1}{2}u_1 - v_1$$
$$\eta = \frac{1}{2}u_1. \tag{118}$$

The resulting two triangles, once again, are mapped into squares, as done with the linear element.

The eight-noded rectangle is treated the same as the four-noded bilinear element when the singularity exists at node 1. The element is split in the same way as the bilinear element, using the same coordinate transformations. If the singularity exists at the second node (or at any mid-side node), the element must be split into three
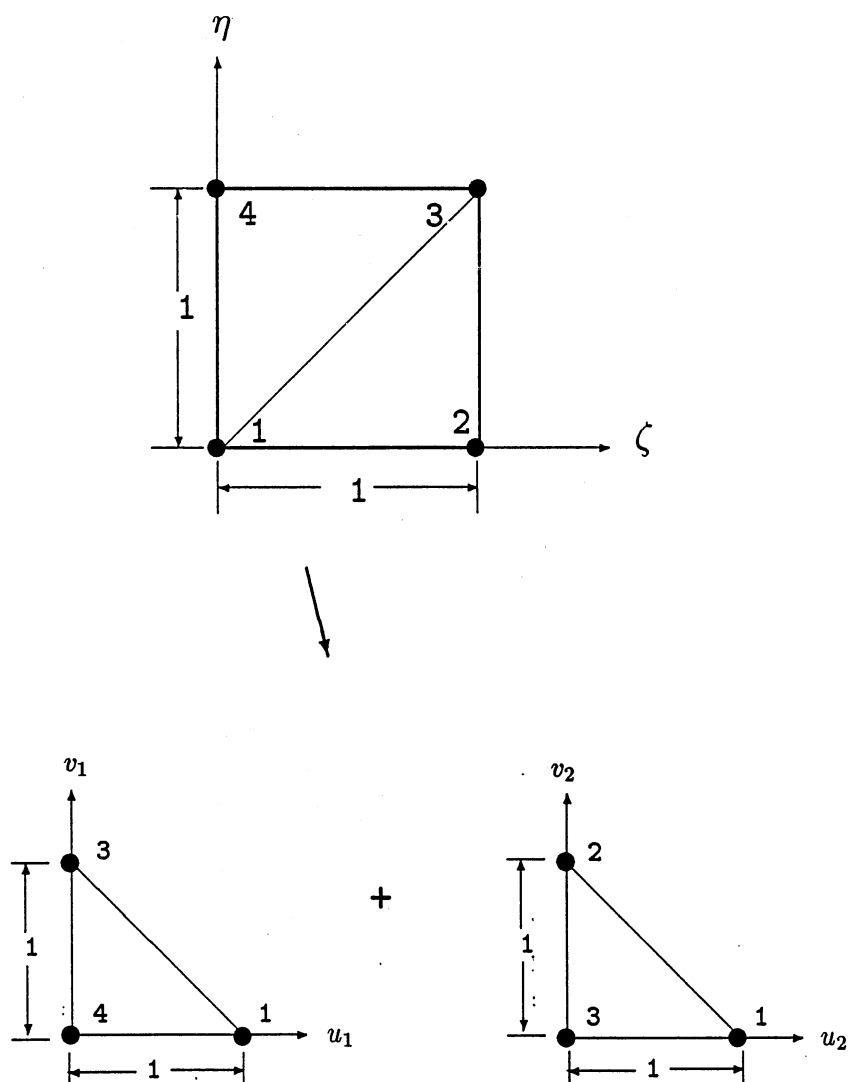
Figure 15. Mapping of Six-Noded Bilinear Element in ζ-η Coordinate System to Two Triangles in u_1-v_1 and u_1-v_1 Coordinate Systems
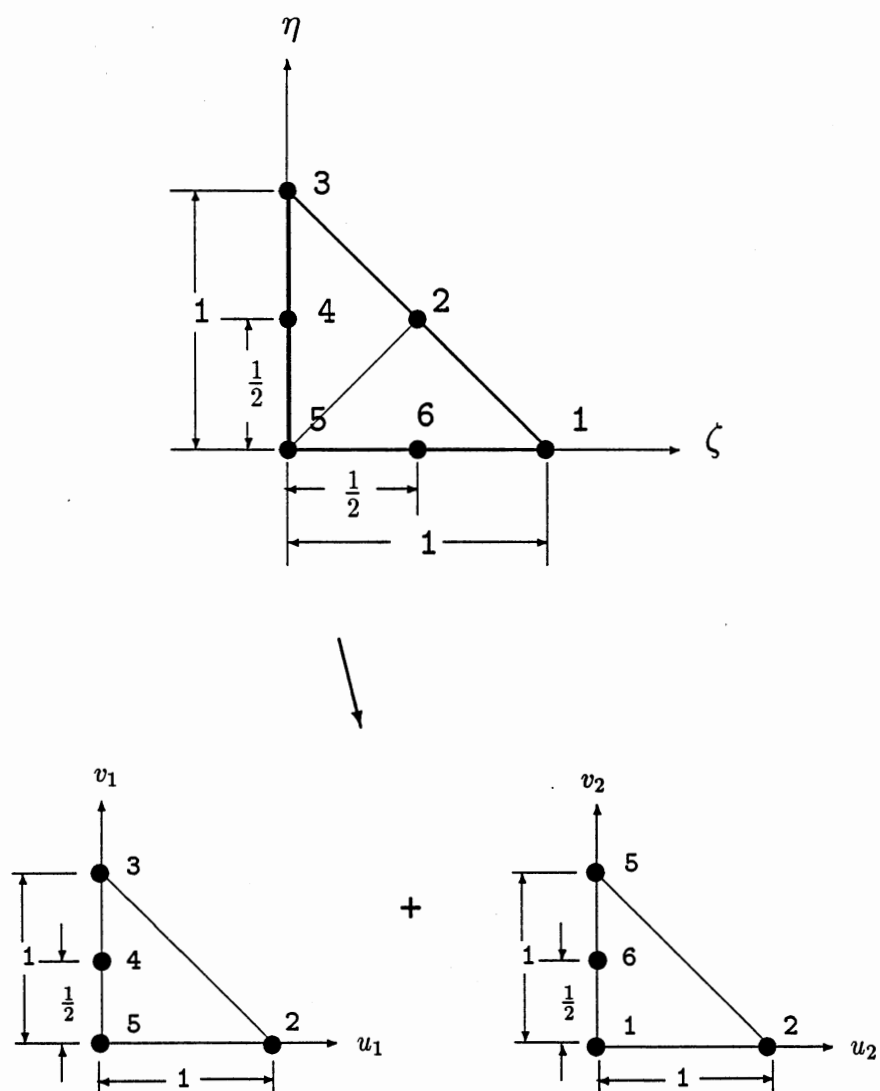
Figure 16. Mapping of Six-Noded Triangular Element in ζ-η Coordinate System to Two Triangles in u_1-v_1 and u_1-v_1 Coordinate Systems

rectangles as shown in Figure 17, using the following coordinate transformations:

$$\zeta = \frac{1}{2}u_1$$

$$\eta = v_1, \tag{119}$$

$$\zeta = \frac{1}{2}u_1 + v_1$$

$$\eta = 1 - u_1, \tag{120}$$

and

$$\zeta = 1 - \frac{1}{2}u_1$$

$$\eta = 1 - u_1 - v_1. \tag{121}$$

The three triangles in the u_1-v_1, u_2-v_2, and u_3-v_3 coordinate systems are then mapped into squares, and the integrals are evaluated in the same manner as the linear triangular elements.
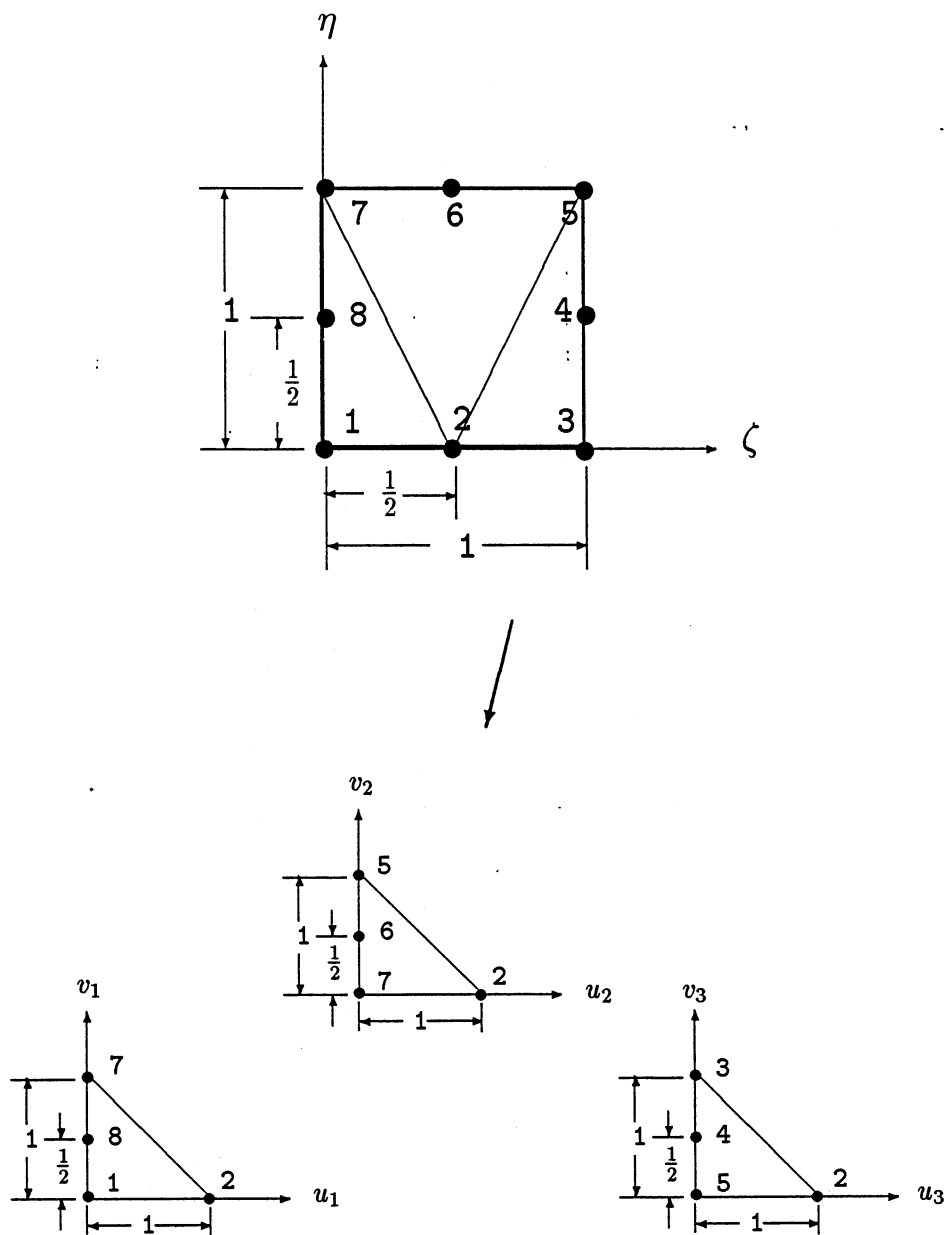
Figure 17. Mapping of Eight-Noded Rectangular Element in
ζ-η Coordinate System to Three Triangles in u_1-v_1,
u_2-v_2, and u_3-v_3 Coordinate Systems

Computer Implementation

The BEM system was implemented in a computer program, using the C programming language, under the Ultrix operating system, on a VAXstation 2000 minicomputer. The program consists of a general purpose boundary element system capable of solving Darcy's equation, for the special cases discussed, in two- and three-dimensional space. The program is also capable of solving axisymmetric problems, where only the curved boundary in the r-z plane is defined. It is a batch-oriented system, where the user creates an input file which is read by the program. Interactive graphical analysis of the input data, and the results are also provided, using the X-windows system under Ultrix.

The input data for the BEM system resides in a file created by the user. The file contains: the locations of all the nodes, including their boundary conditions; the element topology information; the material property information; and the type of analysis which is to be performed.

Readability of the input and output file was one of the main considerations which influenced the creation of the input/output routines. The user of the system should be able to read the contents of the file and easily recongnize what everything represents. To achieve this, keywords are used throughout the input file, indicating to both the user and the BEM system what each part of the data represents. All of the data may be written in "free format", where none of the numbers or keywords needs to be lined

up in columns. Blank lines, as well as comment lines (identified by placing a % sign in the first column of the line), are also allowed, helping to improve readability for the user. Keywords may be written in upper or lower case, and for the most part, only the first few letters of the keyword are necessary.

The interactive graphical previewer and post-processor are invoked with a command line argument, given at run time. A window is created and the program enters a "command mode", where the user is prompted for commands which determine the action of the program. From this command mode, the user can: view the model from any angle desired; begin the analysis process; view isopotential maps of the solution within the domain for two-dimensional problems; view isopotential maps on the surface of three-dimensional models; select specific points within the domain and obtain potential values there in two-dimensional problems; and produce PostScript files of the current contents of the window which can then be printed out on any PostScript laser printer. An online "help" command, which simply lists the commands and their syntax, is also provided.

CHAPTER IV

VERIFICATION

The initial verification of any numerical analysis system is achieved by comparing results from numerical analyses with results from analytical (exact) analyses. Exact solutions are available for only relatively simple problems. Therefore, additional comparisons must be made with experimentally obtained data. In the following sections, the BEM system is used to analyze a number of example problems. Comparisons are made with analytical results and with experimentally obtained data.

Electropotential Distribution Over Coplanar
Electrodes

In this example, the results of the current BEM system are compared with the analytical work of Waber and Fagan [12], where the electropotential distribution throughout an electrolyte above infinitely long narrow electrodes, juxtaposed and alternating in an infinitely long array along a horizontal plane (Figure 18), is studied. This semi-infinite galvanic cell may be modeled as a two-dimensional problem, as shown in Figure 19.
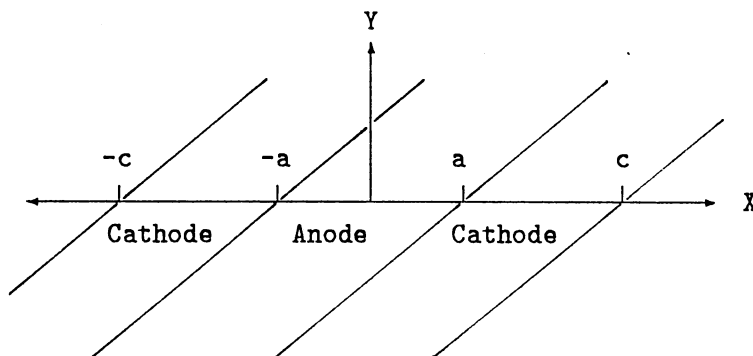
Figure 18. Infinite Array of Infinitely Long Electrodes on the x-z Plane
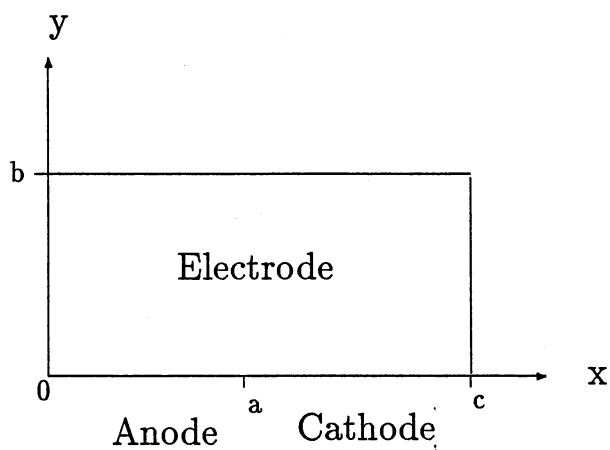
Figure 19. Two-Dimensional Model of the Semi-Infinite Galvanic Cell

The boundary conditions are given by:

$$\lim_{y \to b} \frac{\partial \Phi}{\partial y} = 0$$

$$\left.\frac{\partial \Phi}{\partial x}\right|_{x=0} = \left.\frac{\partial \Phi}{\partial x}\right|_{x=c} = 0$$

$$\Phi(x,0) = \begin{cases} E_a + \left.\kappa\frac{\partial \Phi}{\partial y}\right|_{y=0} & 0 \leq x \leq a \\ \left.\kappa\frac{\partial \Phi}{\partial y}\right|_{y=0} & a \leq x \leq c \end{cases}$$

where κ is a "polarization parameter" [7], and E_a is the difference in potentials between the anode and the cathode extrapolated to zero current flow. The electropotential distribution in the the two-dimensional problem is expressed by Waber as a Fourier series of the form:

$$\Phi(x,y) = \frac{E_a a}{c} + \frac{2E_a}{\pi}\sum_{n=1}^{\infty}\frac{\sin\left(\frac{n\pi a}{c}\right)\cos\left(\frac{n\pi x}{c}\right)\cosh\left[\frac{n\pi}{c}(b-y)\right]}{n\left[\cosh\left(\frac{n\pi b}{c}\right) + \left(\frac{n\pi\kappa}{c}\right)\sinh\left(\frac{n\pi b}{c}\right)\right]}$$

The problem was modeled using the BEM system with a mesh as shown in Figure 20. The parameters a, b, and c were 0.5, 0.5, and 1.0, respectively. The polarization constant E_a was set to 1.0. The model contained 44 nodes and 42 elements. The electrodes were modeled using Overhauser elements, while the sides and top of the electrolyte were modeled using linear elements.

The BEM system converged to a solution after only one iteration. The rapid convergence occurred because the polarization behavior of the electrodes was given
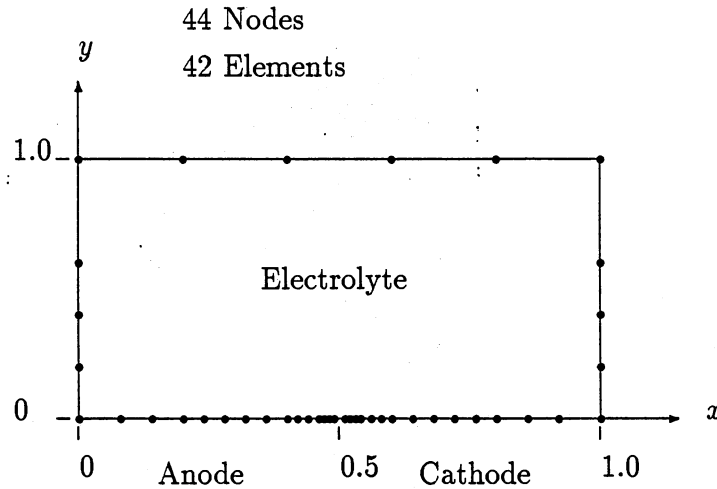
Figure 20. BEM Mesh of Electrolyte Boundary

by a linear function and the resulting set of equations to be solved by the BEM system was linear.

The dimensionless quantity C^*, representing current density at the electrode surfaces, is defined by Waber as:

$$C^* \equiv \left(-\frac{2a}{E_a}\right) \frac{\partial \Phi}{\partial y}\bigg|_{y=0}$$

The results for C^* on the electrodes, at $y = 0$, are shown in Figure 21. As seen from the figure, the results of the BEM analysis are extremely accurate, even at the singularity located at $x/c = 0.5$, where C^* changes sign. The results of the dimensionless potential $P^* = \Phi/E_a$ are shown in Figure 22, where, again, it can be seen that the results of the BEM analysis agree with the Fourier series solution.
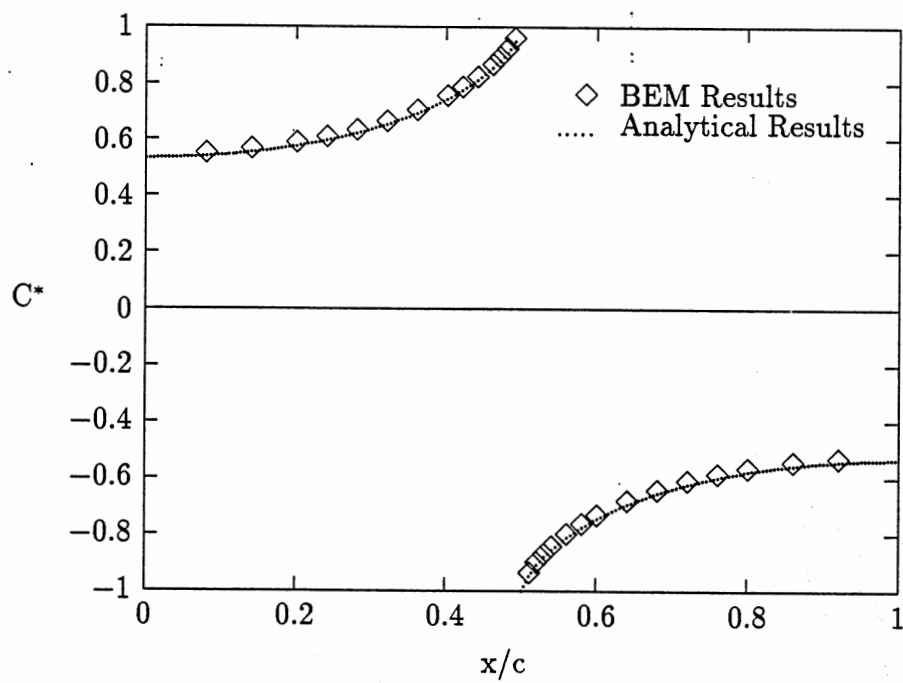
Figure 21. Dimensionless C* Current Flux at Electrode Surfaces
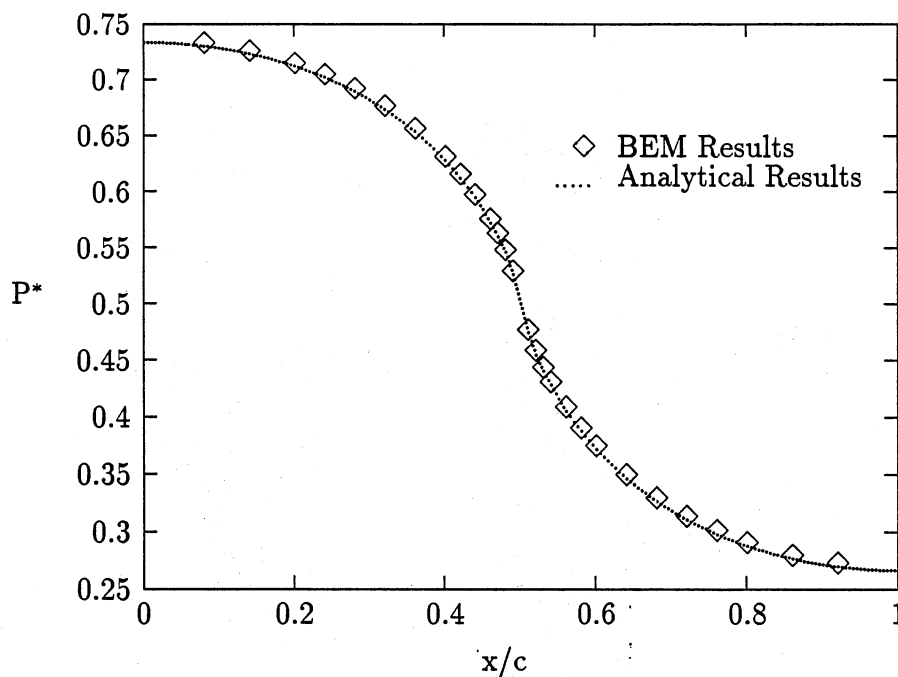
Figure 22. Dimensionless P* Potential at Electrode Surfaces

Comparison of Two-Dimensional Analysis With Experimental Results

A simple galvanic cell involving stainless steel (SUS-304) and gray cast iron (FC-20) immersed in an NaCl solution is used to compare the results of the current BEM system with experimental data. The work of Aoki, et al. [29], involving such a galvanic system, is used here.

The galvanic cell is shown in Figure 23, where the top and sides were assumed to be insulated. To measure the current density, the electrodes were split into strips along the width, separated by very thin insulation. After the galvanic cell reached a

Width = 60 mm
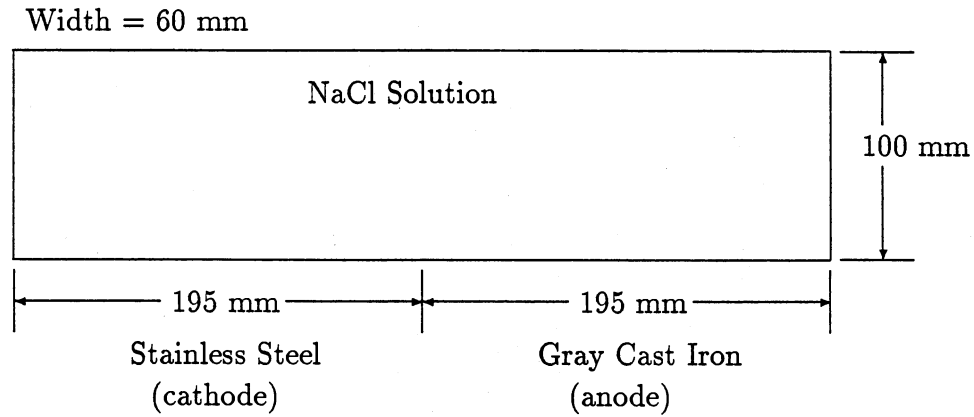
Figure 23. Experimental Stainless Steel-Cast Iron Galvanic Cell

steady state, the current density was measured at each electrode strip.

The polarization behavior of the two metals was given by the following curves [29]:

$$\Phi_e\big|_{\text{iron}} = 12(\log q_e)^2 + 22\log q_e - 681$$

and

$$\Phi_e\big|_{\text{steel}} = -48(\log q_e)^2 - 137\log q_e - 372$$

where the electrode potential Φ_e is measured in mV and the current density q_e at the electrode is measured in $\mu A/\text{cm}^2$. The polarization curves are approximations to the measured polarization behavior of stainless steel and cast iron in the NaCl solution. Aoki et al. [29] did not specify the concentration or the conductivity of the

NaCl solution used in this experiment. For the BEM analysis, the conductivity of the electrolyte was taken as 0.000357 mho/cm. This value is given in the work by Aoki et al. [55] for a 0.016 wt% NaCl solution and is consistent with other values found in the literature [21].

For this analysis a two-dimensional BEM model of the galvanic cell, composed of 74 nodes and 70 elements, was used. The mesh is very similar to the one shown in Figure 20 for the previous problem and therefore it is not shown here. Linear elements were used to model the sides and top of the electrolyte and Overhauser elements were used to model the electrodes. Convergence was achieved after 8 iterations. The results are shown in Figure 24 where it can be observed that the general behavior of the results obtained using the BEM system is the same as that of the experimental results. The actual values differ by as much as 100% at some points, but this is attributed to the fact that the conductivity values used in this work may not be the same as those used in the experimental work, which were not available at the time.

Comparison of Axisymmetric BEM Analysis
With Experimental Results

The work by Fu and Chow [56] is used in this example for the purpose of comparing the results obtained using the axisymmetric formulation of the BEM system with experimental results.

The analysis consists in finding the electropotential distribution in a cathodically
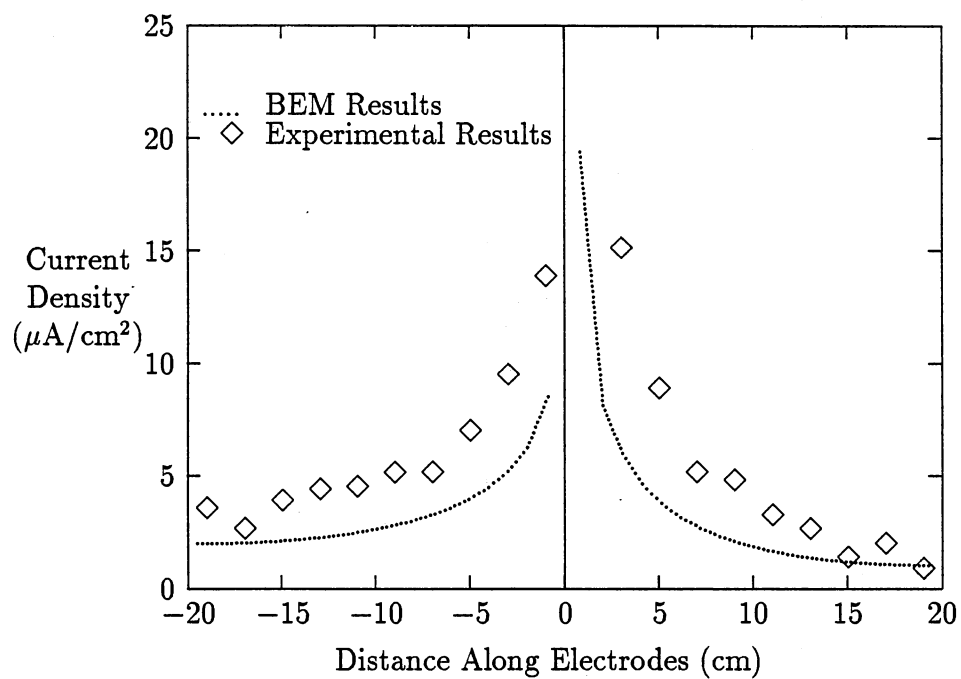
Figure 24. Comparison of BEM Results With Experimental Results For Current Density Along Electrolyte Surface
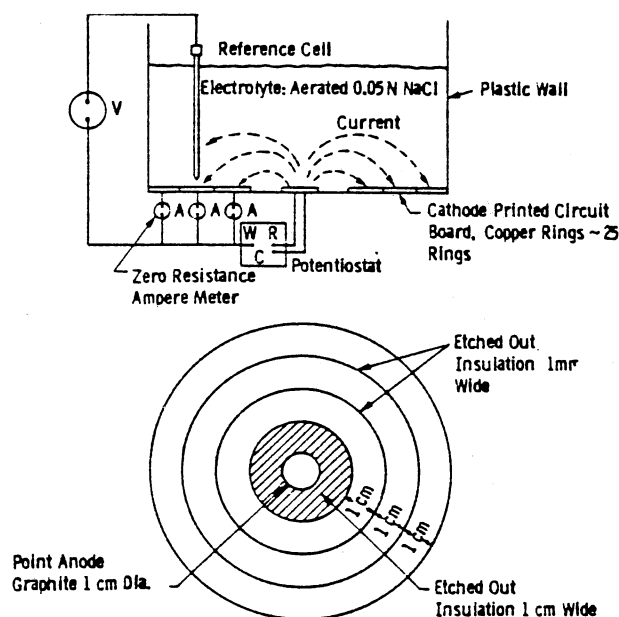
Figure 25. Experimental Axisymmetric Galvanic Corrosion Cell With Concentric Copper Electrodes Surrounding Graphite Anode

protected plastic cylindrical tank with a copper bottom, as shown in Figure 25, reproduced here from Fu and Chow [56]. The bottom of the tank holds a 1 cm dia. graphite anode, at which an impressed current of 20 mA was supplied using a potentiostat, and concentric copper rings separated by thin (1 mm) insulation material. The tank was filled to a depth of 10 cm with an aerated 0.05 N NaCl solution with a specific conductivity of 0.0033 mho/cm.

The BEM analysis was performed using the mesh as shown in Figure 26.

A total of 64 nodes and 62 linear elements were used in the axisymmetric model. The boundary conditions specified were: an outward normal flux on the graphite anode of -25.46 μA/cm^2; a zero normal flux on the top, sides, and insulation between
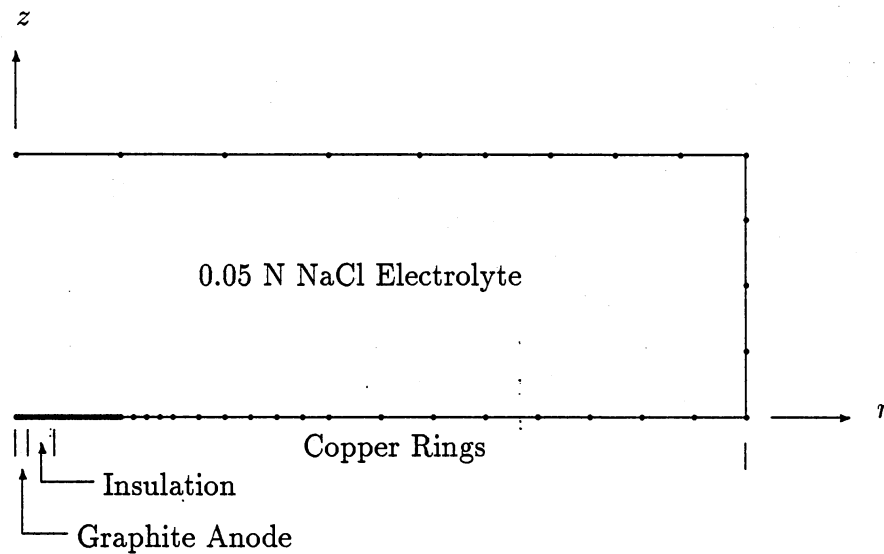
Figure 26. Axisymmetric BEM Mesh of Electrolyte Boundary

Graphite and copper; and $\Phi = f_e(q_e)$ on the copper surface. The approximation of the polarization curve $f_e(q_e)$ given in the work by Fu [56] is shown in Figure 27. The polarization curve shown in Figure 27 is an approximation of the curve given in the work by Fu [56]. This approximation is given by:

$$f_e(q_e) = \alpha \log i + \beta$$

where the values of α and β are given in Table 1.

The BEM analysis converged after 9 iterations. The results obtained from the BEM analysis and the experimental data for the electropotential and the current
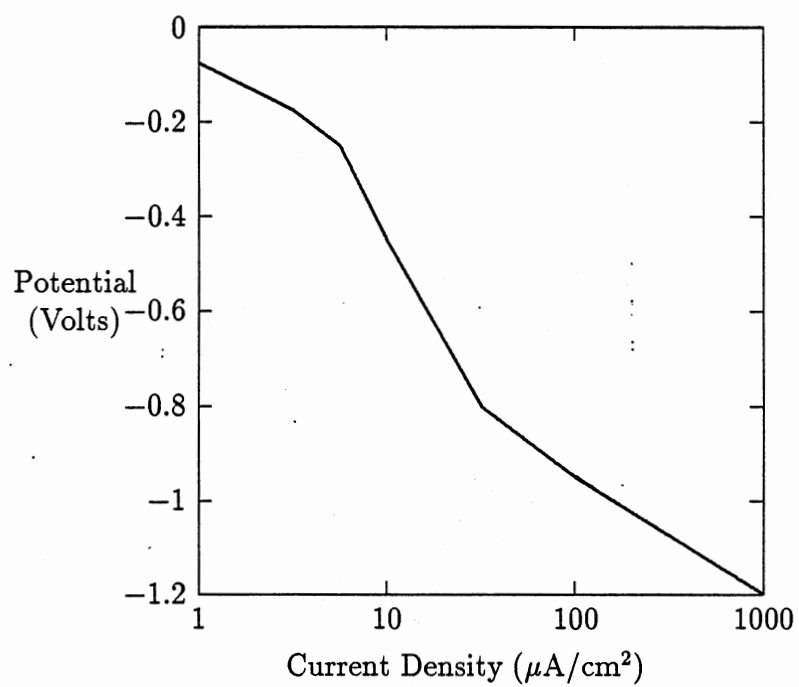
Figure 27. Cathodic Polarization Curve for Copper in a 0.05 N NaCl Solution

Table 1. Coefficients Used to Approximate Polarization Curve of Copper in 0.05 N NaCl Solution

Current Density Range (μA/cm^2)	α	β
$-\infty < i \leq 3.162$	-2.0	-1.275
$3.162 < i \leq 5.623$	-3.0	-1.825
$5.623 < i \leq 1.000$	-8.0	-4.450
$1.000 < i \leq 17.78$	-7.0	-3.951
$17.78 < i \leq 31.62$	-7.0	-3.950
$31.62 < i \leq 100.0$	-3.0	-2.150
$100.0 < i < \infty$	-2.5	-1.950
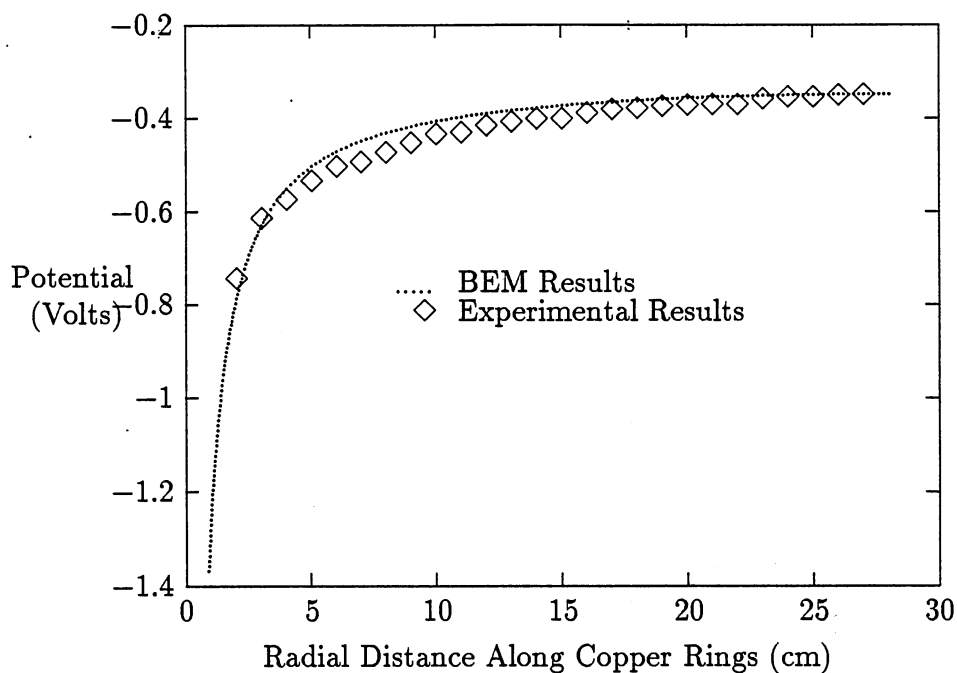
Figure 28. Comparison of BEM Results With Experimental
Results For Electropotential on Bottom of Tank
Along Radial Distance

density along the bottom of the tank are shown in Figures 28 and 29. For the elec-

tropotential along the copper surface, there is generally excellent agreement between

the experimental results and the BEM analysis results. For the current density,

agreement is generally not as good. This is probably because the experimental mea-

surements for the current density may have been flawed. As Fu postulates in his work

[56], the experimental measurements may be flawed by hydrogen bubbles formed on

the copper ring surfaces, especially close to the graphite surface.
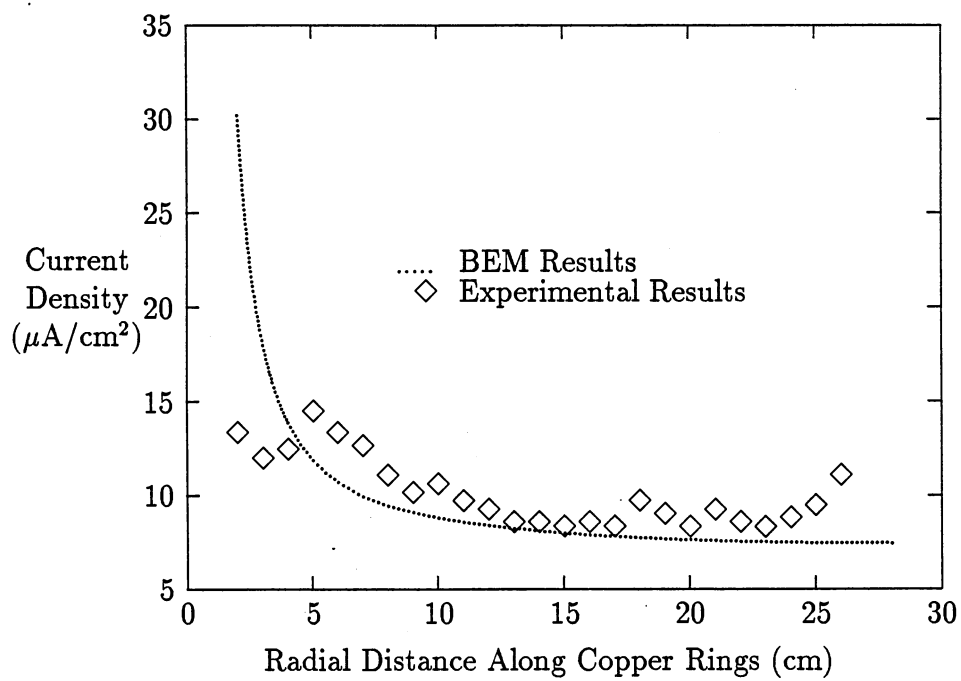
Figure 29. Comparison of BEM Results With Experimental
Results For Current Density on Bottom of Tank
Along Radial Distance
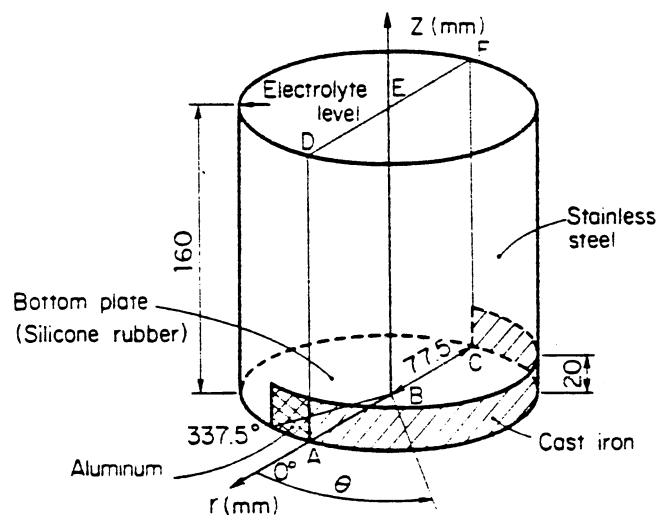
Figure 30. Experimental Stainless Steel-Cast Iron-Aluminum
Cylindrical Tank Filled With NaCl Solution

Comparison of Three Dimensional BEM
Analysis With Experimental Results

The cylindrical tank shown in Figure 30, reproduced from Aoki et al. [55], is used

to compare the results of the three-dimensional BEM analysis with experimental

results. The experimental results are based on the work of Aoki et al. [55].

The tank consists of a cylindrical stainless steel (AISI 304) shell with a silicone

rubber bottom. A cast iron, 20 mm semi-circular strip is attached to the bottom of

the stainless steel side. A small piece (20x20 mm) of aluminum is also attached to the

bottom of the cylinder side (Figure 30). The tank is filled to 160 mm with a 0.0165

wt% NaCl solution with a conductivity of 0.000357 moh/cm.

An approximation of the polarization curves in the work by Aoki et al. is shown

in Figure 31. It is important to note that, although the defined boundary conditions specify a negative current density for anodic surfaces and a positive current density for cathodic surfaces, they are both represented on the positive axis in the log-scale graph. Although the polarization curve of cast-iron appears to be a multiply-valued function, it should be noted that the top portion of the curve represents the anodic behavior, and the bottom of the curve represents the cathodic behavior. The polarization behavior of aluminum is also plotted on the positive axis, though in this case it acts strictly anodically.

The polarization curves are approximated in a piece-wise fashion according to

$$\Phi_e = f_e(q_e) = \alpha \log i + \beta$$

for each segment of the curve. Φ_e is measured in Volts (vs. SCE). The values of α and β for each material are given in Table 2.

The three-dimensional BEM model used in the analysis is shown in Figure 32. The mesh consists of 226 nodes and 384 linear elements. Zero flux boundary conditions were specified at the bottom and top of the cylinder. The boundary condition specified at the remaining nodes was $\Phi = f_e(q_e)$, where f_e is determined by the electrode material pertaining to each element, whose locations are shown in Figure 32.

The BEM system converged after 7 iterations. The results for the electropotential along the Θ direction at a z distance of 10 mm are shown in Figure 33. Averages were calculated for the elemental node values of Φ for each element. It is these average
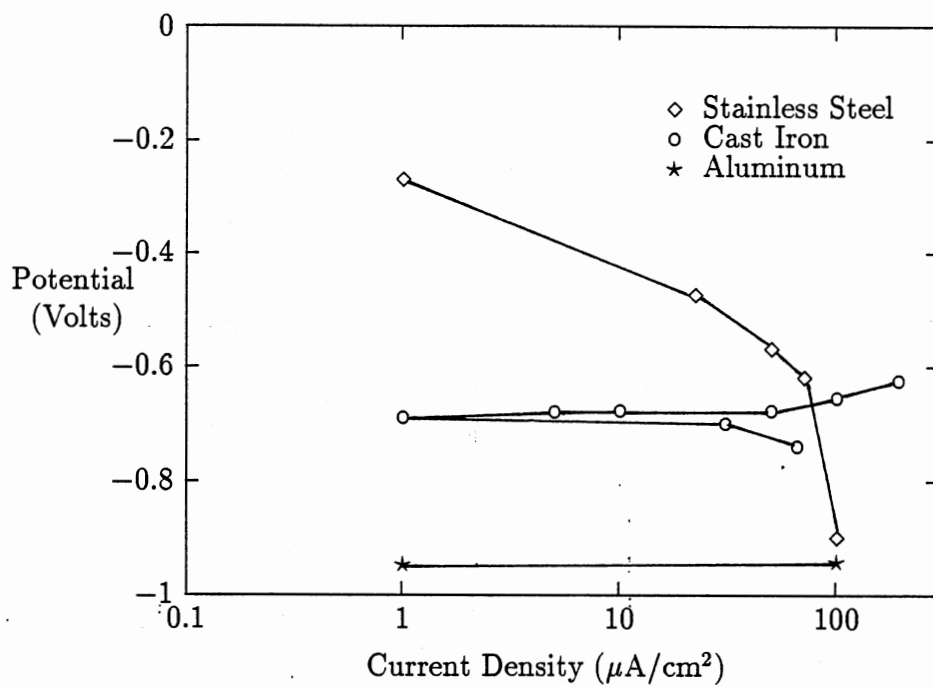
Figure 31. Polarization Curves for Stainless Steel, Cast Iron,
and Aluminum in 0.0165 wt% NaCl Solution

Table 2. Coefficients Used to Approximate Polarization Curves for Stainless Steel, Cast Iron and Aluminum in 0.0165 wt% NaCl Solution

Material	Current Density Range $(\mu A/cm^2)$	α	β
Stainless Steel	$-\infty < i \leq 22.36$	-0.152	-0.270
	$22.36 < i \leq 50.00$	-0.272	-0.108
	$50.00 < i \leq 70.71$	-0.332	-0.006
	$70.71 < i < \infty$	-1.860	2.821
Cast Iron	$-\infty < i \leq -100.0$	-0.105	-0.865
	$-100.0 < i \leq -50.0$	-0.076	-0.808
	$-50.0 < i \leq -5.0$	-0.002	-0.681
	$-5.0 < i \leq 30.9$	-0.009	-0.684
	$30.9 < i < \infty$	-0.121	-0.519
Aluminum	$-\infty < i < \infty$	0.002	-0.946
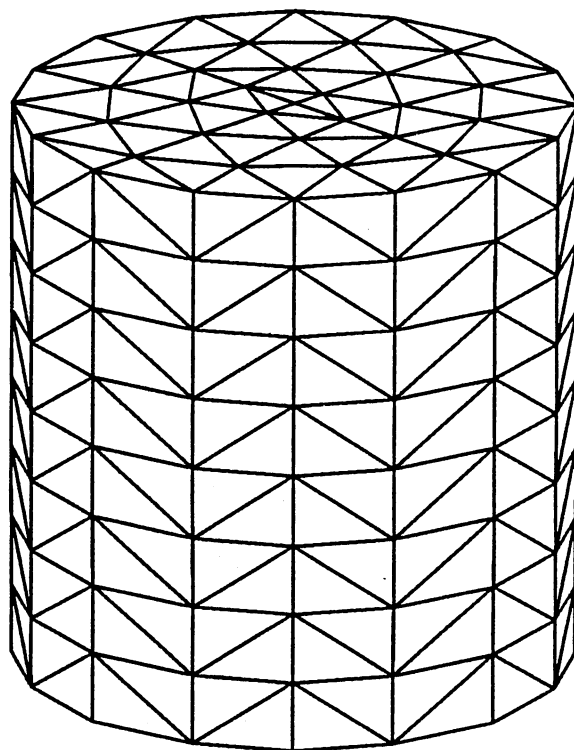
Figure 32. BEM Mesh of Cylindrical Tank - 226 Node and 384 Elements
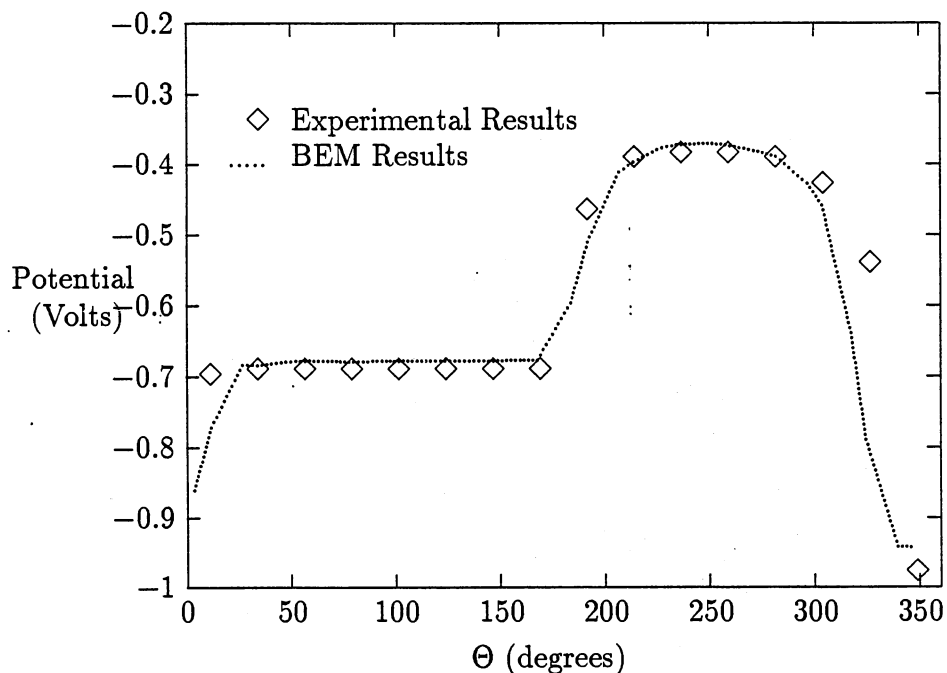
Figure 33. Potential Distribution Along Θ Direction at $z = $ 10mm

values, for elements along the bottom row of elements along the side of the tank, that are plotted as the BEM solution in Figure 33. An average value for q was also calculated in the same manner as the average Φ values, and the results for the same elements in Figure 33 are shown in Figure 34.

An isopotential map of the BEM results on the boundary of the tank is shown in Figure 35, where the boundaries of the different metal surfaces are clearly defined by the potential values. It can be seen that the effects of the aluminum and iron on the stainless steel are very localized. Despite the localized effect of the anodic metals, the stainless steel still acts as the cathode in the galvanic cell. The magnitude of the potential value of all of the nodes in the model is above 300 mV, indicating that the
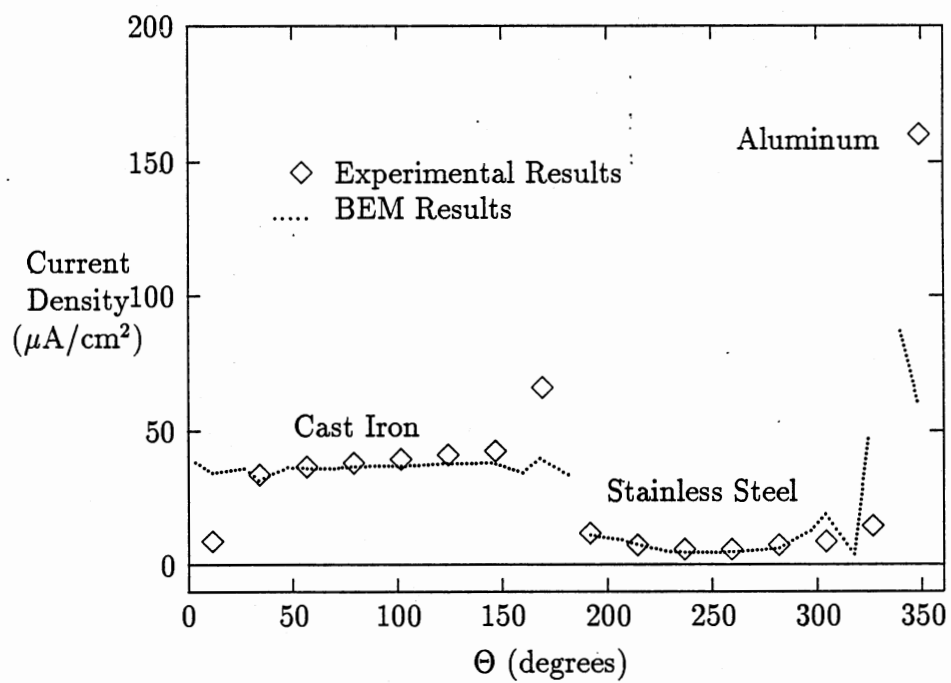
Figure 34. Current Density Distribution Along Θ Direction at
$z = 10$mm
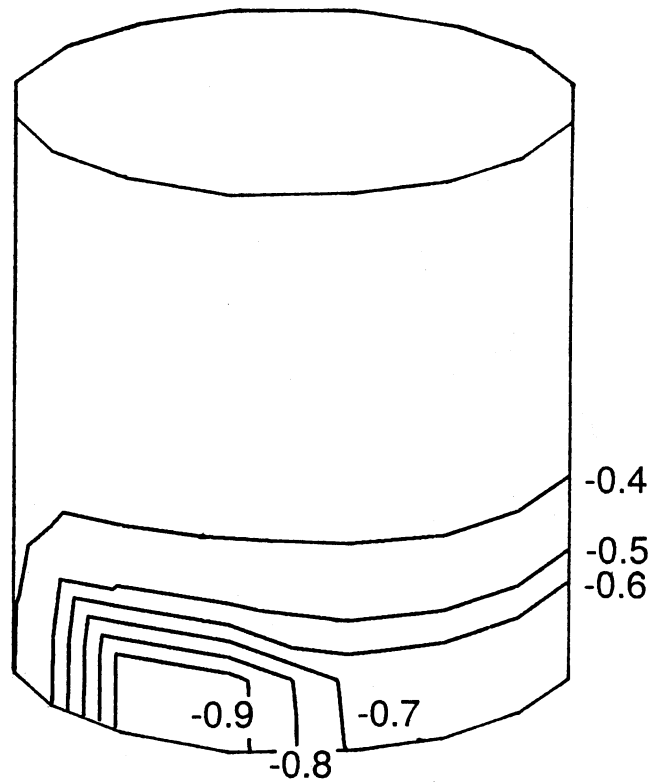
Figure 35. Isopotential Map of BEM Results Along Tank Sides

stainless steel is always acting cathodically.

The results of this example clearly indicate that the current BEM system is very accurate and may be used to calculate electropotential and current density values in galvanic corrosion cells.
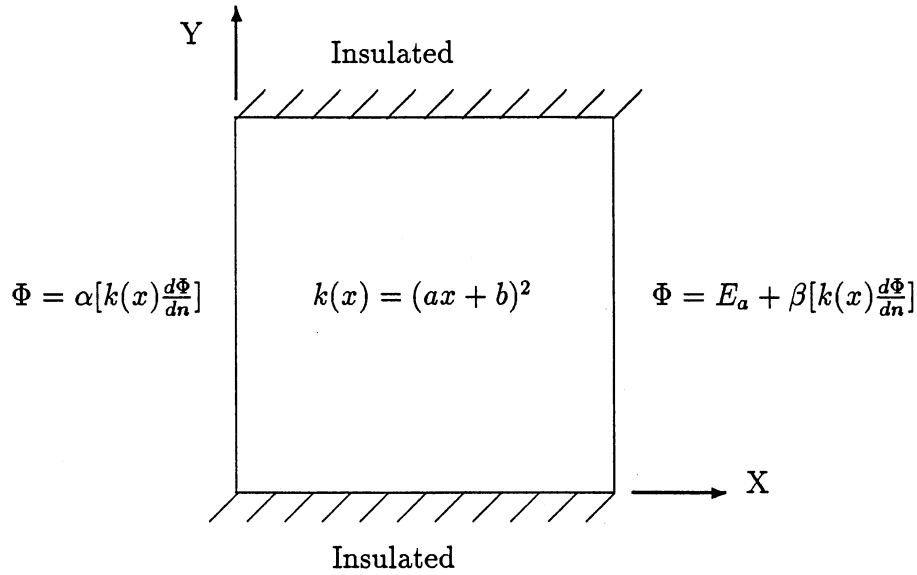
Figure 36. Semi-Infinite Nonhomogeneous Electrolyte Body

Galvanic Corrosion in a Nonhomogeneous Electrolyte

The following example is used to compare the results of the system with analytical results. The problem consists of an electrolyte body which is infinitely long in the z direction and has a square boundary in the x-y plane (Figure 36). The electrolyte is insulated at $y = 0$ and $y = 1$. Electrodes exist at $x = 0$ and $x = 1$. Assuming that the conductivity, k, of the electrolyte behaves according to $(ax + b)^2$, the problem reduces to one dimension, and may be cast in the following manner:

$$\frac{d}{dx}[k(x)\frac{d\Phi}{dx}] = 0$$

with boundary conditions:

$$\Phi(0) = \alpha q(0)$$

$$\Phi(1) = E_a + \beta q(1)$$

where Φ is the electropotential, q is the electric flux, α and β are polarization parameters as defined by Wagner [7], and E_a is the difference between the electrode potentials extrapolated to zero current density. The electric flux is defined by:

$$q(x) = k(x)\frac{d\Phi}{dn}$$

where n is the direction of the outward pointing normal to the electrolyte surface. The solution to this problem, easily found by integration, is:

$$\Phi(x) = \frac{E_a(b+a)[(ab\alpha - 1)x + \alpha b^2]}{(ax + b)[(b^2 + ab)(\beta + \alpha) - 1]}$$

Results were obtained for $\alpha = \beta = -\frac{1}{2}$, $b = 1$, $a = 2$, and $E_a = 1$. The electrolyte surface was modeled with a total of 34 nodes. The top and bottom were modeled with a combination of quadratic and Overhauser [42] elements, while the left and right sides were modeled using linear elements. A comparison of the electropotential values obtained from the BEM system and from the analytical solution are shown in Figure 37. As can be seen from the figure, the agreement between the two solutions is excellent. The exact value of the flux, constant throughout the electrolyte, is 0.75.
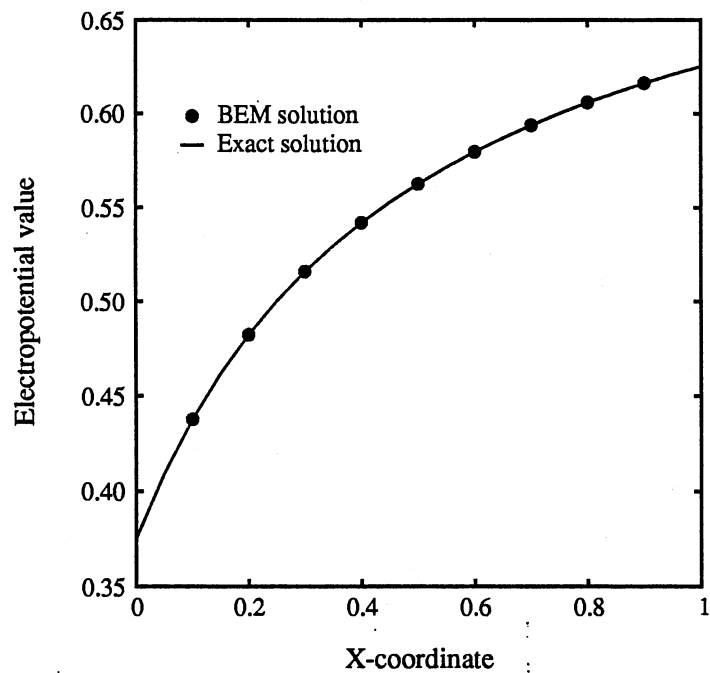
Figure 37. Comparison of Results with Analytical Solution

The calculated value of the flux is accurate to 5 decimal places — an error less than 0.01%, indicating that the current BEM system is very accurate indeed.

CHAPTER V

USE OF THE BEM SYSTEM

To show how the current BEM system may be used for analysis and design of cathodic protection systems, two sample analyses are performed. The first sample consists of the analysis of a hypothetical cathodic protection system for a reinforced concrete deck under the influence of deicing salts. The second sample is an analysis of a cathodic protection system for a culvert valve. The following sections describe the problems, BEM results, and conclusions about the BEM system which may be made from the sample problems.

Concrete Bridge Deck Under the Influence of Deicing Salts

A hypothetical problem will be used to illustrate the advantages of using a BEM system which explicitly accounts for electrolyte nonhomogeneities. The problem consists of a cathodically protected reinforced concrete deck (which is under the influence of deicing salts), as shown in Figure 38. The steel used is $\frac{3}{4}$ in. diameter steel, with a $2\frac{1}{2}$ in. cover. An anode-net system is used for cathodic protection of the deck. The anode-net system consists of a continuous thin layer, or net, of anodic material covering the top of the deck, with an impressed current applied to it.

95

Anode-Net With Impressed Current
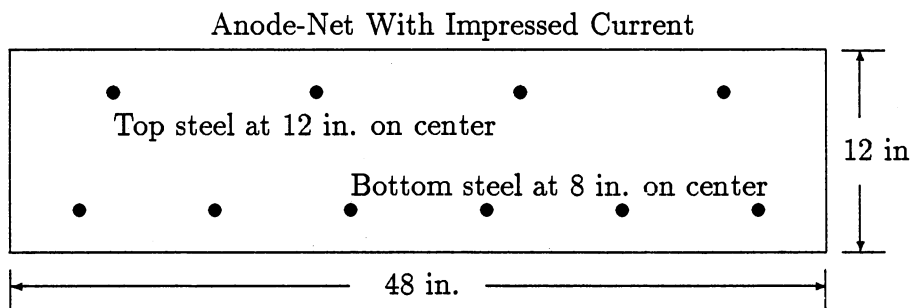
Figure 38. Cathodically Protected Reinforced Concrete Deck

The resistivity of the concrete is inversely related to the chloride concentration within the concrete [6], which decreases with depth. For simplicity, other factors such as moisture, temperature, and concrete density, which affect the conductivity, are ignored. The electrochemical resistivity of this example is assumed to increase with depth from 50 ohm-cm at the top to 10,000 ohm-cm at the bottom of the deck. This resistivity variation is taken from the work by Vrable [27], and is approximated by

$$k = (0.0024 + 0.0003y)^2$$

where y is the height, in inches, measured from the bottom of the deck.

Typical long-term polarization behavior for steel in concrete is assumed [27], as shown in Figure 39. This behavior is represented by piece-wise sections of the form

$$\Phi = \alpha \log q + \beta$$
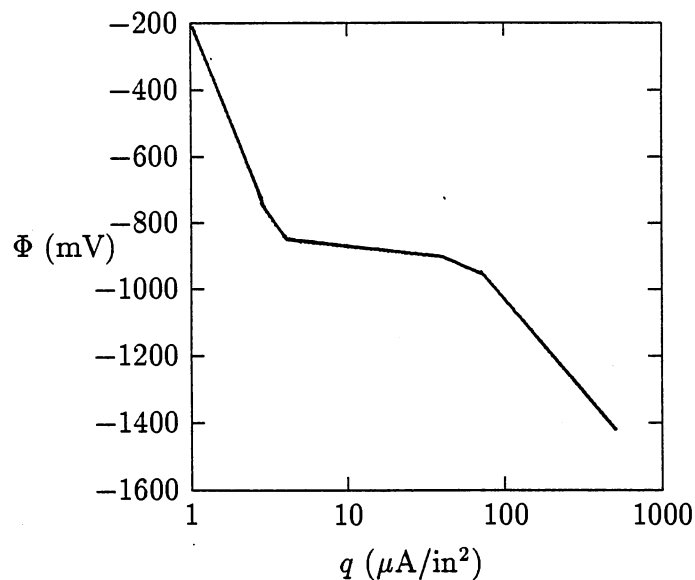
Figure 39. Polarization Behavior of Reinforcing Steel in Con-
crete

where Φ is measured in mV (to $Cu/CuSO_4$ half cell), and q is measured in $\mu A/in.^2$.
The constants α and β are given in Table 3.

The impressed current applied to the system is 1.55 $\mu A/in.^2$. This is the recom-
mended maximum current density for cathodically protected concrete structures, and
it is the operating current density for most net-anode systems now in use [6].

Two different models were used for the analysis of the deck: the first model
discretizes the concrete deck into four different regions, each of which is assumed to
have a constant conductivity; the second model treats the deck as one region with a
variable conductivity. Figure 40 shows the different conductivity functions used for
each of the two models.

The model with different regions, with a total of 134 nodes and 174 elements,

Table 3. Coefficients Used to Approximate Polarization
Curve of Reinforcing Steel in Concrete

Current Density Range $(\mu A/in^2)$	α	β
$-\infty < i \leq 4.00$	-1.0514	-0.2000
$4.0 < i \leq 50.0$	-0.0612	-0.7962
$50.0 < i \leq 80.0$	-0.3233	-0.3507
$80.0 < i < \infty$	-0.5453	-0.0718
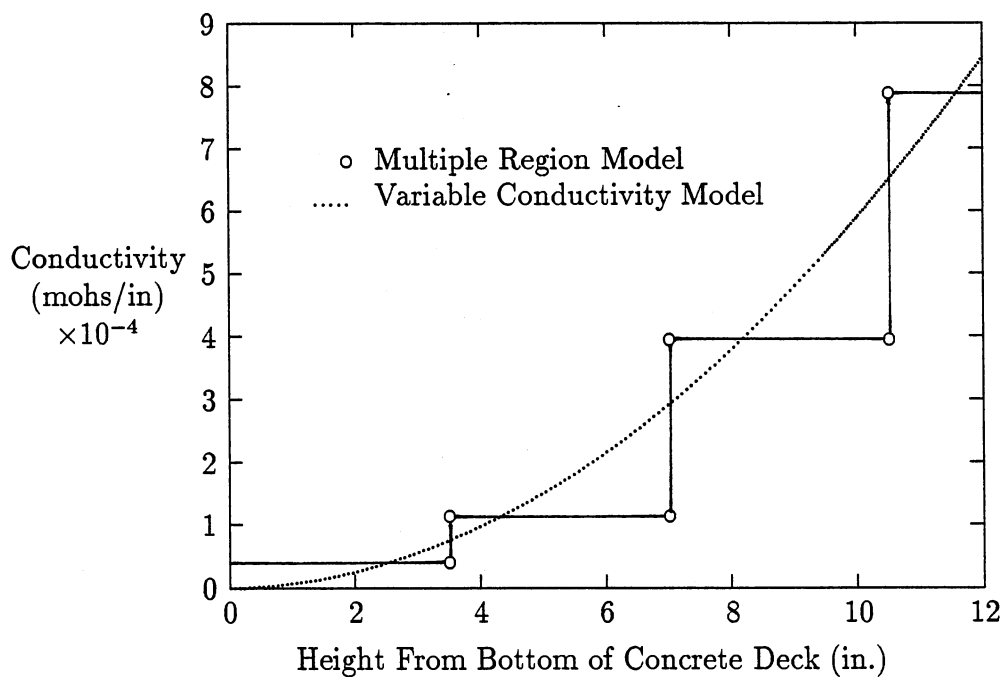
Figure 40. Conductivity Functions For Two Different BEM
Models of Reinforced Concrete Deck
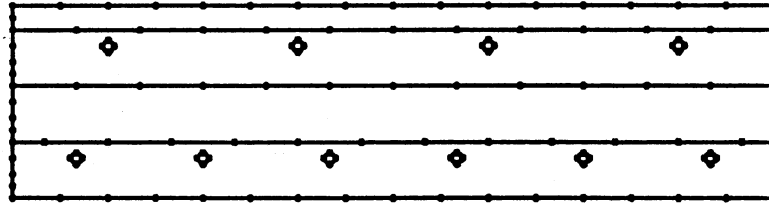
Figure 41. BEM Model of Reinforced Concrete Deck With
Multiple Homogeneous Regions

is shown in Figure 41. The model with variable conductivity, with 100 nodes and 100 elements, is shown in Figure 42. In both models, each reinforcing steel rod was modeled using four Overhauser elements [42] (Figure 43); the remaining boundaries were modeled using linear elements.

The BEM system converged in eight iterations for both cases. The total run time was approximately 20 minutes for the variable conductivity model and approximately 26 minutes for the multiple region model. An isopotential map of the results for the variable conductivity mesh is shown in Figure 44. Similar results were obtained for the multiple homogeneous regions mesh.

For the multiple region model, the average potential value on the top steel was calculated to be -820 mV, while on the bottom steel the average potential calculated
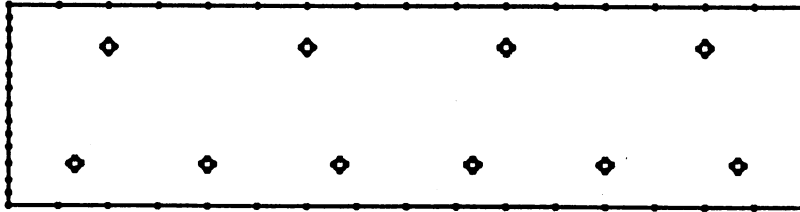
Figure 42. BEM Model of Reinforced Concrete Deck With Variable Conductivity
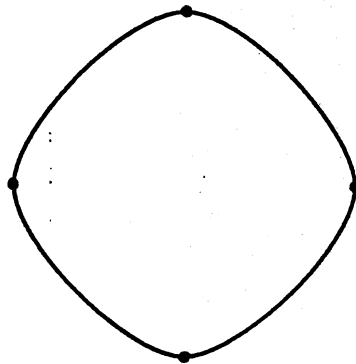
Figure 43. Close Up View of Overhauser Model of Each Reinforcing Steel Rod

-820 mV   -805 mV
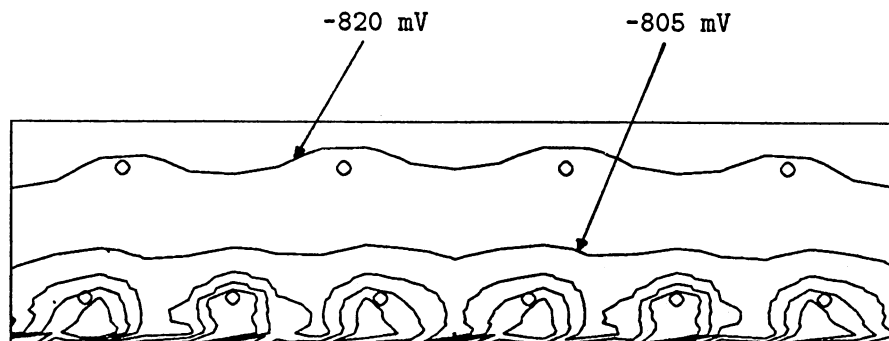
Figure 44. Isopotential Map of Results for Reinforced Con-
crete Deck With Variable Conductivity

was -730 mV. For the variable conductivity model, the average potential value on the

top steel was calculated as -815 mV, while the average potential calculated on the

bottom steel was -735 mV. The results obtained from both models indicate that the

bottom steel is not being protected from corrosion — an electropotential of -770 mV

on the steel is generally assumed to be the minimum magnitude needed for cathodic

protection of reinforcing steel in concrete [6].

The results obtained using the two models are very similar. It is observed though

that the total run time for the model with multiple regions is about 30% greater than

the run time for the variable conductivity model. More importantly, creation of the

input file for the more complex multiple region model is much more time consuming

for the system user. Thus, the variable conductivity model is more effective for analysis and design purposes than the multiple region model.

Cathodic Protection of Culvert Valve

The cathodic protection system of an existing culvert valve is analyzed in this section. The culvert valve is a pressure head releasing device, submerged in fresh water, and made out of ASTM-A36 steel (Figures 45, 46, 47). The radius of the valve is 17 ft. 6 in. from the center of the pivot to the outer edge of the $\frac{3}{4}$ in. thick, 10 ft. 6 in. wide shell. The shell covers an angle of 48.5°. The inside face of the valve is protected from corrosion by a sacrificial anode cathodic protection system. The outside face is protected by a 20% corrosion resistant cladding in combination with a sacrificial anode cathodic protection system. The sacrificial anodes are 7.5 lb. magnesium blocks attached to the shell.

Because the effects of the cathodic protection system are mostly localized to the shell, the culvert valve can be idealized for BEM analysis as a partially cylindrical shell submerged in an infinite electrolyte. Due to lack of polarization and resistivity data for the particular materials involved with this problem, the shell is assumed to be stainless steel, the anodes are assumed to be aluminum, and the electrolyte is assumed to be a 0.0165 wt% NaCl solution. The assumptions are not entirely unfounded; the electrochemical behavior of aluminum is very similar to that of magnesium [4,5], and the resistivity of the 0.0165 wt% solution, taken as 2500 ohm-cm, is the same
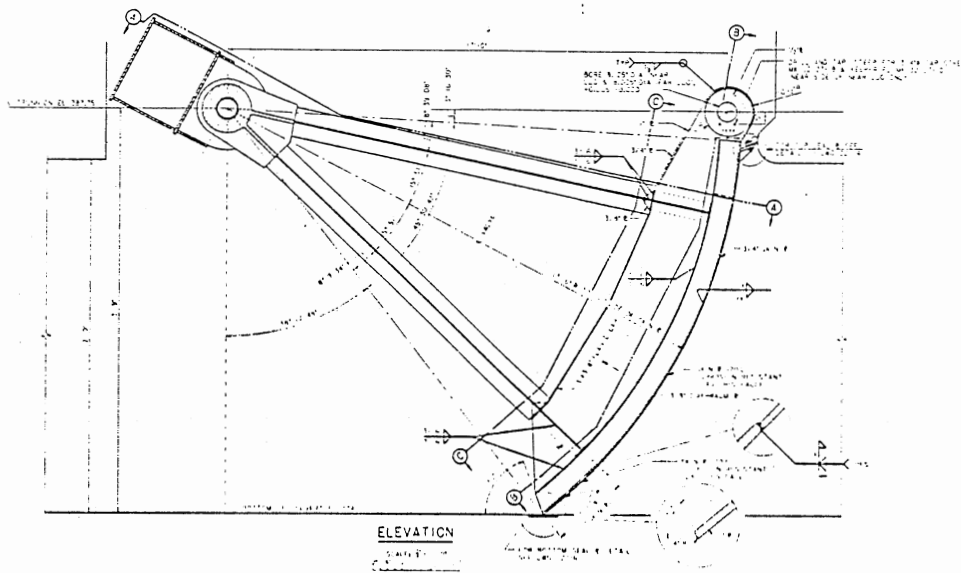
Figure 45. Culvert Valve Submerged in Fresh Water — Elevation
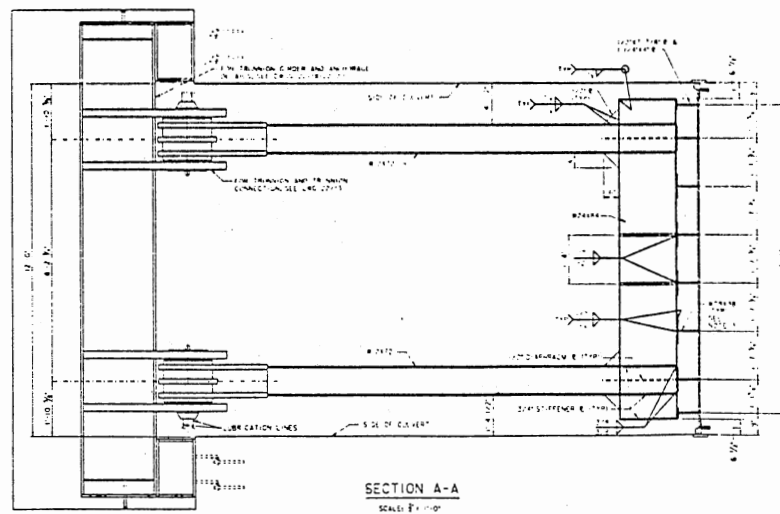
Figure 46. Culvert Valve Submerged in Fresh Water — Section A-A
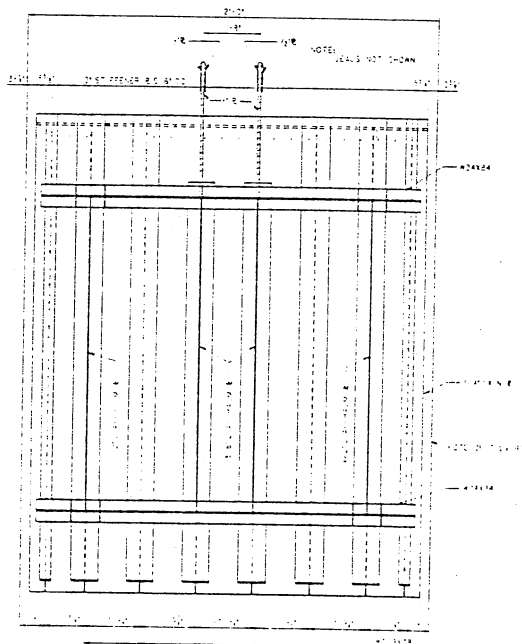
Figure 47. Culvert Valve Submerged in Fresh Water — Section
B-B

as that used for the original design of the culvert valve cathodic protection system.
The polarization curves used, the same as those used in the fourth problem of the
verification chapter (page 84), are repeated here in Figure 48 for convenience.

The boundary element mesh is shown in Figures 49 and 50, where the anode
arrangement is depicted by the filled-in anodic surfaces. The BEM mesh consists of
504 nodes, and 1004 triangular linear elements. It is an "external " problem, in the
sense that the boundary of the electrolyte is the shell itself — the electrolyte medium
extends to infinity in all directions.

The BEM system converged to a solution in 7 iterations, after running on the
VAXstation 2000 system for approximately 21 hours. The results are depicted in the
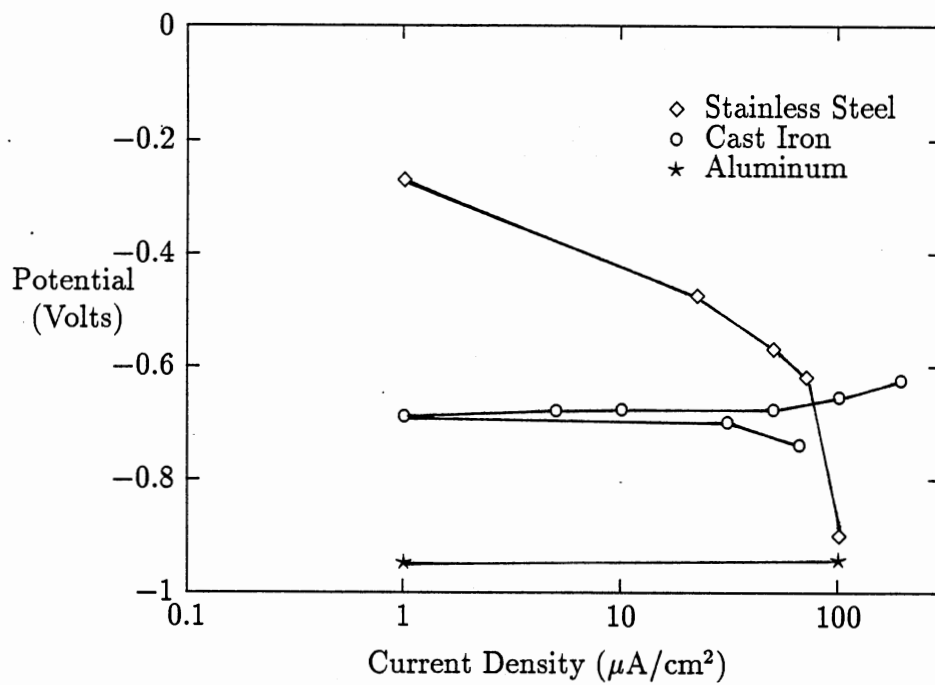
Figure 48. Polarization Curves for Stainless Steel, Cast Iron, and Aluminum in 0.0165 wt% NaCl Solution
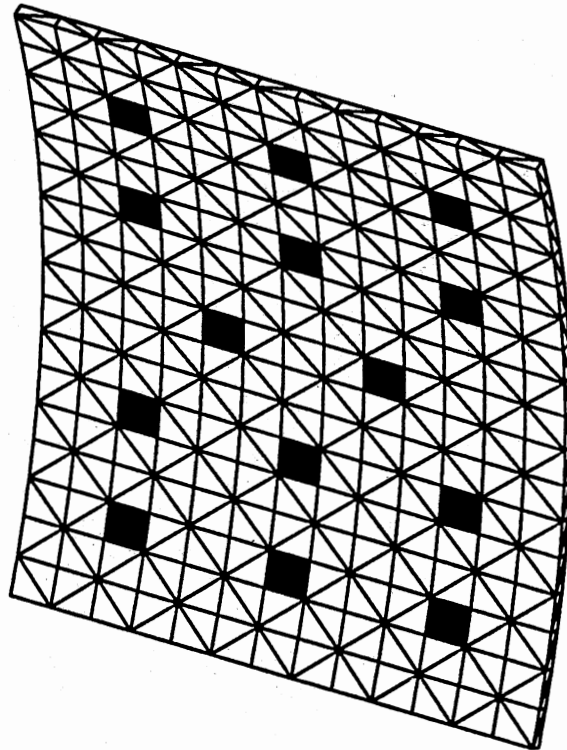
Figure 49. Perspective View of Inside Face of Culvert Valve BEM Mesh
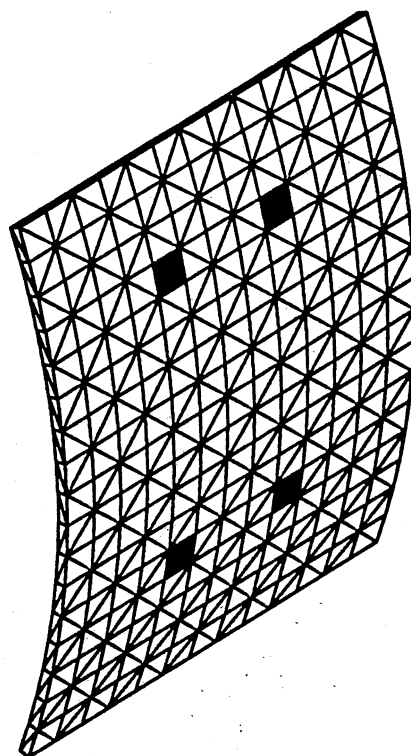
Figure 50. Perspective View of Outside Face of Culvert Valve
BEM Mesh

contour map of equipotentials in Figures 51 and 52.

For complete cathodic protection, the galvanic reaction must be such that the electropotential of the complete surface area of the steel shell is forced far enough into the cathodic region of the polarization curve to ensure that the steel is acting cathodically. A criteria for the maximum potential value for cathodic protection can therefore be taken as -300 mV, a value which is well within the cathodic region of the polarization curve. Based in this value, Figures 51 and 52 indicate that the outside edges of the shell may not be protected from corrosion.

An alternative BEM mesh and anode arrangement for the front of the valve is shown in Figure 53. This arrangement contains one more anode at the center of the shell, and the anodes on the outer edges of the shell have been placed closer to the borders. For the alternative mesh, the BEM system converges to a solution in 8 iterations, after running for approximately $22\frac{1}{2}$ hours. The results are shown in Figure 54, where it can be seen that the electropotential values at outside edges are almost completely under -300 mV. Though, according to the criteria chosen here, the front face of the shell is still not completely protected from corrosion, the alternative anode arrangement results in a larger cathodically protected surface area.

The original anode arrangement was used to test the cathodic protection properties of aluminum with respect to cast iron. Using the same mesh shown in Figures
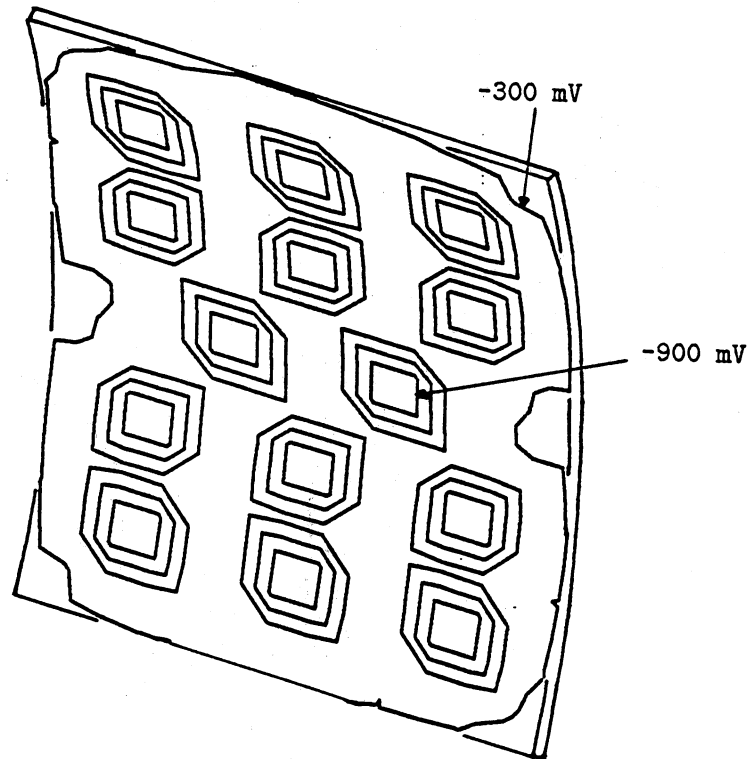
Figure 51. Topographic Map of Calculated Electropotential Values of Front Face of Culvert Valve Shell
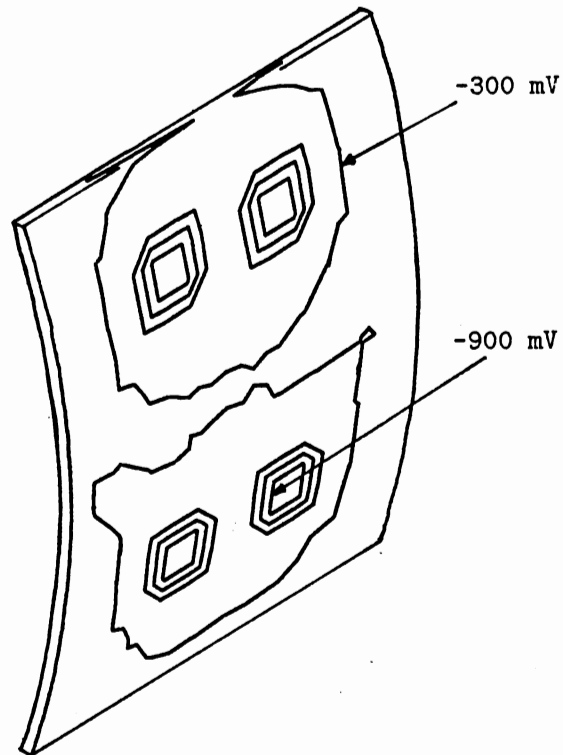
Figure 52. Topographic Map of Calculated Electropotential
Values of Back Face of Culvert Valve Shell
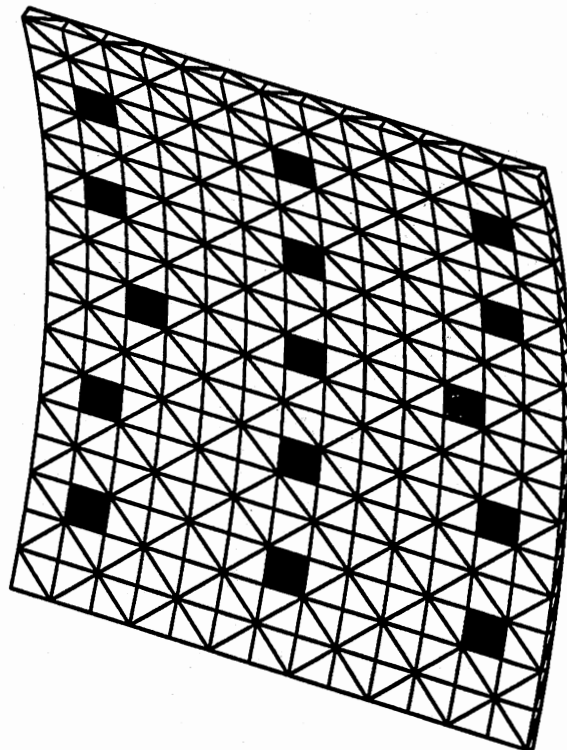
Figure 53. Perspective View of Inside Face of Culvert Valve
BEM Mesh With Alternative Anode Arrangement
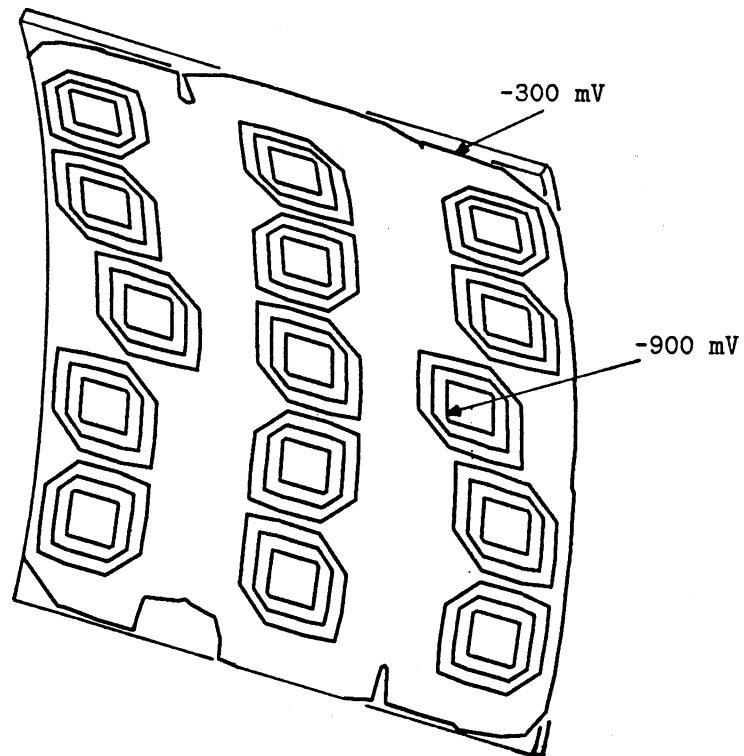
Figure 54. Topographic Map of Calculated Electropotential Values of Front Face of Culvert Valve Shell for Alternative Anode Arrangement

49 and 50, but assuming that the valve shell was cast iron instead of stainless steel, another program run was made. Convergence was achieved after 4 iterations and 20 hours.

Using the same criteria as that used for choosing the critical electropotential value for cathodic protection of stainless steel, the maximum electropotential value for cathodic protection of cast iron is taken as -700 mV. The results shown in Figure 55 indicate that only those areas very close to the aluminum anodes have electropotential values bellow -700 mV. It can be concluded that, based on the criteria chosen here, the aluminum anodes are not very good choices for the cathodic protection of cast iron in fresh water.

Although no concrete conclusions can be made about the cathodic protection system used for the culvert valve, due to insufficient polarization data, it is possible to see how the system BEM can be used as an aid for design of cathodic protection systems. Once the polarization data are obtained and programmed into the polarization database of the BEM system, it is simple to create new models for different anode arrangements, and even different anodic materials, in order to find a suitable cathodic protection system.
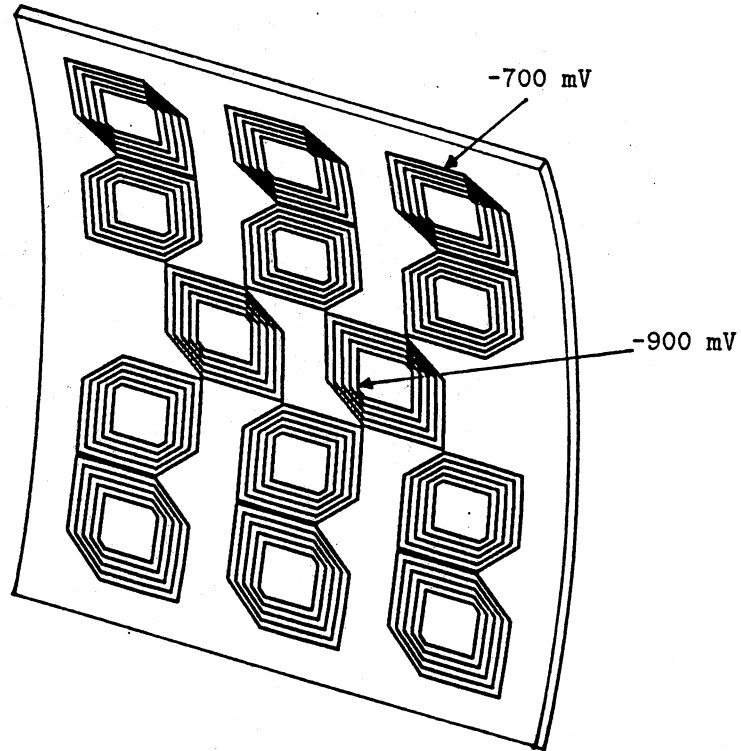
Figure 55. Topographic Map of Calculated Electropotential Values of Front Face of Cast Iron Culvert Valve Shell

CHAPTER VI

CONCLUSIONS

A BEM system which accounts for domains with variable resistivity is advantageous because the alternatives may be too costly in both man-hours and computer time. FEM and FDM differences suffer from the fact that the domain must be discretized. Though domain discretization facilitates the approximation of nonhomogeneities, it leads to large systems of equations to be solved, and large amounts of time consumed in creating the model, especially for three-dimensional problems. Accurate modeling of nonhomogeneous regions with standard BEM systems requires division of the domain into several homogeneous zones, adding to the number of equations to be generated and solved, as well as adding to the time in which the model can be created.

In addition to the aforementioned advantages, the current BEM system, which explicitly treats nonhomogeneous domains, may lead to more accurate results than its alternatives. In general, the resistivity of a particular region must be obtained experimentally. The resistivity function is then approximated by fitting curves through the obtained data. Using either FEM, FDM, or BEM with multiple zones, these curves are then approximated again by discretization of the domain. Using a BEM system

which explicitly treats nonhomogeneous domains, no discretization of the conductivity function within the electrolyte is needed. The functions used to approximate the experimental data may be the same as those used in the BEM analysis.

It is important to note that successful application of this method, and any other numerical method, is highly dependent on the accuracy of the mathematical model used. In previous work, it has been shown that Laplace's equation accurately governs the distribution of electropotentials within an electrolyte in a galvanic cell, but the boundary conditions, given by the electrode polarization functions, have not been as thoroughly investigated. The behavior of the electrode surfaces is dependent a multitude of factors, including temperature, dissolved oxygen within the electrolyte, and Hydrogen ion concentration. The polarization curves used in the analysis of corrosion problems by numerical techniques must take all of these factors into account. Inaccurate polarization curves will invariably lead to erroneous results.

In a large number of applications, the electrode polarization functions will change over time, due to a build up of calcareous deposits. Therefore, quasi-static capabilities for this type of problem would be an important addition to the current BEM system. This type of analyses would use a family of polarization curves, each corresponding to a particular time period. A more accurate representation of the corrosion process would thus be obtained, improving the design and analysis of cathodic protection systems.

Additional work could to improve the user-friendliness of the system is also desirable. A specialized Green's function, capable of explicitly modeling symmetric problems, and tube elements, which would model cylindrical voids within the electrolyte with few nodes, could both be incorporated into the current BEM system in the future. The advantages of these two additions would be a reduction in modeling and computation time required to solve problems.

APPENDIX

USERS'S MANUAL

CPOIS
A Boundary Element System For Galvanic Corrosion

By

Juan C. Ortiz

BSCE Louisiana State University 1984
MSCE Louisiana State University 1986
PhD Oklahoma State University 1989

August 4, 1989

1 Introduction

The program CPOIS is a general purpose boundary element method (BEM) analysis system for the solution of Laplace's equation, Poisson's equation, and some special cases of Darcy's equation. Two and three dimensional problems, as well as axisymmetric problems modeled with two dimensional elements in the r-z plane, can be solved using CPOIS. Non-linear boundary conditions, multiple regions with different material properties, and point sources are additional capabilities of the BEM system. Several element types in both two and three dimensions are available.

CPOIS is a file oriented program which reads in one input file and writes the results into one output file. A command line argument to the program permit the user to activate the interactive graphics previewer and postprocessor. The interactive previewer permits the user to visually check the input data for modeling accuracy and errors. Full two and three dimensional graphics are provided for this purpose. Auto-windowing, hidden surfaces, zooming and selective display are all included features of the interactive graphics previewer.

Postprocessing commands may be invoked upon termination of the system solution without exiting the previewer, or the postprocessor may be invoked after a batch run, for large problems which are not suitable for interactive analysis. The postpro-

cessing capabilities of CPOIS include: plotting of isopotential maps throughout the domain for two dimensional problems, including axisymmetric analyses; plotting of isopotential maps throughout the boundary of three dimensional problems; selection of points within the domain for the calculation of the potential value at that location; and creation of PostScript output to external files.

This manual is intended for those who are already familiar with the boundary element method and its applications. This manual does not attempt to teach BEM concepts nor does it attempt to inform the user of the various applications of Laplace's equation to engineering problems.

2   Program Capabilities

The BEM system, CPOIS, can solve the general two dimensional Laplace's equation in two and three dimensions. Also, axisymmetric problems may be modeled in the r-z plane using the two dimensional elements. The program CPOIS contains a series of additional capabilities making it a powerful tool for the solution of general diffusion-type problems.

Problems with piece-wise homogeneous regions are treated by creating a sub-domain with specific material properties for each different region. The nodes on the

interface between the regions do not have any specific boundary condition specified; CPOIS will internally impose the physical restrictions existing at the interface. The conductivities of each material must be given in each particular direction, thus allowing for materials with orthotropic properties. Problems involving materials with spacialy varying conductivities, in which the square root of the conductivity function satisfies Laplace's equation, can also be solved using CPOIS. The conductivity function may be explicitly defined by the user as a C function (including its derivatives with respect to each coordinate) or the coefficients of the general trilinear function may also be specified in the input file.

The general Poisson's equation, in two dimensional and axisymmetric problems, can also be solved using CPOIS. Poisson terms which satisfy Laplace's equation are treated using a boundary integration technique; Poisson terms which do not satisfy Laplace's equation are treated using the Monte Carlo method developed by G. S. Gipson. The user must supply the program with the Poisson function, as well as its derivatives in both the x and y directions as functions written in C. Concentrated point sources, a special case of Poisson terms which satisfy Laplace's equation, is another available option in CPOIS.

Phreatic surface problems are treated using an integration procedure in which the y coordinate of the phreatic surface, equivalent to the 'head' pressure, is found with

respect to a reference 'head' pressure of zero. Galvanic corrosion problems are solved by specifying an electrode type as a boundary condition, where the electropotential is given as a function of the current density. A Newton-Raphson iteration procedure is used to solve the resulting system of non-linear equations.

3 Element Types

3.1 Two Dimensional Elements

Five different types of two dimensional elements are available. All of the elements may be connected to one another at will. For maximum efficiency, it is recommended that linear elements are used for linear geometries where the behavior of the field variable is expected to behave in a more or less linear fashion, and the higher order elements be used for more complex boundaries.

The elements described in this section are used for both axisymmetric and two dimensional planar problems.

3.1.1 The Constant Element

This very crude element, which assumes a constant distribution of the field variable across the element, consist of 3 nodes, two of which are "dummy" nodes. These

dummy nodes are not actual nodes, but locations which define the endpoints of the elements. The middle node, which is not one of the "dummy" nodes must be located between the other two nodes of the element. It is recommended that these elements not be used on a routine basis, due to the lack of accuracy obtained when they are used. A large number of constant elements is needed to obtain accurate results for all but the most simple of problems. The constant element was originally included in the system only as a debugging tool for the author, and remains in the system for the same purpose.

3.1.2 The Linear Element

The linear element linearly interpolates the field variable between the two nodes of the element, located at the endpoints of the element. The linear element works very well for linear geometries where the resulting potential is close to linear, and, due to the speed at which the integrations are calculated using this element, it is very efficient. Curved geometries must be defined with a large number of linear elements to obtain accurate results, thus it is recommended that the higher ordered elements be used for curved geometries.

3.1.3   The Quadratic and Cubic Elements

These higher ordered elements are very effective for modeling curved and linear geometries. They interpolate the field variable between the nodes using a polynomial of order $n-1$, where n is the number of nodes on the element. The difference between the results obtained using higher ordered elements and those obtained using the linear and constant elements is impressive, specially for problems with curved geometries. The quadratic element is composed of three nodes, two at the endpoints of the element and one at the center. The cubic element is defined by four nodes, two of which are located at the endpoints and the other two evenly spaced between the endpoints.

Higher ordered elements may lead to a phenomenon known as "overspill". This phenomenon is encountered when the nodal spacing within an element is very uneven, causing a non-unique mapping of the function under consideration and creating unwanted warping of the element. These distortions may also appear when the values of the calculated variable vary greatly within an element, as may occur near singularities and locations where high gradients in the field variable are present. Care must be taken when using these elements so as to not cause unwanted distortions, in other words, the nodes within an element should be equally spaced and linear elements should probably be used near singularities.

6

3.1.4 The Overhauser Element

The Overhauser element, which interpolates the field variable with a cubic polynomial between the nodes, produces the most accurate results out of all the element types. It is constructed by four nodes, where the two internal nodes are the endpoints of the elements, and the two outside nodes lie outside of the element. The external nodes are used to define the parametric derivatives existing at the two end nodes (the middle two nodes). By overlapping the Overhauser elements, where nodes 2, 3 and 4 of one element are nodes 1, 2 and 3 of the next element, we insure that the parametric derivative is continuous at the nodes where the elements are joined together.

Overspill problems are not as severe with the Overhauser element as with the other higher ordered elements. Still, nodal spacing should be kept as even as possible between the four nodes that define the element to ensure that the element behaves as expected.

3.2 Three Dimensional Elements

There are four different types of elements available: linear triangles, bilinear rectangles, six-noded quadratic triangles, and eight-noded semi-cubic elements. Not all of the elements may be used in the same mesh though. Only combinations of linear/bilinear elements, and six-noded/eight-noded elements are possible. There are

no transition elements between the linear and bilinear elements and the higher order elements.

All of the surface elements used for three dimensional analysis are created by nodes which are numbered in a counterclockwise fashion around the edges of the element. The order in which the nodes are placed on the element is important, since it determines where the domain to be analyzed is located in space. The direction of a vector normal to the surface element which points away from the domain to be modeled is determined by using the right-hand rule: using your right hand wrap your fingers in the direction the elemental nodes and your thumb should point in the outward normal direction.

3.2.1   The Linear and Bilinear Elements

The linear elements are constructed with 3 nodes, which form a plane triangle in space. The linear element linearly interpolate the field variable between the two nodes of the element, located at the vertices of the triangle. The linear element works very well for flat geometries where the resulting potential behaves in a more or less linear fashion. Due to its low number of nodes, and hence, low number of calculations needed in the integrations, the computation times for models using the linear element are comparably lower than those for models using higher ordered elements.

The bilinear elements represent a mild improvement over the linear elements. Four nodes are used to create a bilinear rectangular element, the nodes of the element located at the corners of the rectangle. The bilinear element linearly interpolates the field variable in each parametric direction, hence the name "bilinear".

The linear element can be used only in conjunction with other linear element or with bilinear elements, and vice-versa.

3.2.2 The Six-Noded and Eight-Noded Elements

In general, results obtained using the higher ordered elements are more accurate than results obtained using the linear and bilinear elements. The six- and eight-noded elements are especially suited for curved geometries and problems in which the field variable does not behave in a linear fashion.

The six-noded triangular element interpolates the field variable with a quadratic surface between the nodes six nodes it is composed of. The first node of the element *must* be at one of the vertices of the triangle which is formed by the nodes. Thus, nodes 1, 3, and 5 of the triangle are at the vertices, and nodes 2, 4 and 6 are at the midpoints of the sides of the triangle.

The eight-noded rectangular element interpolates the field variable with a semi-cubic surface between the nodes eight nodes it is composed of. The first node of the

9

element *must* be at one of the corners of the rectangle which is formed by the nodes. Thus, all even numbered nodes, within the element, are located at the midpoints of the sides of the rectangle, and the uneven numbered nodes are located at the corners of the rectangle.

4 Data Input

This section explains how to create the input file for the program CPOIS. The underlying principles of the input file is readability: the user should be able to read the contents of the file and easily recognize what everything represents. To achieve this, keywords are used through out the input file, indicating to both the user and the BEM system what each part of the data represents.

All of the data may be written in "free format", where none of the numbers or keywords need to be lined up in columns. Blank lines, as well as comment lines (identified by placing a % sign in the first column of the line), are also allowed, helping to improve readability for the user. Keywords may be written in upper and/or lower case, and for the most part, only the first few letters of the keyword are necessary.

The general order of the data is: (1) title, (2) problem type, (3) control data, (4) nodes, and (5) regions. This order *must* be followed. Except for the title, the problem

type, and the control information, each major section of data is identified by a key word on the line before it.

The elements, material properties, internal points, etc. are all defined in the region data. The order in which this information is listed is not important, but again, each section of data is identified by a key word on the line before it.

The following sections describe each section of data and how the information is included in the input file. Keywords in the following sections are given in upper case boldface (**LIKE THIS**), and an asterisk appears where the keyword may be terminated, as in **AXIS*YMMETRIC**, where only the first four letters **AXIS** are required by the program.

4.1 Title

There must be a title line at the top of the file. No comments or blank lines are allowed before the title line. The title line can be up to 80 characters long.

4.2 Problem Type

This line must be after the title line. It defines the type of analysis to be performed, which may be either planar two dimensional analysis (**TWO**), axisymmetric analysis (**AXIS*YMMETRIC**), or three dimensional analysis (**THREE**). Examples:

three

TwoDimensional

AXIS

Notice that once the required part of the keyword is recognized by the program, the rest of the keyword is ignored. Also, it does not matter whether the words are in upper or lower case, or a mixture of both.

4.3   Control

Several of the program's options may be invoked by the optional control data. The control data determines (a) whether to echo the input data, or not (**ECHO** or **NOE-CHO**, (b) the value of the tolerance used in the iteration solution of galvanic corrosion problems (**TOLE*RANCE**), and (c) the maximum number of iterations allowed (**ITER*ATIONS**).

Examples:

tolerance n

iterations n

echo

noecho

where n is a number specifying the number of iterations or the tolerance.

4.4   Nodal Points

The nodal point information should be after the problem type line and before the material lines. The keyword **NODE*S** must precede the coordinate line list. Each coordinate line also contains the boundary condition at each node. Nodes may be generated in a straight line, therefore, the nodes must all be input in ascending order. Syntax:

$$n \quad x \quad y \quad z \quad bc \quad v$$

where n is the node number, x, y, and z are the coordinates of the node, bc is the keyword specifying the boundary condition type, and v is either the value of the boundary condition or the electrode metal type. The z coordinate must be omitted for three dimensional analysis. For axisymmetric analysis, the x and y coordinates are the r and z coordinates in polar coordinates, respectively. The keyword used to specify the boundary condition type are: **POTE*NTIAL, FLUX, DUMM*Y, INTER*FACE**, or **ELEC*TRODE**, which are self explanatory. Only nodes with either the potential or the flux must have a specified boundary condition value v. Electrodes must have a metal type specified which may be: **TESTA, TESTB, STEELS, STEELC, COPPERS, SSTEELS, ALUMINUMS, IRONS, SUS304, FC20,**

INSSTEELS , or **INALUMINUMS.** The file 'initmetals.c' contains the definitions and sources for the polarization curves corresponding to each of these metal types.

Examples:

    1 1.0 5 30.25 temperature 1.0

    2 10.0e+03 1.0e+02 10 flux 10.0

    3 1 1 1 dumm

    4 20000.003 20.0 20 PHRE

    5 3 3 3 INTERFACE

    6 1.0 1.0 11.0 electrode ssteels

4.5   Materials

Each material must have its own list of elements, internal points and properties. The keyword **MATE*RIAL** must be specified before the properties, elements and internal points of each material is given. The material number must also be given. Materials must be in order, i.e. material 2 must follow material 1, and so on. If the material is an external one this must also be specified.

Syntax:

    material *n code*

where n is the material number, and *code* is the optional keyword **EXTE*RNAL**.

Examples:

> MATE 1 external
>
> material 2

4.5.1 Elements

The element line list must be preceded by the key word **ELEM*ENTS**. Each element line contains the element type, topology information and number of Gauss points used for integration. Elements are generated when the difference between two consecutive element numbers is greater than one, therefore, all elements must be in order.

Syntax:

> n *type* n_1 n_2 ... n_N *ngauss*

where n is the element number, *type* is the keyword for the element type. For two dimensional elements these may be **CONS*TANT, LINE*AR, QUAD*RATIC, CUBI*C**, or **OVER*HAUSER**. For three dimensional elements they may be: **LINE*AR, BILI*NEAR, TRIA*NGULAR**, or **RECT*ANGULAR**.

n_1 n_2 ... n_N are the N nodal point numbers which define the element. The nodal points which define the element must be in order, and remember that for regular problems they go counterclockwise and for external problems they go clockwise. *ngauss*

is the number of Gauss points used for integration, which is optional – the default value is four (4), the maximum value is fifteen (15).

Examples:

1 LINE 1 2

2 quadratic 2 3 4

3 CUBIC 4 5 6 7 12

4 overh 6 7 8 9 5 line 1 2 3

6 bili 45 57 34 22 10

7 TRIANG 34 22 12 23 45 67

8 rectangular 1 2 3 4 5 6 7 8 5

4.6 Material Properties

The optional list of material properties lines must be preceded by the key word **PROP*ERTIES**. The default is no Poisson terms or sources, conductivities of 1.0 in all directions and 0.0 angle of orthotropy. Orthotropic properties, conductivities, Poisson terms, and points sources are all included in this section.

4.6.1   Conductivities

The conductivity **COND*UCTIVITY** of each material is by default 1.0 in all directions. They may be changed and different conductivities may be given in different directions. For two dimensional and axisymmetric problems, only the conductivities of the x and y direction may be given.

Syntax:

COND*UCTIVITY c_x c_y c_z

where c_x, c_y, and c_z are the values of the conductivities in the x, y, and z directions respectively. You must omit c_z for two dimensional and axisymmetric problems. Variable conductivities are also allowed, as long as the square root of the conductivity satisfies Laplace's equation, and it is the same conductivity in all directions (i.e. varies only with respect to position). The variable conductivity may be specified either as a the coefficients of the square of the general trilinear polynomial function,

$$(a + bx + cy + dz + exy + fxz + gyz + hxyz)^2$$

where a-h are constants, or as a specific function written in C.

Syntax:

COND*UCTIVITY *type h g f e d c b a*

17

where *type* is either **TRILI*NEAR** or **VARI*ABLE** (used for specific variable function) and the constants *a-h*, correspond to the coefficients of the trilinear function given above (not given if **VARI*ABLE** is used. Note the order of the coefficients when specifying trilinear conductivity functions. The file 'kfun.c' contains the variable conductivity function and its derivatives.

Examples:

conductivity 0.5 0.5 0.5

cond trilinear 0 0 0 0 0 5.0 0 5.0

cond variable

4.6.2 Poisson Terms and Point Sources

Poisson terms are classified into three different types in CPOIS, and each type must be differentiated in the input file. The three classifications are: general Poisson terms, treated with the Monte Carlo method; cases in which the Poisson term satisfies Laplace's equation, treated by a surface integration; and concentrated sources, which are treated with a simplified boundary integration. Poisson terms are specified in the file 'fun.c' which contains the Poisson term function and its derivatives.

Monte Carlo Method   Specifying the total number of random points to be used for Monte Carlo integration of the Poisson term automatically indicates to CPOIS that a general Poisson term exists. The keyword is **RAND*OM POINTS**.

Syntax:

RANDOM POINTS n

where n is the number of random points used.

Poisson Terms Which Satisfy Laplace's Equation   The boundary integration technique is implemented when a Poisson terms which satisfy Laplace's equation is specified by using the keyword **POIS*SON**, with no other parameters.

Syntax:

POISSON

Point Sources   For point sources, the information needed by the program is the location of the source and its intensity. The keyword **SOUR*CES** is used with a list of the location of source points, with their intensity, following.

Syntax:

SOURCES n x y z val

where n is the number of the source, x, y, and z are the source location coordinates (z coordinate not specified for two dimensional or axisymmetric analyses), and *val* is the value of the intensity of the point source (may be negative for concentrated sinks). Sources may be generated in a straight line similar to the nodes, which is the only reason why there is a number specified with each source.

4.7   Internal Points

The list of internal points must be preceded by the keyword **INTE*RNAL POINTS**. Internal points may also be generated in a straight line, as the nodes are, which implies that each internal point has a number associated with it, and that the numbers must be in order.

Syntax:

$n \; x \; y \; z$

where n is the internal point number, starting with one (1) for each material, and x, y, and z are the coordinates of the internal point (omit the z coordinate for two dimensional and axisymmetric problems).

5 Sample Data Files

A sample data file follows. It is the data file used for the first verification problem in the previous text.

```
Verification Test -- Waber 1956 paper (no. IV)
twod
%                       This is the control data
%

                        noecho
                        tolerance      1.0e-10
                        iterations   10
%
%                       These are the nodal points
%
% node     X        Y              BC    BC VALUE/ELECTRODE TYPE
nodes
    1     0.0      0.0        flux            0.0
    2     0.0      0.0        electrode       testa
    3     0.08     0.0        electrode       testa
    4     0.14     0.0        electrode       testa
    5     0.20     0.0        electrode       testa
   10     0.40     0.0        electrode       testa
   13     0.46     0.0        electrode       testa
   16     0.49     0.0        electrode       testa
   17     0.51     0.0        electrode       testb
   20     0.54     0.0        electrode       testb
   23     0.60     0.0        electrode       testb
   28     0.80     0.0        electrode       testb
   29     0.86     0.0        electrode       testb
   30     0.92     0.0        electrode       testb
   31     1.00     0.0        electrode       testb
   32     1.00     0.0        flux            0.0
   35     1.00     0.3        flux            0.0
```

21

```
   36      1.00       0.5       flux            0.0
   41      0.00       0.5       flux            0.0
   42      0.00       0.3       flux            0.0
   43      0.00       0.2       flux            0.0
   44      0.00       0.1       flux            0.0
%
%              This is the material data
material 1
properties
conductivity 1.0 1.0
%
%              These are the elements
%
%   NUMBER      TYPE         ELEMENT NODES          GAUSS POINTS
elements
        1      line      2       3                        15
        2      over      2       3       4       5        15
       28      over     28      29      30      31        15
       29      line     30      31                        15
       30      line     32      33                        15
       41      line     43      44                        15
       42      line     44       1                        15
end
```

BIBLIOGRAPHY

[1] Adey, R.A. and Niku, S.M. Boundary Element Simulation of Galvanic Corrosion—The Story of a Major Success for Boundary Elements. In C.A. Brebbia, editor, *Boundary Elements X, Vol.2 Heat Transfer, Fluid Flow and Electrical Applications*, pages 453–481. Computational Mechanics Publications, Southampton, U.K., 1988.

[2] R.S. Munn. Microcomputer Corrosion Analysis for Structures in Inhomogeneous Electrolytes. In Heidersbach, Fu, J., and Erbar, R., editors, *CORROSION/86 Symposium on Computers in Corrosion Control*, pages 240–255. NACE, Houston, TX, 1986.

[3] R.F. Stratfull. How Chlorides Affect Concrete Used With Reinforcing Steel—Laboratory and Field Tests. *NACE, Materials Performance*, 7(3):29–34, 1968.

[4] J.H. Morgan. *Cathodic Protection*. The Macmillan Company, New York, NY, 1960.

[5] Fontana, M.G. and Greene, N.D. *Corrosion Engineering*. McGraw Hill Book Company, New York, NY, 1978.

[6] Mudd, C.J., Mussinelli, G.L., Tettamanti, M., and Pedeferri, P. Cathodic Protection of Steel in Concrete. *NACE, Material Performance*, pages 18–24, September 1988.

[7] C. Wagner. Theoretical Analysis of the Current Density Distribution in Electrolytic Cells. *Journal of Electrochemical Society*, 98(3):116–128, 1951.

[8] Stern, M. and Geary, A.L. Electrochemical Polarization — I. A Theoretical Analysis of the Shape of Polarization Curves. *Journal of Electrochemical Society*, 104(1):56, 1957.

[9] J.T. Waber. Mathematical Studies on Galvanic Corrosion — I. Coplanar Electrodes With Negligible Polarization. *Journal of Electrochemical Society*, 101(6):271, 1954.

[10] Waber, J.T. and Rosenbluth, M.J. Mathematical Studies on Galvanic Corrosion — II. Coplanar Electrodes With One Electrode Infinitely Large and With Equal Polarization Parameters. *Journal of Electrochemical Society*, 102(6):344, 1955.

[11] J.T. Waber. Mathematical Studies on Galvanic Corrosion — VI. Limiting Case of Very Thin Films. *Journal of Electrochemical Society*, 103(10):567, 1956.

[12] Waber, J.T. and Fagan, B.J. Mathematical Studies on Galvanic Corrosion — IV. Influence of Electrolyte Thickness on the Potential and Current Distributions Over Coplanar Electrodes Using Polarization Parameters. *Journal of Electrochemical Society*, 103(1):64–72, 1956.

[13] Kennard, E. and Waber, J.T. Mathematical Study of Galvanic Corrosion—Equal Coplanar Anode and Cathode With Unequal Polarization Parameters. *Journal of Electrochemical Society*, 117(7):880, 1970.

[14] Parrish, W.R. and Newman, J. Current Distributions on Plane, Parallel Electrodes in Channel Flow. *Journal of Electrochemical Society*, 117(1):43–48, 1970.

[15] Nanis, L. and Kesselman, W. Engineering Applications of Current and Potential Distributions in Disk Electrode Systems. *Journal of Electrochemical Society*, 118(3):454–461, 1971.

[16] Newman, J. and Harrar, J.E. Potential Distribution in Axisymmetric Mercury-Pool Electrolysis Cells at the Limiting Current. *Journal of Electrochemical Society*, 120(8):1041–1044, 1973.

[17] Alkire, R. and Varjian, R. Resistive Wire Electrodes. *Journal of Electrochemical Society*, 121(5):622–631, 1974.

[18] Doig, P. and Flewitt, P.E.J. A Finite Difference Numerical Analysis of Galvanic Corrosion for Semi-Infinite Linear Coplanar Electrodes. *Journal of Electrochemical Society*, 126(12):2057–2063, 1979.

[19] Helle, H.P.E., Beek, G.H.M., and Ligtelijn, J.TH. Numerical Determination of Potential Distributions and Current Densities in Multi-Electrode Systems. *Corrosion/NACE*, 37(9):522–530, September 1981.

[20] R.S. Munn. A Mathematical Model for a Galvanic Anode Cathodic Protection System. *NACE, Material Performance*, pages 29–36, August 1982.

[21] J.W. Fu. A Finite Element Analysis of Corrosion Cells. *Corrosion/NACE*, 38(5):295–296, May 1982.

[22] Fu, J.W. and Chan, S. A Finite Element Method for Modeling Localized Corrosion Cells. *NACE, Material Performance*, 40(10):540–544, October 1984.

[23] M.R. Haroun. Cathodic Protection Modeling of Nodes in Offshore Structures. Master's thesis, Oklahoma State University, Stillwater, OK, 1986.

[24] Str⌀mmen, R. and R⌀dland, A. Computerized Techniques Applied in Design of Offshore Cathodic Protection Systems. *NACE, Material Performance*, pages 15–20, April 1981.

[25] Kasper, R.G. and April, M.G. Electrogalvanic Finite Element Analysis of Partially Protected Marine Structures. *Corrosion/NACE*, 39(5):181–188, May 1983.

[26] Keim, W. and Str⌀mmen, R. Computer Modeling in Offshore Platform CP Systems. *NACE, Material Performance*, pages 25–28, September 1988.

[27] J.B. Vrable. Cathodic Protection for Reinforced Concrete Bridge Decks. Technical Report 180, National Cooperative Highway Research Program, Washington, D.C., 1977.

[28] G.S. Gipson. A Survey Report on the Boundary Element Method Applied to Cathodic Protection Problems. Technical report, U.S.A.E. Waterways Experiment Station, Vicksburg, MS, October 1986.

[29] Aoki, S., Kishimoto, K., and Sakata, M. Boundary Element Analysis of Galvanic Corrosion. In Brebbia, C.A. and Maier, G., editors, *International Conference on Boundary Element Methods in Engineering*, pages 1-63 – 1-72. Computational Mechanics Publications, Southampton, U.K., 1985.

[30] Telles, J.C.F., Wrobel, L.C., Mansur, W.J., and Azevedo, J.P.S. Boundary Elements for Cathodic Protection Problems. In Brebbia, C.A. and Maier, G., editors, *International Conference on Boundary Element Methods in Engineering*, pages 1-73 – 1-83. Computational Mechanics Publications, Southampton, U.K., 1985.

[31] Adey, R.A., Niku, S.M., Brebbia, C.A., and Finnegan, J. Computer Aided Design of Cathodic Protection Systems. In Brebbia, C.A. and Maier, G., editors, *International Conference on Boundary Element Methods in Engineering*, pages 14-21 — 14-23. Computational Mechanics Publications, Southampton, U.K., 1985.

[32] Adey, R.A., Brebbia, C.A., and Niku, S.M. Beasy-CP—A System for Analysis of Galvanic Corrosion and Cathodic Protection Using Boundary Elements. In Connor, J.J. and Brebbia, C.A., editors, *Proceedings of BETECH 86*, pages 85–107. Computational Mechanics Publications, Boston, MA, 1986.

[33] Str⌀mmen, R., Keim, W., Finnegan, J., and Mehdizadeh, P. Advances in Offshore Cathodic Protection Modeling Using the Boundary Element Method. *NACE, Material Performance*, pages 23–28, February 1987.

[34] C.A. Brebbia. *The Boundary Element Method for Engineers*. Pentech Press, London, 1978.

[35] A.H.-D. Cheng. Darcy's Flow With Variable Permeability: A Boundary Integral Solution. *Water Resources Research*, 20(7):980–984, 1984.

[36] G.S. Gipson. Boundary Element Fundamentals—Basic Concepts and Recent Developments in the Poisson Equation. In Brebbia, C.A. and Connor, J.J, editors, *Topics in Engineering Vol. 2*. Computational Mechanics Publications, Southampton, U.K., 1987.

[37] Press, W.H., Flannery, B.P., Teukolsky, S.A., and Vetterling, W.T. *Numerical Recipes*. Cambridge University Press, Cambridge, MA, 1986.

[38] Hamberg, A., Orton, M.D., and Smith, S.N. Cathodic Protection of Offshore Well Casing. *NACE, Materials Performance*, pages 26–30, March 1988.

[39] Brebbia, C.A., Telles, J.C.F., and Wrobel L.C. *Boundary Element Techiques, Theory and Applications in Engineering*. Springer-Verlag, Berlin, 1984.

[40] O.C. Zienkiewicz. *The Finite Element Method*. McGraw Hill, London, 1977.

[41] Juan C. Ortiz. An Improved Boundary Element System for the Solution of Poisson's Equation. Master's thesis, Louisiana State University, 1986.

[42] Ortiz, J.C, Walters, H.G., Gipson, G.S., and Brewer, J.A. Development of Overhauser Splines as Boundary Elements. In Brebbia, C.A., Wendland, W.L., and Kuhn, G., editors, *Boundary Elements IX, Vol. 1, Proceedings of the Ninth International Conference on Boundary Element Methods*, pages 401–407. Springer-Verlag, Berlin, 1987.

[43] Walters, H.G., Ortiz, Juan C., Gipson G.S., and Brewer, J.A. Overhauser Splines as Improved Boundary Element Types. In T. A. Cruse, editor, *Advanced Boundary Element Methods*, pages 461–464. Springer-Verlag, New York, 1987.

[44] H.G. Walters. Techniques for Boundary Element Analysis in Elastostatics Influenced by Geometric Modeling. Master's thesis, Louisiana State University, 1986.

[45] Stroud, A.H. and Secrest, D. *Gaussian Quadrature Formulae*. Prentice-Hall, Englewood Cliffs, NJ, 1966.

[46] Gradshteyn, I.S. and Ryzhik I.M. *Tables of Integrals, Series, and Products*. Academic Press, New York, 1980.

[47] Abramowitz, M. and Stegun, A. *Handbook of Mathematical Functions*. Dover, New York, 1972.

[48] Aliabadi, M.H. and Hall, W.S. Taylor Expansions For Singular Kernels in The Boundary Element Method. *International Journal for Numerical Methods in Engineering*, 21:2221–2236, 1985.

[49] Lachat, J.C. and Watson, J.O. Effective Numerical Treatment of Boundary Integral Equations: A Formulation for Three-Dimensional Elastostatics. *International Journal for Numerical Methods in Engineering*, 10:991–1005, 1976.

[50] Aliabadi, M.H. and Hall, W.S. Analytical Removal of Singularities and One-Dimensional Integration of Boundary Element Method Kernels. *Engineering Analysis*, 4(1):21–24, 1987.

[51] Aliabadi, M.H., Hall, W.S., and Hibbs, T.T. Exact Singularity Cancelling For The Potential Kernel in The Boundary Element Method. *Communications in Applied Numerical Methods*, 3:123–128, 1987.

[52] Aliabadi, M.H. and Hall, W.S. Weighted Gaussian Methods For Three-Dimensional Boundary Element Kernel Integration. *Communications in Applied Numerical Methods*, 3:89–96, 1987.

[53] Lean, M.H. and Wexler, A. Accurate Numerical Integration of Singular Boundary Element Kernels Over Boundaries With Curvature. *International Journal for Numerical Methods in Engineering*, 21:211–228, 1985.

[54] Li, H-B., Han, G-M., and Mang, H.A. A New Method for Evaluating Singular Integrals in Stress Analysis of Solids By the Direct Boundary Element Method. *International Journal for Numerical Methods in Engineering*, 21:2071–2098, 1985.

[55] Aoki, S., Kishimoto, K., and Miyasaka, M. Analysis of Potential and Current Density Distributions Using a Boundary Element Method. *Corrosion/NACE*, 44(12):926–932, 1988.

[56] Fu, J.W. and Chow, S.K. Cathodic Protection Designs Using an Integral Equation Numerical Method. *NACE, Material Performance*, 21(10):9–12, October 1982.

VITA

Juan Carlos Ortiz

Candidate for the Degree of

Doctor of Philosophy

Dissertation: USE OF THE BOUNDARY ELEMENT METHOD
FOR ANALYSIS OF GALVANIC CORROSION
IN NONHOMOGENEOUS ELECTROLYTES

Major Field: Civil Engineering

Biographical:

Personal Data: Born in Caracas, Venezuela, October 13, 1961, the son of Juan and Graciela Ortiz.

Education: Graduated from Liceo Gustavo Herrera, Caracas, Venezuela, in July, 1980; received Bachelor of Science degree in Civil Engineering form Louisiana State University in August, 1984; received Master of Science degree in Civil Engineering from Louisiana State University in August, 1986; completed requirements for Doctor of Philosophy degree in Civil Engineering at Oklahoma State University in August, 1989.

Professional Experience: Teaching and Research Assistant, School of Civil Engineering, Louisiana State University, August, 1984 to July, 1986; Teaching and Research Assistant, Civil Engineering Department, Oklahoma State University, August, 1986 to August, 1989.